THE USE OF BIOPOLYMER FUNCTIONALIZED SINGLE WALLED CARBON NANOTUBES FOR EFFECTIVE TARGETED PHOTODYNAMIC THERAPY OF COLON CANCER STEM CELLS

A thesis submitted to the Faculty of Health Sciences, University of Johannesburg, in fulfilment of the requirements for the degree of Doctor of Technology, Biomedical Technology

By

Prabhavathi Sundaram

(Student Number: 201807307)

Supervisor:

_____ 23November 2020

Prof. Heidi Abrahamse Date

DECLARATION

I **Prabhavathi Sundaram** declare that this thesis is my own, unaided work. It is being submitted for the Degree of Doctor of Technology at the University of Johannesburg. It has not been submitted before for any degree or examination in any other University.

Doctoral Candidate: _____ 23 November 2020

Prabhavathi Sundaram Date

OUTPUTS OF THE STUDY

ACCREDITED INTERNATIONAL PUBLICATIONS: (Appendix E)

- **Sundaram, P**.; Abrahamse, H. (2020). Effective Photodynamic Therapy for Colon Cancer Cells Using Chlorin e6 Coated Hyaluronic Acid-Based Carbon Nanotubes. *International journal of molecular science*, 21(13), 4745. DOI: 10.3390/ijms21134745. **Impact Factor: 4.556.**
- **Sundaram, P**.; Abrahamse, H. (2020). Emerging Phototherapy combined with 1D & 2D carbon nanomaterial applications in cancer therapy. *Materials*, 13, 4830; doi:10.3390/ma13214830. **Impact Factor: 3.057**
- **Sundaram, P**.; Abrahamse, H. Cellular uptake kinetics and stability analysis of photosensitizer chlorin e6 and its photodynamic effect on colon cancer cells. *Journal of photochemistry and photobiology B: Biology*. (In draft). **Impact Factor: 4.383**
- **Sundaram, P**.; Abrahamse, H. Isolation, characterization and targeting of colon cancer stem cells with carbon nanotube enabled photodynamic therapy. *Cancer Research*. (In draft). **Impact Factor: 9.727**

CONFERENCES AND WORKSHOPS PRESENTATIONS:

- Universitas 21 Health Sciences Group Doctoral Student Forum (Virtual conference) conducted by UCD, Dublin, Ireland. Poster presentation, Sundaram, P (2020).
- Africa Laser Council (ALC) Symposium, Biophotonics in cancer: redefining trends in cancer therapy, Hosted by the Laser Research Centre (LRC), University of Johannesburg, South Africa. Poster presentation, Sundaram, P (2019).

ABSTRACT

Cancer is one of the leading causes of mortality with approximately 14.1 million new cases and 8.2 million deaths worldwide reported by GLOBOCAN Colorectal cancer (CRC) is the third most diagnosed cancer in males and second in females worldwide. In the South African population, CRC incidence rate was 6.5% and the death rate was 6.4% from total number of cancer cases (Cancer country profile, WHO, 2020). Present cancer treatments include radiation therapy, surgery and conventional chemotherapy which is limited due to nonspecific targeting, poor solubility, and rapid drug clearance (Senapati et al., 2018). Major issues with cancer cells are metastasis, invasion, and recurrence. After treatment small populations of cells actively form tumours within the same organ or nearby organs due to the presence of cancer stem cells (CSCs). Cancer stem cells are a small subset of neoplastic cells capable of tumourgenesis, they have characteristics like normal stem cells (SCs) which include, self-renewal and pluripotency through which the generation of heterogeneous cells can construct the entire tumour (Lundin et al., 2013).

In recent years, nanotechnology coupled with photodynamic therapy (PDT) has received considerable attention in terms of improving the effectiveness of drug delivery in cancer therapeutics. Photodynamic therapy is a principle whereby a photosensitizer (PS) absorbs a photon of energy at a specific wavelength of light and transfers that energy into singlet oxygen molecules (Eun et al., 2016). PDT is a minimal invasive cancer treatment that has clinically been approved by the FDA and used to treat various tumours, is compatible, low cost, effective and has with minimal side effects (Mukai et al., 2016). Chlorin e6 (Ce6), is a naturally derived heterocyclic aromatic PS molecule and it is synthesised from chlorophyll-a. Ce6 accumulate in target tissue, has a strong absorption wavelength between 650-670 nm and no side effects to biological tissue (Juzeniene et al., 2009).

Single walled carbon nanotubes (SWCNTs) are nanosized hollow cylindrical tubes made up of C60 carbon atoms in the form of benzene rings.

It has a wide surface area to carry drugs, PSs, and biological substances, and, when the SWCNTs are coupled with biological molecules they are biocompatible, excellent nanocarriers and non-toxic to normal cells while excreted through the urine. The development of functionalised single walled carbon nanotubes (SWCNTs) has become revolutionary in targeted PDT delivery since it improves the therapeutic index of drugs (Singh et al., 2012).

Hyaluronic acid (HA) is a biocompatible and well-known biodegradable biopolymer which is widely distributed in human epithelial, neural and connective tissues (Fallacara et al., 2018). Furthermore, it has a high affinity towards CD44 receptors which are overexpressed in various CSCs, including colon cancer. Thus, HA can act as a targeting ligand when coupled with SWCNTs to favourably target colon cancer stem cells (CCSCs) and aid in delivering active molecules such as anticancer PS drugs for PDT treatment.

The aim of this study was to synthesise nanobiocomposites using SWCNTs, HA and Ce6. Carboxylated SWCNTs and amine activated HA were covalently coupled by carboxyl-amine cross linking. Then the loading of Ce6 on SWCNTs couple HA was achieved by non-covalent π-π interaction techniques. The newly synthesised nanobiocomposite (SWCNTs-HA-Ce6) effectively targeted the CD44 receptors in the CCSCs. The physicochemical characterisation of synthesised SWCNTs-HA-Ce6 was analysed using ultraviolet Visible (UV-Vis) spectrophotometer, Fourier transformation infrared spectroscopy (FTIR), particle size and zeta potential analysis using DLS method, morphological evaluation by high-resolution transmission electron microscope (HR-TEM) and X-ray diffraction (XRD).

The dispersibility of SWCNTs-HA-Ce6 was significantly improved than SWCNTs alone due to the coupling of the biopolymer HA. CCSCs were isolated using the magnetic bead antigen antibody technique from Caco-2 colon cancer cell lines. SWCNTs coupled HA and coated with Ce6 were successfully synthesized and the results of physicochemical characterisation of SWCNTs-HA-Ce6 showed positive outcomes for cancer

PDT applications. The maximum absorbance peak for Ce6 was measured with UV- vis spectrophotometer and it appeared at two different wavelengths, 664 nm and 404 nm. The surface chemistry and chemical bond shifting of the synthesised SWCNTs-HA-Ce6 were analysed using FTIR. Crystallinity and purity of the samples were analysed using XRD-write out first time used, and the results were closely corresponding to the planes of graphite's, according to the JCPDS #751621. The particle size and surface charge of the synthesised SWCNTs-HA-Ce6 were analysed using dynamic laser scattering (DLS) method and it showed approximately 203 ± 6.6 nm and -18.9±1 mV, respectively. Structural morphology of synthesised SWCNTs-HA-Ce6 were analysed using HR-TEM, it showed the tubular structure of nanotubes, and the shape was consistently maintained without breaking until the final product.

The stability of the synthesized SWCNTs-HA-Ce6 were tested against both physiological pH 7.4 and intracellular pH 5.5 and showed significant stability in both conditions. This study revealed enhanced stability of Ce6 on SWCNTs-HA. Ce6 loading percentage was achieved at 70% on SWCNTs-HA and *in vitro* Ce6 release study showed the slow and sustained release of Ce6 at pH 7.4 & 5.5. The results obtained from *in vitro* release studies were fitted with different mathematical equations (zero order model, first order model, Higuchi model and Korsmeyer-Peppas model). It indicated that the Ce6 release pattern from the SWCNTs-HA-Ce6 followed the Higuchi kinetic release and the release mechanism followed the Korsmeyer-Peppas equation. The Ce6 release mechanism was followed the Non-Fickian transport mechanism and it was controlled by more than one process, it may be the coupling of fickian diffusion and polymer matrix relaxation.

Intracellular localisation of synthesised SWCNTs-HA-Ce6 molecules showed more fluorescence intensity in the mitochondrial region of Caco-2 cells and comparatively very less fluorescence intensity of SWCNTs-HA-Ce6 in lysosomes and the nuclei region. CCSCs were isolated from Caco-2 cancer cell lines by magnetic bead method and morphological

characterisation of isolated CCSCs indicated spheroid formation. It was further confirmed by both flow cytometry analysis and immunofluorescence.

The effect of PDT on isolated CCSCs were studied at 660 nm laser irradiation with two different laser fluences of 5 and 10 J/cm^2 at 24 and 48 h. In 10 J/cm^2, the cytotoxicity results of SWCNTs-HA-Ce6 on CCSCs showed 86.7% at 48 h and 74.8 % at 24 h of incubation. The metabolic activity of the isolated CCSCs was tested before and after treatment by evaluating the ATP luminescence signal produced by viable cells. When the metabolic rate or ATP production in cells are low, it leads to inactivity and pronounced cell death. The results of 0, 5 and 10 J/cm^2 laser fluences were compared and 10 J/cm^2 showed more promising outcomes after 24 and 48 h. ROS production of CCSCs after laser irradiation were analysed and the fluorescence intensity of Cy5 showed its highest peak at 10 J/cm^2 compared to 5 J/cm^2. The stages of cell apoptosis were analysed using FITC Annexin V and PI stain using 0, 5 and 10 J/cm^2 at 24 and 48 h. There were less apoptotic cells seen in 0 and 5 J/cm^2, whereas 10 J/cm^2 showed an increased range of early and late apoptotic counts. The study suggested that there was prominent cell death using 10 J/cm^2 compared to both 0 and 5 J/cm^2.

Therefore, the combined effect of PDT and SWCNTs-HA-Ce6 showed increased cytotoxic and cell apoptosis at a laser fluence of 10 J/cm^2 at 48 h. In conclusion, the combined effect of photodynamic therapy and synthesised Ce6 loaded SWCNTs-HA-Ce6 on CCSCs are effective inducers of cell death and a promising new cancer therapy.

DEDICATION

To my beloved husband

Dr D Sathish Sundar

&

my precious little boy

Maruthasimhan

To my successor's mom, dad and all my family members.

ACKNOWLEDGEMENTS

I thank my supervisor and mentor, Prof Heidi Abrahamse for her assistance, guidance, motivation, incentive support during difficult times. Without her persistent help, the goal of this project would not have succeeded.

Thanks to Prof Nicolette Houreld, for your tireless assistance and advice whenever needed. Thank you so much for the personal and professional guidance.

Thanks to Dr Sathish Sundar for guidance, continuous support, and impactful contribution to this project. Sincere, thanks to all Laser Research Centre staffs for their kind help and support.

Thanks to Dr Anine Crous for your encouragements and support whenever needed. Thanks to all my fellow research colleagues for your enthusiasm, may you all never get weary of helping others.

Thanks to Ms Christine Fernandez, for your timely help and tireless assistance.

This research was supported by the South African Research Chairs Initiative of the Department of Science and Technology and National Research Foundation of South Africa (SARChI/NRF-DST) (Grant No 98337).

The author sincerely thanks the University of Johannesburg and the National Laser Centre for their facilities and laser equipment. Thanks to all the staffs at the National Laser Centre for their assistance, guidance and setting up of the lasers.

To my family, for all their continuous support, love and for their belief in me.

Most of all my friends who put up with me through all this time, giving me encouragement and confidence at tough situation.

Thank you to the department of Applied Chemistry and spectrum laboratory at the University of Johannesburg for the use of their specialised equipment.

TABLE OF CONTENTS

LIST OF FIGURES

LIST OF TABLES

LIST OF SYMBOLS

CO_2	Carbon Dioxide
cm	Centimetre
cm^{-1}	Centimetre inverse
Da	Dalton
°C	Degree Celsius
ddH2O	Double-Distilled Water
eV	Electron Volt
Ex/Em	Excitation/ Emission wavelength (nm)
h	Hours
[IC50]	Inhibitory concentration of 50 %
J/cm^2	Joules per Centimetre Squared
J mol−1	Joules per moles
kV	Kilovolt
µg	Microgram
µl	Microlitre
µM	Micromolar
mA	Milliampere
mg	Milligram
ml	Millilitre
mm	Millimetre
mM	Millimolar
mW	Milliwatt
min	Minutes
O_2	Molecular Oxygen
nm	Nano Meter
nM	Nanomolar

ppm	Parts per Million
%	Percent
pH	Potential of Hydrogen
®	Registered
rpm	Revolutions per Minute
$^{1}O_{2}$	Singlet Oxygen
™	Trademark
$^{3}O_{2}$	Triplet Oxygen

LIST OF ABBREVATIONS

4′,6-diamidino-2-phenylindole	DAPI
Adenosine triphosphate	ATP
ATP-binding cassette	ABC
Bovine serum albumin	BSA
Cancer association of South Africa	CANSA
Cancer stem cells	CSCs
Carbon nanotubes	CNTs
Chlorin e6	Ce6
Cluster of differentiation	CD
Colon cancer stem cells	CCSCs
Colorectal cancer	CRC
Cyanine	Cy5
Dimethyl formamide	DMF
Double stranded Nucleic acid	DNA
Double walled carbon nanotubes	DWCNTs
Dulbecco's modified eagle's medium	DMEM
Dynamic laser scattering	DLS
Dynamic light scattering	DLS
Epidermal growth factor	EGFR
Equation	Eq
European medicines agency	EMA
Extra	Etc
Fluorescein isothiocyanate	FITC
Foetal bovine serum	FBS
Food and drug administration	FDA
Fourier transmission electron microscope	FTIR
Fourier transmittance infra-red	FTIR
Hank's balanced salt solution	HBSS

Hedgehog	Hh
High resolution-transmission electron microscope	HR-TEM
Human papillomavirus	HPV
Hyaluronic acid	HA
Immunofluorescence	IFL
Multiwalled carbon nanotubes	MWCNTs
Nanobiocomposite	SWCNTs-HA-Ce6
N-ethylcarbodiimde hydrochloride- N-hydroxysuccinimide	EDC HCL-NHS
Nitric acid	HNO_3
Phosphate buffer solution	PBS
Photo biomodulation	PBM
Photo thermal therapy	PTT
Photodynamic therapy	PDT
Photosensitizers	PS
Phycoerythrin	PE
Polyethylene glycol	PEG
Potassium bromide	KBr
Potential of hydrogen	pH
Propidium iodide	PI
Psoralen and Ultraviolet A	PUVA
Radiofrequency ablation	RFA
Reactive oxygen species	ROS
Single walled carbon nanotubes	SWCNTs
Stem cells	SCs
Transmission electron microscope	TEM
Ultraviolet	UV
World health organisation	WHO
X-ray diffraction	XRD
X-ray diffraction	XRD

THE USE OF BIOPOLYMER FUNCTIONALIZED SINGLE WALLED CARBON NANOTUBES FOR EFFECTIVE TARGETED PHOTODYNAMIC THERAPY OF COLON CANCER STEM CELLS

CHAPTER 1 INTRODUCTION

1.1. Background

Cancer is a major burden on global health and in South Africa. Worldwide large populations are affected, and mortality rate is high, lack of excise, food habits, obesity, Ultraviolet (UV) radiation, genetic disorder are the main causes of cancer (Anand et al., 2008). Colorectal cancer (CRC) is the third most common cancer diagnosed in men and women, and if the CRC metastasizes to other parts of the body, the patient's 5-year survival rate is 15% (Rebecca et al., 2019).

Photodynamic therapy (PDT) is a relatively innovative and emerging technique to treating cancer, which involves three sources: light source such as laser (Light amplification by stimulated emission of radiation), photosensitizers (PS) and reactive oxygen species (ROS). When the PS molecule is subjected to target cells and then irradiated at a specific wavelength, it stimulates the production and activation of a singlet oxygen that leads to cell necrosis or apoptosis (Moan et al., 2003). PDT successfully treats various medical field such as dermatology, urology, gynaecology and oncology (Kharkwal et al., 2011; Sperandio et al., 2013; Luo et al., 2017).

Stem cells (SCs) are referred to as pluripotent, multipotent or unipotent, self-renewing cells, and are broadly classified into two types: embryonic stem cells and adult stem cells based on their characteristics and origin (Orlic et al., 2002). Cancer stem cells (CSCs) are characterised by self-renewal and asymmetrical division properties and the ability to form tumour cells with different phenotypes (Adams et al., 2008). CSCs were present in most types of cancer, including CRC, breast, brain, melanoma, leukemia and liver cancer (Phi et al., 2018; Batlle et al., 2017).

Nanotechnology deals with nanosized particles for innovative applications in a different field, nanomedicine is one of the applications specifically involved in drug delivery, targeting, diagnostics, imaging and regenerative medicine (Alexiou et al., 2015). Carbon nanotubes (CNTs) are nanosized hollow cylindrical structured tubes, classified into three types: single walled carbon nanotubes (SWCNTs), double walled carbon nanotubes (DWCNTs) and multi-walled carbon

nanotubes (MWCNTs). SWCNTs are monolayered graphite sheet rolled into the tubular structure between 0.2-3 nm in diameter, wide application in the fields such as biomedical, nanocarrier, imaging (Baughman et al., 2002). Pristine CNTs are generally toxic to the normal cells, and it often need surface modification with biological compounds. The biodistribution of CNTs are excellent when coupled with long polymers or biological substances. SWCNTs are the best nanocarriers in terms of high surface area, biological distribution, biocompatibility, and enter in and out activity on the cells (Ali-Boucetta et al., 2013).

1.2. Problem Statement

In South Africa, CRC is the second most common cancer in men and third most common cancer in women, according to the reports published by cancer association of South Africa (CANSA, 2019). Currently available cancer treatments are chemotherapy, radiotherapy, monoclonal antibodies immunotherapy and surgery, while present therapies have severe side effects such as killing healthy cells, non-specificity and poor bioavailability. Scientists are optimistic about the potential of nanomaterials to increase the bioavailability of the drug by targeting cancer cells (Badea et al., 2020).

Cancer stem cells are small populations of cells that resist chemotherapy and then regenerate into tumours, leading to the failure of cancer treatment (Mansoori et al., 2017). Recent studies have shown that a group of cells that begin initiating the tumour occurrence and recurrence after treatment commonly referred to as cancer stem cells. Researchers are now focusing on targeting the heart of cancer named as CSCs, which will completely eradicate the tumour from the affected organs.

In the nanobiocomposite synthesis for drug delivery system, the main issues are solubility (hydrophobic and hydrophilic nature of the nanoparticles), dispersion of particles, cell targeting, engulfment of cells, drug release in target cells, stability of the nanobiocomposite. The size of the nanoparticles also plays an important role in transporting the drug to cancer cells (Patra et al., 2018). Nanobiocomposite should be designed and integrated to target the CSCs based on the criteria mentioned above.

The combination of photodynamic therapy and nanomedicine is a novel emerging treatment that target and kills the CSCs to destroy cancer from affected organs. The novel application of PDT and SWCNTs nanobiocomposite to eradicate CCSCs for the treatment of colon cancer. This approach will significantly reduce the side effects, recurrences, metastatic effect and reduce the cancer death rate.

1.3. Specific Aim

Isolation of CCSCs from Caco-2 colon cancer cell lines using surface markers CD 44, CD133 and CD24. Isolated cells were cultured in ultra-low attachment flasks to maintain the stemness for further studies. In order to evaluate the effects of PDT and nanobiocomposite (SWCNTs functionalised HA and loaded photosensitizers Ce6) on CCSCs, the synthesised nanobiocomposite were incorporated into the isolated CCSCs and treated with PDT at 660 nm.

The following objectives were achieved:

- Synthesised HA functionalized SWCNTs loaded with chlorin e6.
- The physicochemical characterisation of the newly synthesised nanobiocomposite analysed using UV spectrophotometer, Fourier transmission electron microscope (FTIR), X-ray diffraction (XRD), particle size analysis and zeta potential (DLS method), High resolution-transmission electron microscope (HR-TEM).
- The photosensitizer stability analysis using different pH conditions.
- *In vitro* photosensitizer release study using dialysis technique.
- Isolation of Caco-2 CCSCs using CD133, CD44, CD24 markers by magnetic bead method.
- Characterisation of isolated CCSCs using immunofluorescence microscopy technique and flow cytometry analysis.
- The anticancer activity of the newly synthesised nanobiocomposite under PDT treatment on CCSCs.
- The Nuclear damage of the CCSCs under PDT treatment analysed using Hoechst/propidium iodide staining.
- The oxidative stress of the CCSCs under PDT treatment analysed using reactive oxygen species (ROS) analysis using intracellular ROS assay imaging under live microscope.

UNIVERSITY
OF
JOHANNESBURG

CHAPTER 2 LITERATURE REVIEW

2.1. Cancer

The term cancer refers to a deadly disease in the present era. Globally, the burden of cancer affects every individual family due to physical, emotional and financial crisis. Cancer, a group of mutated cells in an uncontrollable growth condition, forms a tumour at a specific site and spreads throughout the body. The metastasizing process is the leading cause of death for cancer. Other names for cancer include malignant tumour, neoplasm, lymphoma etc (Lopez-Lazaro et al., 2016; Martin et al., 2013). Worldwide, cancer is the second leading cause of death, around 9.6 million deaths or one in six deaths in 2018, according to a WHO report (WHO, 2018).

Cancer is caused by genetical disorder, physical inactivation, poor diet, smoking, alcohol & tobacco consumption, obesity, ultraviolet (UV) rays, constipation, stress in modern habits and certain infections also causing cancer like Human papillomavirus (HPV), Epstein-Barr virus, Hepatitis B and C viruses (Bray et al., 2018). The physical, chemical and biological cause of cancer are explained in Figure 2.1.

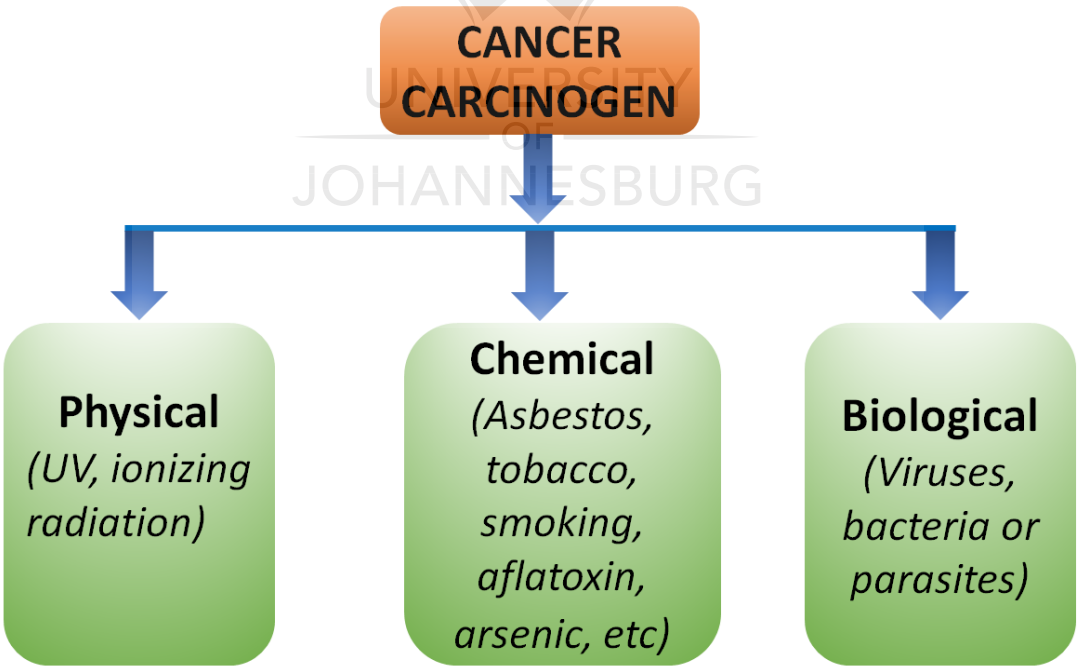

Figure 2. 1 Three different types of cancer carcinogen-physical, chemical and biological cause.

Metastasis, invasion and recurrence are the major issue in the cancer treatment, in the process of metastasis, the malignant phenotype must be obtained to separate the tumour cell from the primary tissue and passes through the extracellular matrix, basal membrane and intravasate into circulation of the body (Spano et al., 2012). Some examples of metastatic sites for specific cancers are listed in Table 2.1. Cancer invasion involves in migration of cancer cells through the cellular matrix and spreads into neighbouring tissues. After treatment or removal of tumour, few subpopulation cells survive and reach metastasis and invasion (Darvishi et al., 2020).

Table 2. 1 Few lists of primary tumour and metastatic sites in the body (Martin et al., 2013).

Primary tumour	Metastatic sites
Colorectal cancer	Liver and lung
Lung cancer	Brain, bone, adrenal gland and liver
Breast cancer	Bone, lungs, liver and brain
Prostate cancer	Bone
Skin melanoma	Lung, brain, skin and liver

Local recurrence after surgical resection is a foremost complication in the treatment of cancer, and it plays major role in decreased survival and quality of life for patients. Drug resistance cancer cells can quickly form tumours in distant organs. Most researchers find that recurrence of cancer due to the cancer stem-like cells are resistant to all treatments (Hiller et al., 2018; Meyerhardt et al., 2006).The term cancer is a main challenge for clinicians and researchers who interested in the field of diagnosis and treatment.

In the current scenario many unknown types of cancer are growing in the human body, researchers and doctors are naming the cancer based on the type of cell, the specific organ that grows the tumour, and the type of gene. The well-known

types of cancer are listed in Figure 2.2. The most common types of cancer in men are lung, prostate, colorectal, liver & stomach and the most common types of cancer in women are breast, colorectal, lung, thyroid and cervical cancer (Bray et al., 2018).

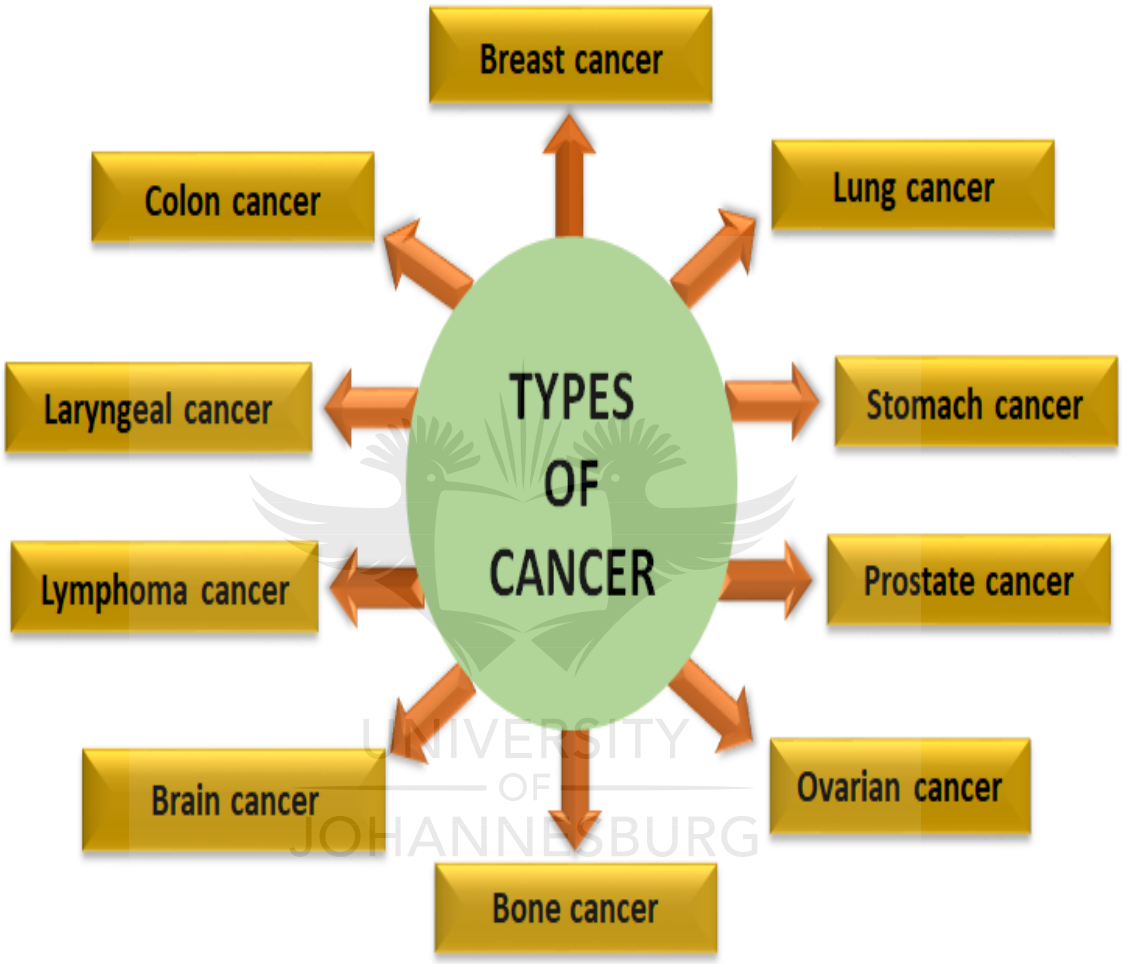

Figure 2. 2 Different types of cancer.

2.1.1. Colorectal cancer

Colorectal cancer (CRC) is also known as bowel cancer or colon cancer or rectal cancer. Colon cancer treatment leads to failures due to the metastasis and invasion (Zheng et al., 2014). The main cause for the CRC accretion of genetic and epigenetic alterations, it forms additional layer of complexity to induce CRC (Valastyan et al., 2011). The polyp (abnormal or noncancerous growth of tissue) grows slowly over a long period of time in the inner parts of colon or rectum

eventually forms a tumour in a region referred to as CRC and later stage it has capable of spreading and growing to the nearby organs through lymph and blood stream. CRC is very difficult to diagnose in the early stages of tumour (Marley et al., 2016). The structure of colon and tumour in the colon region is illustrated in the Figure 2.3.

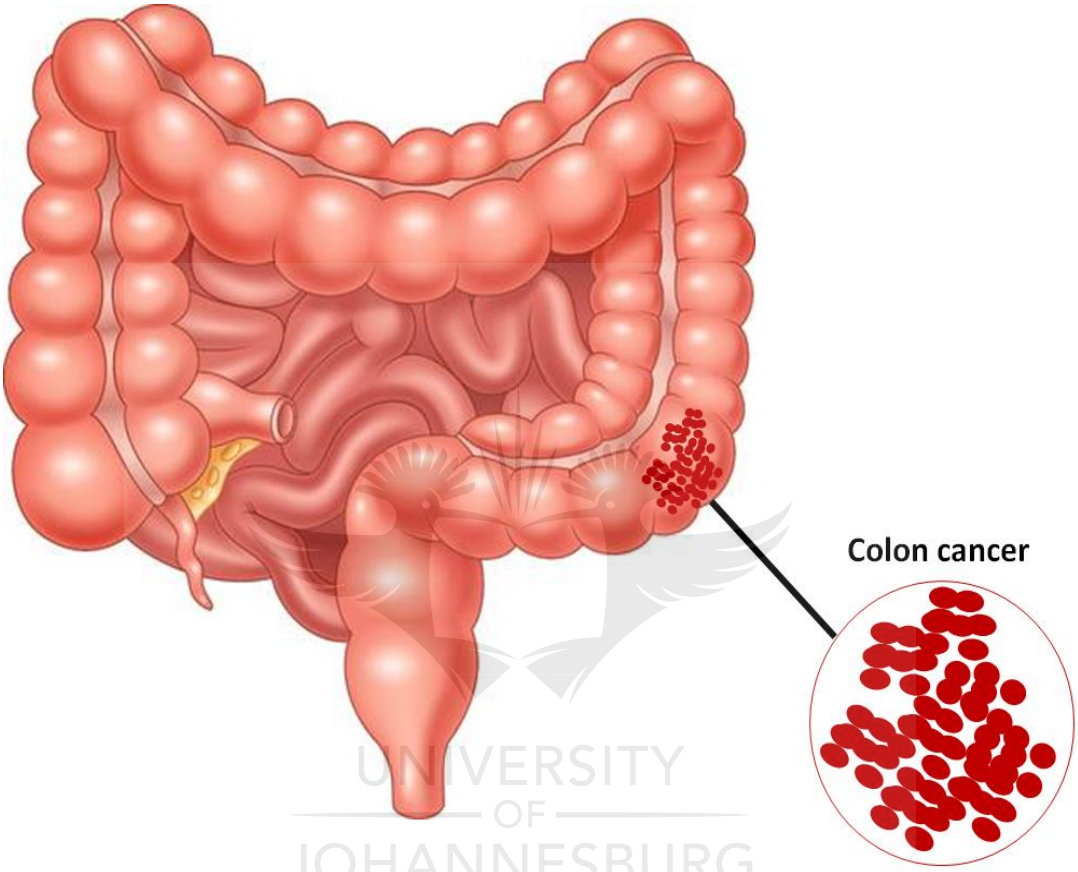

Figure 2. 3 Structure of colon and tumour present on the walls of colon.

In modern culture, changes in their daily habits can lead to the risk of CRC such as poor diet (Boyle et al., 2000) (high fat consumption and low fibres), lack of exercise, tobacco usage, alcohol consumption (Bishehsari et al., 2014), age factor (Raycraft et al., 2019), obesity (Ding et al., 2020), Crohn's disease and ulcerative colitis in colon (Pacal et al., 2020). Common symptoms of CRC constipation, changes in stool colour & shape (narrowed stool), diarrhoea, blood in the stool, abdominal cramps and pain, fatigue, vomiting and appetite loss (Verhaar et al., 2015).

Based on the tumour region CRCs are classified as carcinoid tumours (cancer cells grow in the hormone producing intestinal cell region), gastrointestinal tumour (tumours in the cajal region), sarcomas (colorectal walls and stromal region) (Chelliah et al., 2019). The four stages of CRC listed in the table 2.2.

Table 2. 2 Different stages of colorectal cancer (Chelliah et al., 2019).

CRC	Commonly known	Description	Symptoms
Stage 0	Carcinoma in-situ	Abnormal cells are located on the inner lining of colon or rectum	No symptom
Stage 1	Carcinoma penetration	Cancer cells penetrate the lining or mucous into the muscles of colon or rectum	Constipation, diarrhoea, abdominal pain
Stage 2	Early stage	Cancer cells spreads to nearby tissues through the walls of colon or rectum	Blood in rectum or stool, abdominal cramps
Stage 3	Late stage	Cancer cells moved to lymph nodes	Excessive fatigue, weight loss, vomiting, bowel moments
Stage 4	Late stage	Cancer cells moved to distant organs liver and lungs.	Jaundice, swelling of hands and legs, blurry vision, bone fractures, breathing difficulties, chronic headache

2.1.2. Statistics report of colon cancer in South Africa

South Africa is a modern and westernized cultured country and CRC ranks in the top five on the list of most diagnosed cancers (Bray et al., 2012; The World bank 2016). CRC is a second most common cancer among men and fourth most common cancer among women in South Africa (CANSA, 2010). Total population of South Africa around 57.78 million in the year 2018 and total cancer cases in the year 2018 was 107,467 cases, then death cases in 2018 was 57,373. The rate of CRC incidence was 6.5 % and the mortality was 6.4% from total number of cancer cases (WHO, 2020). Figure 2.4 shows the percentage of males and females affected by colon cancer in South Africa. The total population of South Africa was covered by four different races, and the percentage of colon cancer among them is given in Figure 2.5.

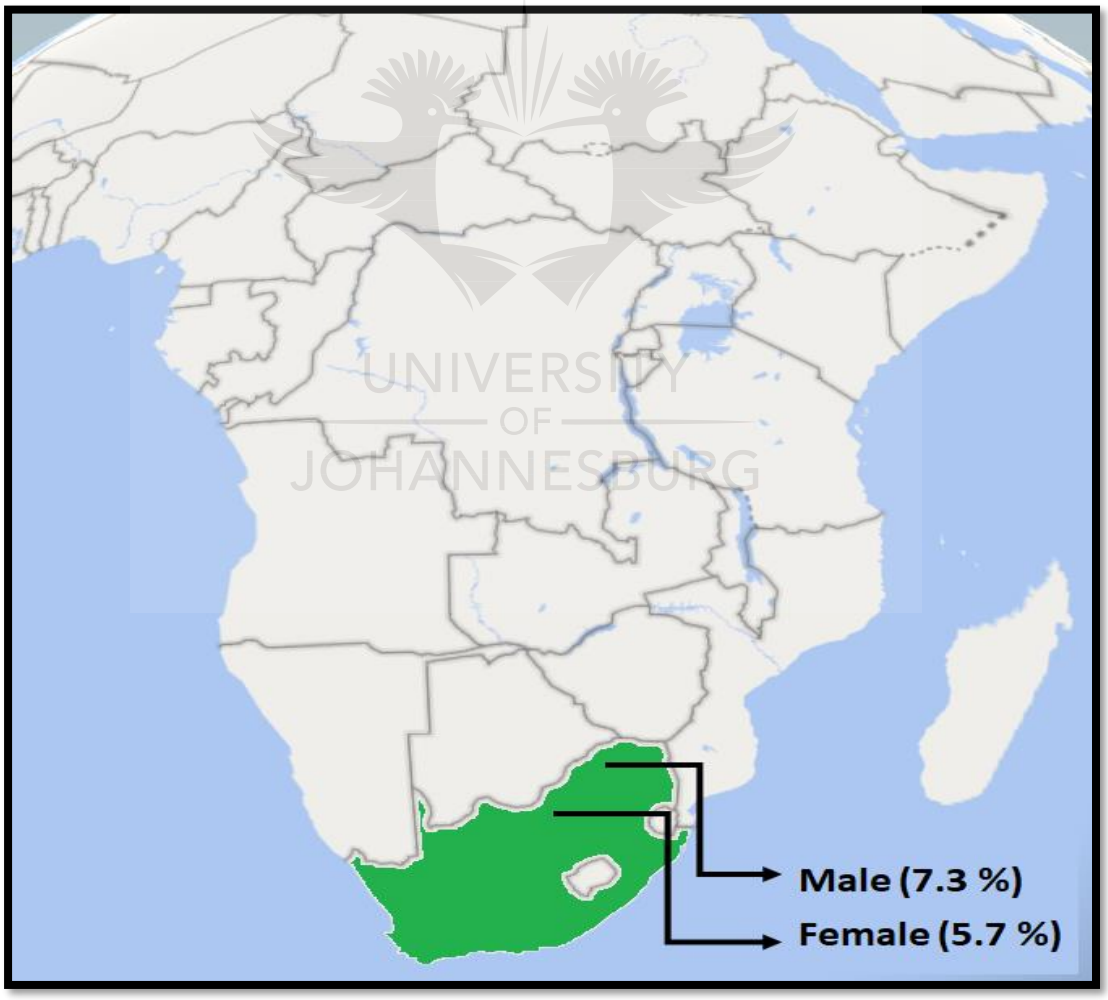

Figure 2. 4 Percentage of colon cancer affected male and female in South Africa.

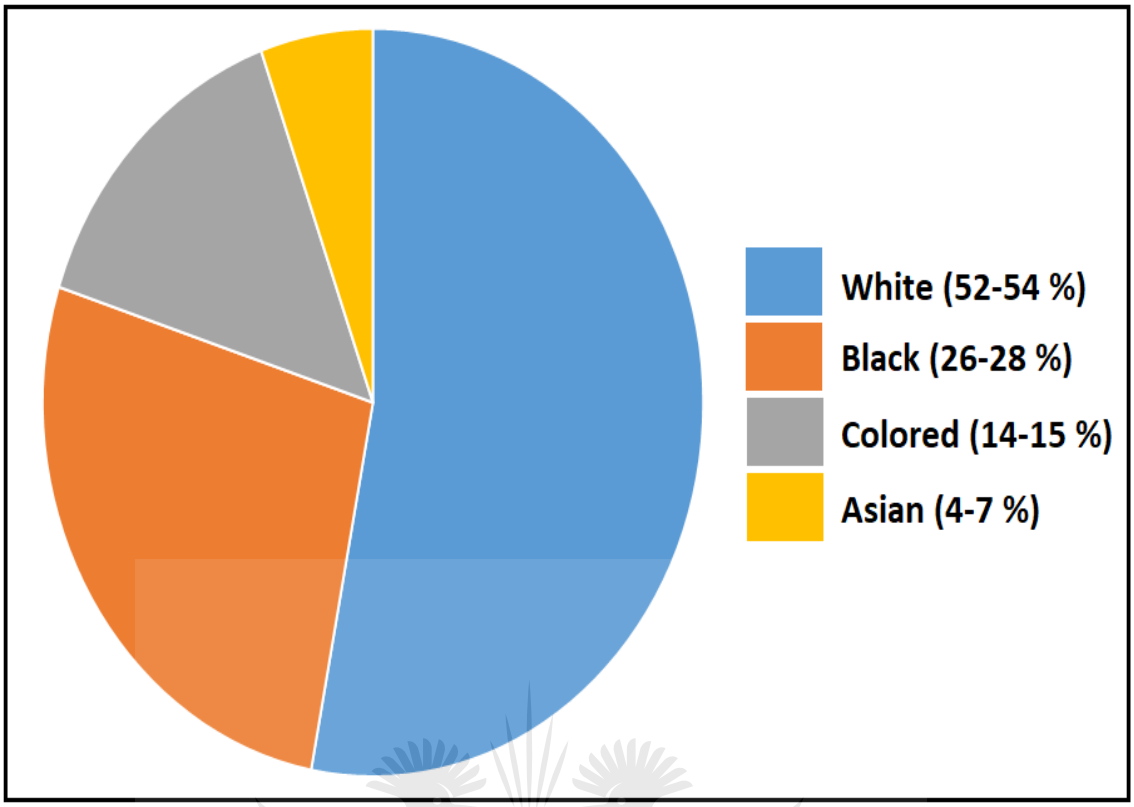

Figure 2. 5 Pie chart for percentage of people population affected by colon cancer in South Africa.

2.1.3. Present cancer treatments

To treat cancer patients, there are currently two ways of treatments available local and systematic treatments, which are mentioned in Figure 2.6. Local treatment such as surgery and radiation therapy involve treating the tumour without affecting any other parts of the body. Systematic treatment involves chemotherapy, immunotherapy, gene therapy using a drug that is administered orally or directly into the bloodstream and it reaches all over body and destroying the cancer cells (Bidram et al., 2019; Ventimiglia et al, 2019).

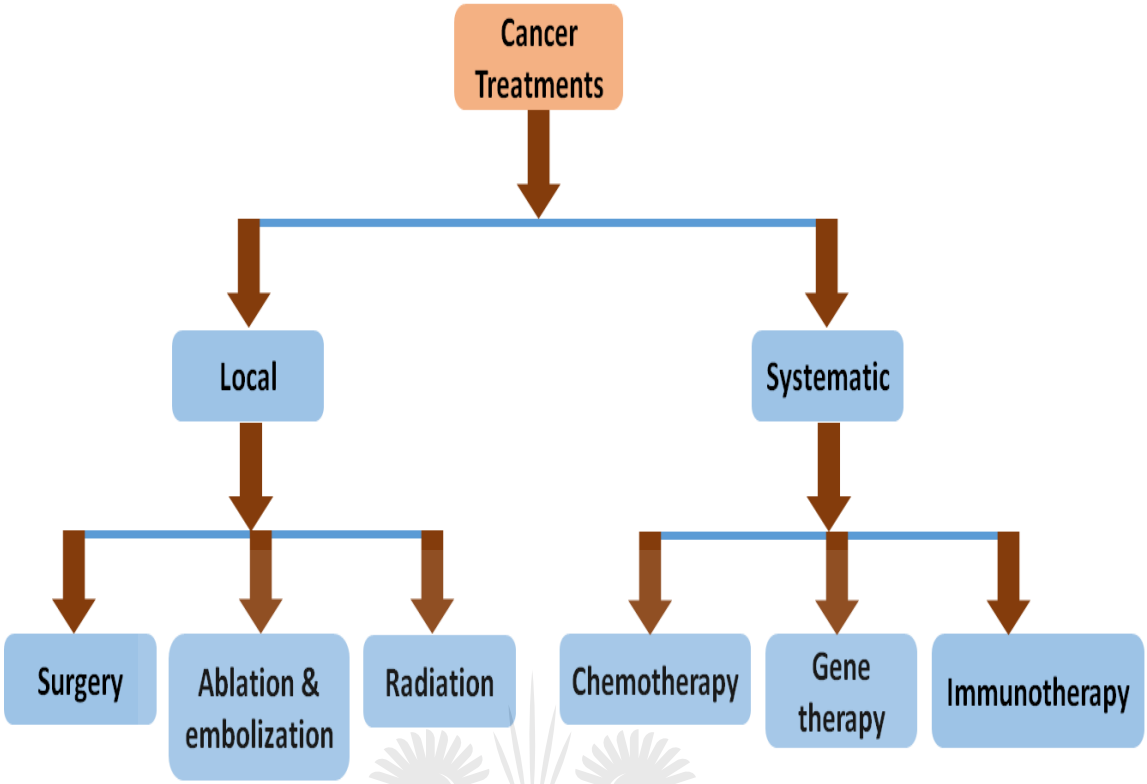

Figure 2. 6 Schematic diagram of cancer treatments.

CRC treatment involves laparoscopic surgery, colostomy for rectal cancer, radiofrequency ablation (RFA) or cryoablation if the tumour size was small or has reached metastatic stage. Chemotherapy and radiation therapy also using for CRC but have many side effects (Seligmann et al., 2020).

2.2. Stem Cells

2.2.1. Characteristics and types of stem cells

Stem cells are a group of cells must have the ability to differentiate and unlimited self-renewal to produce progeny exactly similar like parent cell. SCs plays an important role in every stages of body growth from embryo formation, pluripotent represents progenitors for development of tissues, SCs differentiate and develop every organs of the body. SCs are mainly characterised as self-renewal, differentiation, quiescence, migration, recreation of functional tissues (NIH, Stem cells 2008).

SCs can differentiate in two ways and it based on the different cell type and biological properties. Essentially, SCs describe cell development as “embryonic” and “adult” SCs, which classify these types based on the origin of cell production

Recently, researchers discovered how to turn differentiated adult cells into embryonic stem cells. The adult SCs are also known as somatic SCs found in the placenta, fetus, and umbilical cord (Bajada et al, 2008).

SCs are classified into two types based on their biological properties: pluripotent and multipotent SCs. Pluripotent SCs are capable of differentiating in all types of cells which are present only very short time in the embryo before differentiation. Multipotent SCs are specialized cells of the tissues in the body, the cells of germ line, that multiply themselves into restricted specialized cells (Molfsky et al., 2004). The derivation of SCs are explained in the Figure 2.7.

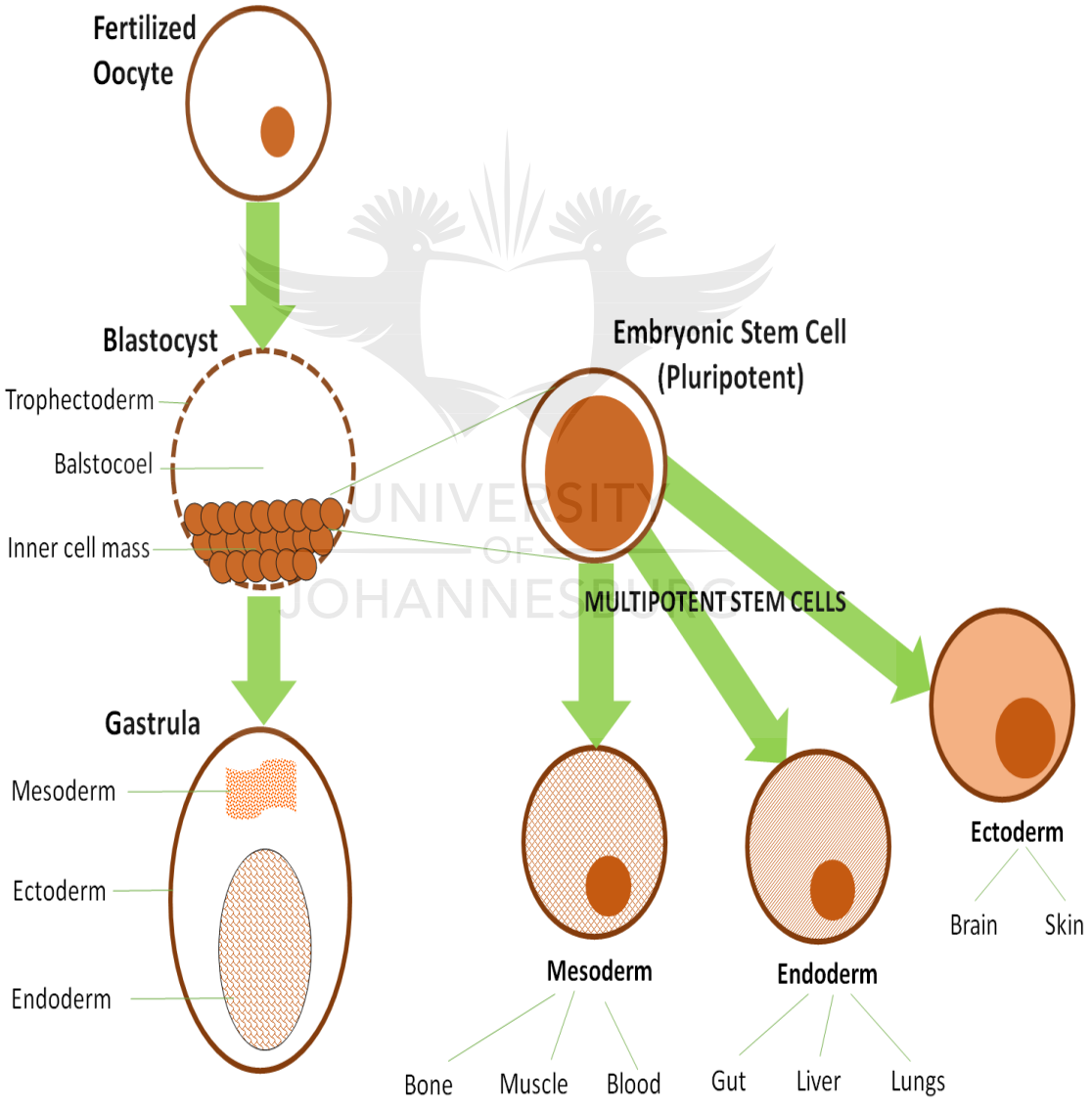

Figure 2. 7 Derivation of stem cells from fertilized oocyte (Adapted from Biehl and Russel 2009).

2.2.2. Cancer stem cells

2.2.2.1. Theories of cancer stem cells

In recent years, cancer therapies have faced a serious failure due to the recurrence of the tumour. The researchers found that a group of cells resisted chemo drugs and regenerated the tumour rapidly, with these cells having the properties of stem cells with the ability of forming tumours called cancer stem cells. The first CSCs were identified in solid tumours of human breast cancer. The small population of human breast cancer cells were administered in immune-compromised mice for tumour formation. CSCs have been positively identified in and isolated from various human solid tumours including colon, pancreatic, head & neck, cervical and brain cancer.

CSCs similar to normal SCs homogenous and heterogenous division concept. CSCs can divide both symmetrically producing two daughter CSCs and asymmetrically producing different daughter cells (Santoro et al., 2016). Three important criteria of CSCs in solid tumours are:

i. Not all the cancer cells CSCs, only small population of cancer cells have the ability to form tumours.
ii. The small population cells are identified by cell surface markers such as CD 133, CD 24, CD44, CD 90, Myc, KLF 4, ALDH, EPCAM etc.
iii. CSCs can form secondary tumour with full phenotypic heterogeneity of the primary tumour.

2.2.2.2. Cancer stem cell markers and pathways

In different types of cancer, cell surface markers will vary, and CSCs are identified based on markers. These cell surface markers are membrane proteins, specific to particular antibodies that helps to differentiate CSCs and non-CSCs population. Some CSCs markers, origins and functions are listed in table 2.3.

Table 2. 3 Cancer stem cell markers, origin and functions.

S.NO	CSCs markers	Origin and function	Expression in CSCs	Ref
1	CD133	Hematopoietic stem cells.	Breast, prostate, colon, glioma, liver, lung, ovary	(Grosse-Gehling et al., 2013; Irollo et al., 2013; Yin et al., 1997; Sundberg et al, 2009)
2	CD326	Cell adhesion, signal transduction	Colon, pancreas, Liver	(Li et al., 2007; Ng et al., 2010; Patriarca et al., 2012)
3	CD24	B cell proliferation	Breast, gastric, Pancreas	(Al-Hajj et al., 2003; Zhang et al, 2011)
4	CD44	Hyaluronic acid receptor	Breast, colon, liver, ovarian, pancreas, gastric	(Thapa et al., 2016; Lapidot et al., 2005; Zuk et al., 2002; Zoller et al., 2011)
5	CD49f	Cell adhesion	Glioma	(Yu et al., 2012; Lathia et al., 2010)
6	SSEA 3	hESC marker	Teratocarcinoma, Breast	(Thomson et al., 1998; Kuroda at al., 2010)
7	CD96	T cell-specific receptor	Leukemia	(Hosen et al., 2007)

The isolation and characterisation of CSCs depend on the cell surface antigen of respective cancer cells. Confirmation of CSCs by surface antigens is linked with their operational characteristics because of factors influencing their expression (Tirino et al., 2013).

Isolated small population of CSCs are clearly identify using low Hoechst 33342 dye staining, this stain eluding the dye by ATP-binding cassette (ABC) (Ozvegy-Laczka et al., 2005). ABC are transmembrane proteins that binds to adenosine triphosphate and hydrolyses, these proteins that acts as receptors and multidrug transporters that use ATP to discharge cell endogenous molecules and cytotoxic agents. Due to these mechanism CSCs are multidrug resistance and leads to failure of cancer treatment (Bleau et al., 2009). CSCs are also resistance to chemotherapy due to the enzyme aldehyde dehydrogenase oxidizing aldehydes, which converts retinol into retinoic acid (Russo et al., 1998).
CSCs are aggressive and uncontrolled cell division in tumour, pathway dysregulation of SCs leads to CSCs. Cell cycle and arrest mechanism are regulated by Wnt-β-catenin in SCs and self-renewal of SCs regulated by Notch pathway (Gedaly et al., 2014; Chiang et al., 2013). The Hedgehog signalling pathway was named after the origin of the polypeptide ligand and intercellular signalling molecule.

Importantly, three homologues have been identified in Hedgehog pathway, they are human's Hedgehog, desert Hedgehog, Indian Hedgehog and the most widely studied Sonic hedgehog (Rubin et al., 2006). The Sonic Hedgehog pathway involves in the activation of SCs to create different SC models, but in CSCs the signalling process of self-renewing genetic programs are activated by this mechanism (Visvader at al., 2012; Zhang et al., 2015). CSCs are resistance to all therapy due to activation of several signalling pathways, such as Notch, Wnt/β-catenin, TGF-β, Hh, RAS, PI3K/Akt/mTOR and JAK/STAT pathways (Islam et al.,2015). Mainly in colon cancer or bowel diseases, the inflammation in colon might be activated by Notch or Hedgehog signalling further expands to colon stem cells (Krok et al., 2004).

2.2.3. Colon cancer stem cells

The colon cancer stem cells (CCSCs) are derived from malignant transformation of normal tissue stem cells present in colon region or from dedifferentiation of matured cells (Friedmann- Morvinski et al., 2014). Recent studies suggest the existences of CCSCs or colon cancer initiating cells isolated from known colon cancer tumours. In human breast cancer, stem cells are isolated and identified using cell surface antigens in flow cytometry. This is corresponding to the tumorigenic phenotype of stem cells (Rubin et al., 2006).

In CCSCs are mainly identified on the basis of cell surface antigens. O'Brien et al., (2007) isolated CCSCs using CD133 markers from seven different primary colon cancers and ten different extracolonic or metastatic sites. The isolated tumorigenic cells were then injected into nonobese diabetic/severe combined immunodeficiency (NOD/SCID) mice. CD133+ cells are analysed on both tumour region and normal cells area. The tumour region ranged about 3.2-24.5% of CD133+ in tumour cells and the normal cells ranged about 0.4-2.1% (O'Brien et al., 2007).

To prove the pluripotent potential of CCSCs in their subpopulation, CD133 markers are used to identify and isolate the tumorigenic cells from colon cancer. These isolated cells were immortalized *in vitro* as floating colonies or tumour spheres and maintained in several passages. Then the CD133+ spheres mixed with CD133+ and CD133 populations, but only the CD133+ cells are tumorigenic (Ricci-Vitiani et al., 2007).

In CCSCs, the most familiar and cell surface marker was CD44 which plays role in cell and cell matrix interaction through its hyaluronic acid, involves in cell-adhesion and assemble the growth factors on the cell surface (Marhaba et al., 2004). CD44 variants isoforms roles are not completely understood, even though some are mediated in colon cancer metastasis (Du et al., 2008; Banky et al., 2012). CD44 receptor immunoprecipitated with ErbB tyrosine kinases family especially with epidermal growth factor receptor (EGFR) (Wobus et al., 2002).

Downstream signalling of CSCs via phosphor-inositol 3 kinase (PI3K)/AKT pathway mainly regulated by EGFR (Ma et al., 2013).

In 50-68% of tumour cells in CRC patients expressed CD24 antigens, and CD24 is a cell surface protein that is expressed in the outer region of the plasma membrane. The CD24 marker has some specific role in the immune system and central nervous system (Weichert et al., 2005; Choi et al., 2010). In the colon cancer, the CD24 positive side populations possess stemness or stem cell like properties (Ke et al., 2012). In this study, the isolation and characterisation of CCSCs is based on three markers CD133, CD44 and CD24.

2.3. Photodynamic Therapy

2.3.1. History of phototherapy

In ancient times, sunlight was used as a source to treat different diseases in many countries such as China, India and Egypt. From the 15th to the mid-19th century, people were treated for skin ailments following sun therapy, called heliotherapy. After the introduction of modern medicine people started forgetting about sun treatment (Grzybowski et al., 2016). In china, ancient medicine based on different colours for each disease and then sunlight for men and moonlight for women's (Needham et al., 1983). Indian way of treatment based on to apply the plant extract or oil (seed oil or ayurvedic oil) on the affected area and exposure to sunlight (Pathak et al., 1992). Modern phototherapy was looming in the field of biomedical to treat different diseases.

The first ultraviolet therapy was used to treat Lupus vulgaris by chemical ray's lamp, succeeded by Niels Ryberg Finsen who was named as father of ultraviolet therapy (Honisgsmann et al., 2013). In 19th Century slowly the treatment evolved into ultra vitalux lamp, fluorescent tubes (Wiskemann et al., 1963) and photochemotherapy psoralen and Ultraviolet A (PUVA) (Wolff et al., 1976). During 1980's, extra corporeal photochemotherapy (extracorporeal photopheresis, ECP) was termed as phototherapy, this technique was introduced to treat palliative of erythrodermic cutaneous T-cell lymphoma approved by FDA (Trautinger et al., 2006).

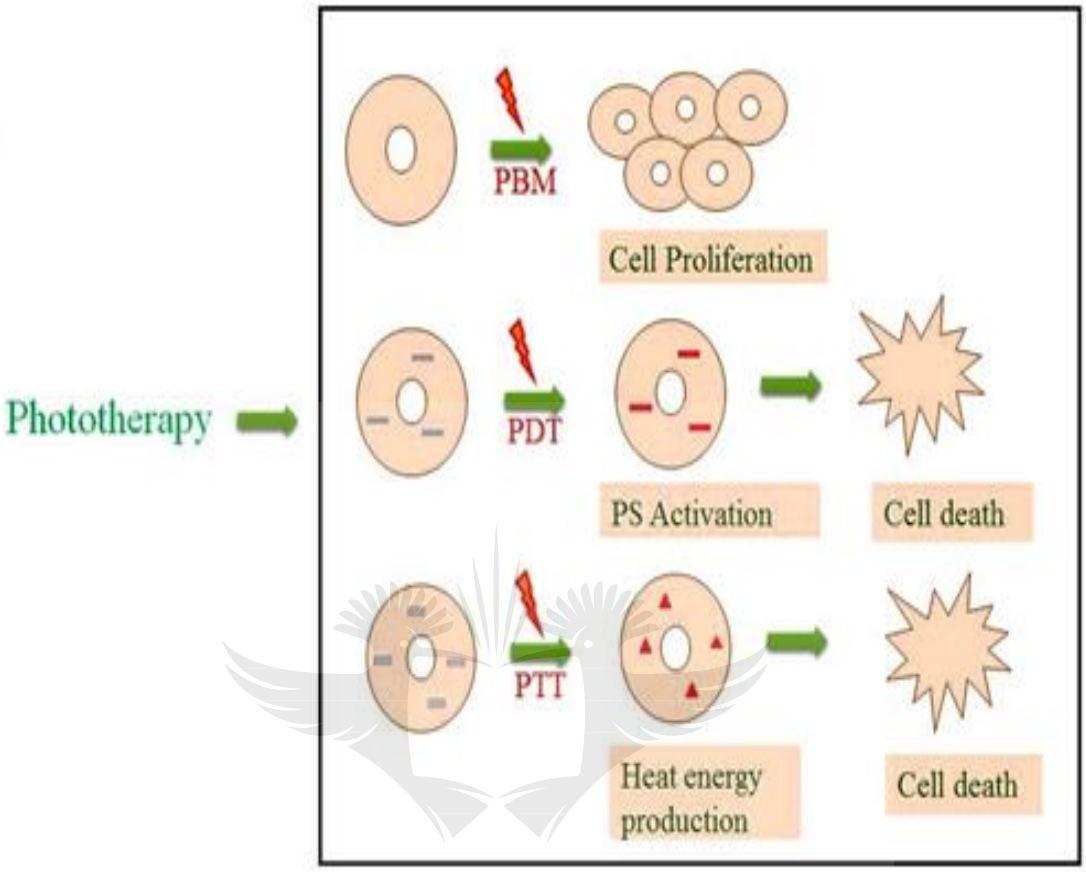

Figure 2. 8 Mechanism action of phototherapy. Photosensitizers, PBM- Photo biomodulation mechanism of light source on cells leads to cell proliferation. PDT- Photodynamic therapy mechanism of incorporation of PS into the cells with light source emission leading to PS molecule activation induces singlet oxygen production and cell death. PTT- Photothermal therapy mechanism of addition of nanomaterials, which has thermal property after the introduction of light source, produces heat energy leading to cell death. (Sundaram et al., 2020b).

Thus, phototherapy attracted research scientists and discovered enormous therapeutic techniques for various diseases. The phototherapy was mainly classified as photo biomodulation (PBM): the low-level light source at a particular wavelength applied into the cells it will stimulate or enhances the cells (Asgari et al., 2020), photodynamic therapy (PDT): the PS molecule in the ground state, when the molecule activated by light source reaches excited state and convert to triplet state by electron spinning. The triplet state interacts with surrounding oxygen molecule and produce ROS through type I and type II reaction (Eun et

al., 2016), and photothermal therapy (PTT): The particle (PS or nanoparticles) will be activated by the light source and produce thermal energy to destroy cells (Junqi et al., 2019). The mechanism action of phototherapy was shown in Figure 2.8.

2.3.2. Overview and Mechanism of photodynamic therapy

Photodynamic therapy is an emerging medical treatment and in-depth research is underway during this period to introduce new treatments for deadly diseases. This treatment deals with three major components light source, photosensitizers and singlet oxygen. When the light source emits at a specific wavelength to activate the PS molecule and it produce singlet oxygen in the cell then it leads to cell death, specifically cancer cells (Dolmans et al., 2003; Hopper et al., 2000).

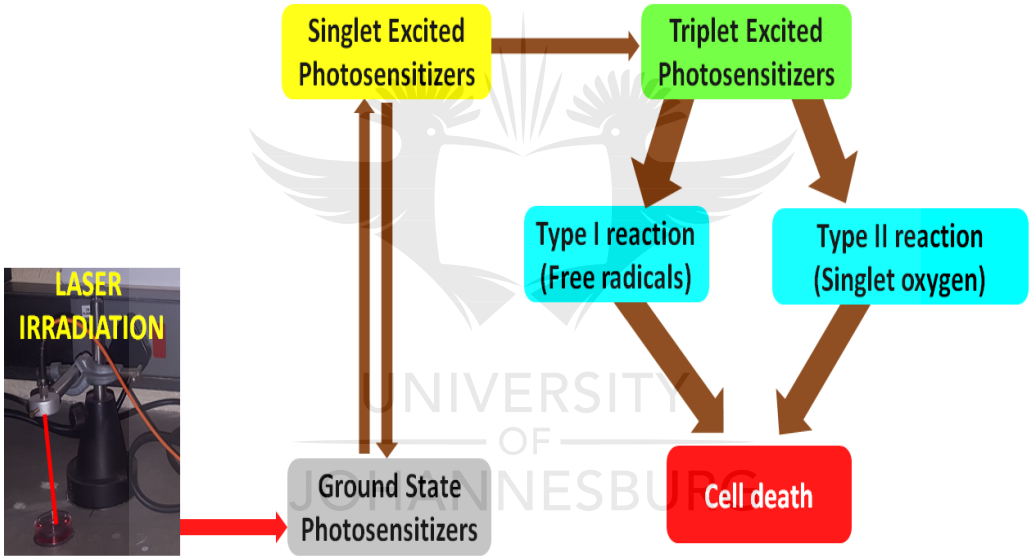

Figure 2. 9 Mechanism action of photosensitizers (PS), activation of PS molecule and its Type I and Type II reactions on cell.

In 1978, Thomas Dougherty and co-workers first and successfully tested PDT in clinical test to treat cancer in preclinical models at Rosewell park cancer institute (Patrice et al., 2003). PDT has more therapeutic efficacy and improving outcomes for cancer treatment in comparison to commercially available chemo and radiotherapy (Detty et al., 2004). The mechanism action of PDT involves two main types, both are based on production of oxygen molecules inside the cells shown in Figure 2.9.

Type I mechanism of PDT: The activated PS molecule in the excited triplet state can transfer energy from its surroundings to the biomolecules. The excited triplet PS molecule and the substrate tissue, an electron or hydrogen is transferred, which leads to the formation of free radicals and anions. These electrons interact with the oxygen molecule to produce reactive oxygen species (ROS) (Nowak-Stepniowska et al., 2013; Luksiene et al., 2003).

Type II mechanism of PDT: The activated PS molecule in the excited triplet state can transfer energy directly to the oxygen molecule (PS to O_2) it is possible to transfer because they have the same spins. Based on the ROS production level cause photodamage of proteins (Kessel et al., 2010), cell membrane destructions (Plaetzer et al., 2003), damage of fats and other molecules, damage of lysosomes or endoplasmic reticulum provoke autophagy in the targeted area or leads to the tumours cells apoptosis (Buytaert et al., 2007).

2.3.3. Role of photosensitizers in PDT

Photosensitizers are naturally derived or chemically formed compounds, that are highly sensitive to light source. These compounds are widely used in PDT, at specific wavelength PS molecules activated and reaches excited state and electron transfers to produce ROS leads to cytotoxicity (Allison et al., 2004). The minimum absorption wavelength range between 400-600 nm prevents excessive sensitivity from sunlight, 600-800 nm are the maximum absorption wavelength, above 800 nm will not provide excess oxygen production (Agostinis et al., 2011; Kou et al., 2017).

PS molecules are actively used in cancer therapy, often the PS molecules are derived from the tetrapyrrole compounds, which resembles haemoglobin due to the presence of protoporphyrin prosthetic group which can easily penetrate into cells (Abrahamse et al., 2016). PS compounds differs into three categories based on evolution such as first, second and third generation. In 1904, Oscar Raab explained to his professor Von Tappeiner that acridine dyes are killing protozoa under radiation (Allison et al., 2010). In 1970's commercially available PS molecule was introduced by Thomas Dougherty and colleagues.

In 1980's, second generation PS molecules based on the hematoporphyrin derivatives and synthetic PS, were used in clinical trials for anticancer activity (Yoon et al., 2013). These generation molecules penetrate deep into the tissues and produce more oxygen molecules; they are activated between 650-800 nm (Nowak-Stepniowska et al., 2013). Third generation PS molecules are derived and synthesised to treat cancer cells, they have high affinity to the tumour cells, will not affect the normal cells during PDT. Most of the molecules are metal based compounds (Kataoka et al., 2013). Some examples of porphyrinoids PS molecules and its structure were shown in Figure 2.10.

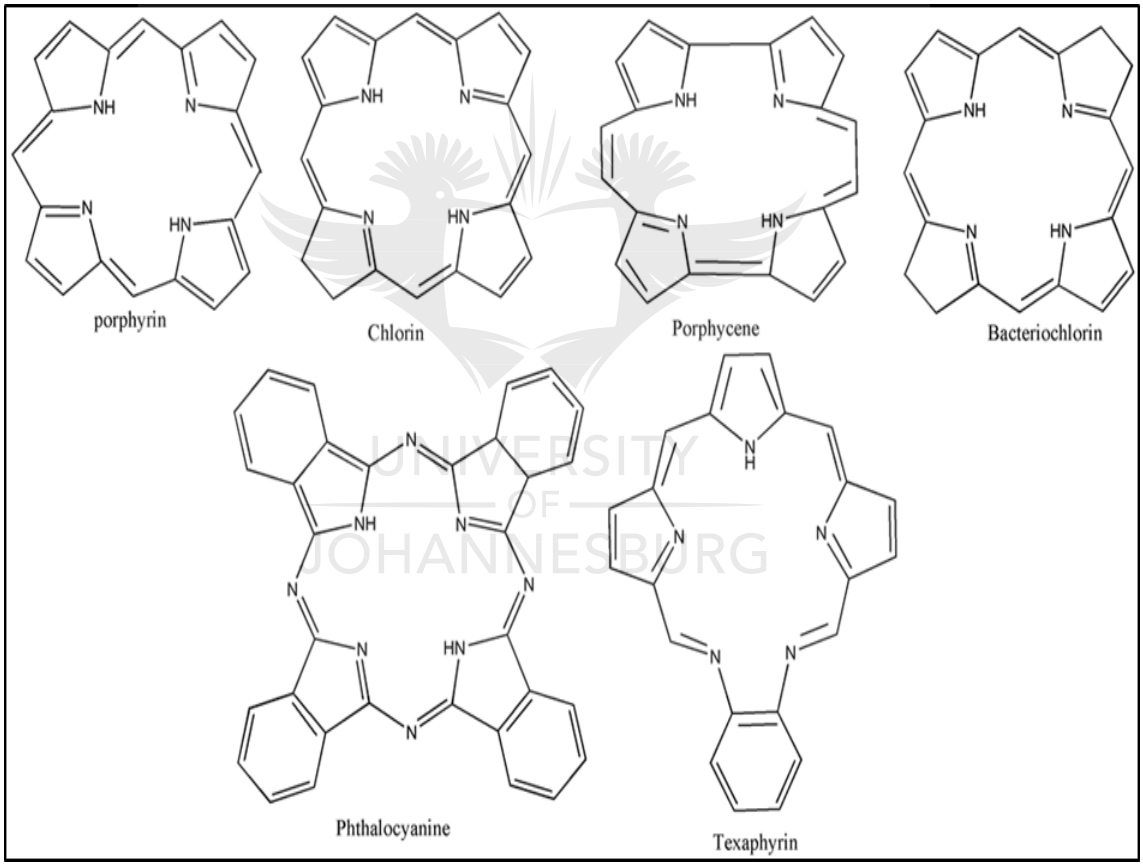

Figure 2. 10 Examples of Porphyrinoids photosensitizers: Porphyrin, Chlorin, Porphycene, Bacteriochlorin, Phthalocyanine, Texaphyrin. (Sundaram et al., 2020b).

2.3.3.1. Chlorin e6

Chlorin e6 also known as phytochlorin is a naturally derived chlorophyll-a derivative, and a second-generation PS molecule. It emerges as the prospective

PS for PDT, the main advantage of Ce6 are low toxicity, easy synthesis and production, fast and selective accumulation in target tissue, strong absorption wavelength between 650-670nm, high singlet oxygen quantum yield, and almost no side effects to skin (Juzeniene et al., 2009). The molecular formula and weight of the Ce6 are given in Table 2.4.

Chlorin e6 coupled with nanoparticles or any chemical compounds, there is no change in the chromophore, and it has significant photostability. Ce6 decorated with doxorubicin and encapsulated with chitosan tripolyphosphate nanoparticles to treat breast cancer cells near infra-red ranges. When PS molecules coupled with nanoparticles are aimed to improve their photo-controlled stability and photoactivity during cancer treatment (Anindita et al., 2019). In drug delivery systems, Ce6 molecules coupled with polymers improves the biocompatibility and bioavailability of Ce6 (Penelllche et al., 2019).

Table 2. 4 Molecular formula, weight and IUPAC name of Ce6 (Pubchem).

Name	**Chlorin e6**
Molecular formula	$C_{34}H_{36}N_4O_6$
Molecular weight	596.7 g/mol
IUPAC Name	(17S,18S)-18-(2-carboxyethyl)-20-(carboxymethyl)-12-ethenyl-7-ethyl-3,8,13,17-tetramethyl-17,18,22,23-tetrahydroporphyrin-2-carboxylic acid

2.4. Nanomedicine in Cancer

2.4.1. Introduction of nanomedicine

Nanomedicine is one of the applications of nanotechnology, mainly involves in diagnosis, imaging, therapeutics and regenerative medicine. Newly synthesised or chemically available nanosized particles are used in the medical fields. Over the past ten-years, most of the researchers have been attracted towards the

nanomedicine to treat cancer, diagnosis or imaging process (Fadeel et al., 2020; Alexiou et al., 2015). The applications of nanomedicine are listed in table 2.5.

Table 2. 5 Applications of nanomedicine.

S. No	Applications
1.	Nanoparticles in nanomedicine to target
2.	Nano valves for drug delivery
3.	Imaging
4.	Diagnosis
5.	DNA analysis
6.	Gene therapy
7.	Delivery system
8.	Cleaning robots
9.	Implant materials
10.	Wound healing bandages
11.	Body surveillance
12.	Artificial tissue and organs

Nanosized particles can be in the range of 1-100 nm, with polymers, dendrimers, liposomes, fullerene, silver and gold nanoparticles, metal based-nanoparticles, carbon nanotubes, graphene, micelles, quantum dots, silica, hydrogel etc. In clinical practice, the benefits of a nanoparticle-based drug delivery system, in comparison with commercially available drugs, include protecting from drug solubility and inactivation of drug or biodegradation(Bernabeu et al., 2017), prolonged circulation without rapidly clearing from body (Gabizon et al., 1994), targeting the specific site increases the concentration of drug to kill the tumours(Gabizon et al., 2003), possible to load multiple drug for synergistic effects on targeted area(Lancet et al., 2016), sustained and controlled release of drugs (Dou et al.,2017), enhancing therapeutic efficacy(Lyon et al., 2018). Currently available and approved nanomedicines are listed in table 2.6.

Table 2. 6 Clinically available and approved cancer nanomedicines.

Product	Drug	NPs size	Approved year	Manufactures	References
Doxil®	Doxorubicin	80-90 nm	FDA 1995 EMA 1996	Johnson & Johnson	(Harrington et al., 2000; Allen et al., 2004; Silverman et al., 2015)
Myocet®	Doxorubicin	150 nm	EMA 2000	Teva	(Swenson et al., 2001)
Abraxane PTX®	Paclitaxel	130 nm	FDA 2005 EMA 2009	Abraxis Biosciences	(peer et al., 2007)
Mepact®	mifamurtide	-	EMA 2009	Takeda pharmaceutical	(Ando et al., 2011)
marqibo®	Vincristine sulfate	115 nm	FDA 2012	Talon therapeutics	(Bedikian et al., 2006)
Onivyde®	Irinotecan	110 nm	FDA 2015 EMA 2016	Merrimack pharmaceutical	(Adiseshaiah et al., 2016)
Vyxeos®	Cytarabine and daunorubicin	100 nm	FDA 2017 EMA 2018	Jazz pharmaceutical	(Brunetti et al., 2017)
Apealea®	Paclitaxel	20-30 nm	EMA 2018	Oasmia pharmaceutical	(Borga et al., 2019)

*FDA-Food and drug administration *EMA-The European medicines agency

Very few drugs in nanomedicine research have been approved by the FDA and EMA, and some cancer nanomedicines have undergone stage 2 and 3 clinical trials (Mukai et al., 2016). Recently, researchers are focusing on carbon nanoparticles such as carbon nanotubes, graphene oxide, and fullerenes as drug carriers to destroy cancer cells (Liu et al., 2011).

2.4.2. Single walled carbon nanotubes

Carbon nanotubes are nanosized cylindrical tubes that are rolled up by graphene sheets where both ends are opened, and carbon atoms are exclusively arranged like a benzene ring. The structural representation of the CNTs are armchair, zigzag and chiral, with allotropic forms were both sp^2 planar and sp^3 cubic (Mehra et al., 2016). Based on the graphene sheets CNTs are classified as single walled carbon nanotubes (SWCNTs) sized between 1-3 nm in diameter and several micrometres in length. Double layered graphene sheets are rolled to form a nanotube named as double walled carbon nanotubes (DWCNTs). Multiple sheets that rolled up and formed a tube was named as multi walled carbon nanotube (MWCNT) sized between 1-3 nm inner diameter 2-100 nm outer diameter and a length ranging from 0.2 to several micrometres (Singh et al., 2012).

The synthesis method of CNTs includes the discharge method, chemical vapor deposition (CVD), and laser ablation techniques. Very few natural syntheses of CNTs techniques are available but there is no proper yield or standardized method (He et al., 2013) The purity of the CNT is achieved by the acid reflux method, air oxidation, and surfactant-based sonication to remove the extra metals. Purity is considered as an important criterion when it comes to biological applications (Donaldson et al., 2006).

Carbon nanotubes play a unique role as nanocarriers to deliver drugs, polymers, photosensitizers, and specific ligands to target siRNA and DNA. In cancer therapy, conventional treatment such as surgery, chemotherapy or radiotherapy has numerous side effects and does not completely get rid of the disease, due to poor targeting, bioavailability, and damaging organs (Hou et al., 2002). Many scientists are focusing on the CNTs combined biological delivery such as polymers, drugs, DNA, PS to target cancer cells (Lei et al., 2014).

SWCNTs have unique size & shape, large surface area and physicochemical properties that improve their quality as nanocarriers (Sajid et al., 2016). When SWCNTs flows in the body circulation and directly penetrate the cells but

MWCNTs enter via the endocytosis pathway (Mu et al., 2009). SWCNTs are act as a leading nanocarrier for loading different types of polymers, drugs, and photo drugs (Marangon et al., 2016). SWCNTs facilitates both covalent and non-covalent functionalization of targeting moieties that make them unique nano carriers in drug delivery systems (Tuncel et al., 2011). The carboxylated SWCNT shows excellent biocompatibility in cancer therapy (Tan et al., 2014).

2.4.3. Hyaluronic acid

Hyaluronic acid is a well-known natural polymer, also known as glycosaminoglycans belongs to a heteropolysaccharides group. HA is found in human bodies around the joints, umbilical cord, skin and connective tissues (Fallacara et al., 2018). HA also produced through microbial fermentation based on the oligosaccharides and molecular weight separated as commercial product (Tavianatou et al., 2019). HA molecule shows increased stability at physiological pH, which is a good quality to act as nanocarrier in drug delivery systems (Kobayashi et al., 1994).

The HA molecule widely exists in the extracellular matrix and primarily cleared by the lymphatic system (Choi et al., 2010). It has excellent properties of water solubility, biocompatibility, it is a biodegradable molecule, has high tumour targeting capacity and non-immune toxicity (Liu et al., 2011; Toole et al., 2002). Hyaluronic acid specifically recognized for its CD44 receptor and has been identified as a potent targeting ligand for tumours over expressing CD44, the CD44-HA interaction provides a new approach to targeted diagnosis and treatment of specific cancers (Virginia et al., 2008).

Hyaluronic acid functionalized SWCNTs coupled to gadolinium is a promising compound for high-resolution magnetic resonance and molecular imaging of tumours (Hou et al., 2015). Hyaluronic acid functionalized SWCNTs coupled with Salinomycin successfully targeted the CD44 receptors on a gastric cancer cell line. The nanocomposite material proved to have a greater cytotoxic effect than the drug alone on cancerous cells as well as avoided side effects seen when using commercially available chemo agents (Yao et al., 2014).

Chemical modifications in HA nanoparticles leads to the possibility of ligand modification and poor biocompatibility (Zhang et al., 2014). Many studies have been reported that HA-based nanoparticles can be used as an effective nanocarrier in tumour accumulation or ablation by phototherapy (Kim et al., 2013; Choi et al., 2010).

To identify gastric CSCs, CD44 cell surface markers are targeted using HA, because the samples collected from gastric cancer patients, CSCs are isolated and tested that CD44 receptors are high. The patients isolated cells possess stem cell-like properties such as invasive, spheroid formation *in vitro* condition, drug resistance capacity, migration and tumour formation (Sun et al., 2013; Zhang et al., 2011a). Scientific reports further indicate that CD 44 expression in some carcinomas may act as a prognostic indicator for tumour progression, metastasis and patient survive (Ghaffarzadehgan et al., 2008; Yoo et al., 1999). The complete eradication of the tumour from the body is to target the CSCs and to destroy the cells using specific markers of CSCs (Kusunoki et al., 2013).

2.4.4. Mechanism of loading and coupling of biological compounds on single walled carbon nanotubes.

2.4.4.1. Physical loading mechanism

In the drug delivery system, physical loading mechanism involves the surface loading of chemotherapeutic drugs, DNA, polymers, PS etc, by non-covalent method. Non-covalent bonding process involves hydrophobic interaction, π-π interactions, Van der Waal's force of attractions. SWCNTs without any functional groups with hydrophobic nature and the loading molecules interact with non-polar attraction absorb on the walls of SWCNTs (Shi et al., 2014). Van der Waal's force involves dipole interaction between the nanoparticle and PS molecule by intermolecular force, which facilitate to the PS aggregated on the surface of the nanoparticle. Both mechanisms are not well preferred in drug delivery system due to poor stability, loading efficiency and release moiety.

π-π stacking is another physical adsorption method to load PS on the nanoparticle. SWCNTs has aromatic ring carbon particle when the PS molecule has similar structure both stack on the surface and non-covalent bonding interaction takes place by π bonds. Hence, this mechanism named as π-π stacking. The long chain polymers or peptides will fold on the nanoparticles by π-π stacking to load drugs (Chen et al., 2001).

The advantages of non-covalent bonding there is no structural damage of the drugs; the properties of the nanoparticle will remain the same (Bilalis et al., 2014; Besteman et al., 2003). Most of the PS molecules such as m-tetrahydroxyl phenylcholrin (mTHPC), Zinc phthalocyanine, Zinc monoaminophthalocyanine, Chlorin e6 are coupled non-covalently by π-π stacking to treat various cancer cells using phototherapy, commonly PDT and PTT are used in cancer cells (Ogbodu et al., 2013; Wu et al., 2017). In recent study, Single walled carbon nanotubes were coupled with encapsulated albumin chlorin e6 PS molecule by the ultra-homogenization technique for PTT has effect on squamous cell carcinoma (SCC 7) cell lines for *in vitro* and the *in vivo* studies on BALB/c nude female mice model (Xie et al., 2016).

2.4.4.2. Chemical loading mechanism

The covalent functionalization is like a defect in the sidewalls of nanomaterial, there will be an addition of different functional groups (Park et al., 2006). The main aim of the covalent functionalization is to avoid change in physical properties such as solubility, purity, sp^2 and sp^3 hybridization of carbon molecules. Those properties of carbon make wide application in the field of medical science and nanotechnology (Zhang et al 2008). The functional groups are added to the CNTs such as carboxyl group, hydroxyl, amine, fluoride, disulphide bonds (Banerjee et al., 2005). The carboxyl group and amine group of Polyethylene glycol (PEG) coupled using EDC-NHS method to act as high loading nanocarrier. Due to the solubilizing nature and biocompatibility of the functionalized carbon nanomaterials, it is opted to add different polymeric chains, proteins, DNA and drugs (Zhang et al., 2011b). In recent study, polyethyleneimine functionalized SWCNTs are tested on melanoma cells *in vitro*

and *in vivo* using PDT. The single walled carbon nanotubes covalently functionalized composite showed excellent photo cytotoxic action against cancer cells, the activity of the composite was based on the functionalization method (King et al., 2014). The loading mechanism of PS on SWCNTs were shown in Figure 2.11.

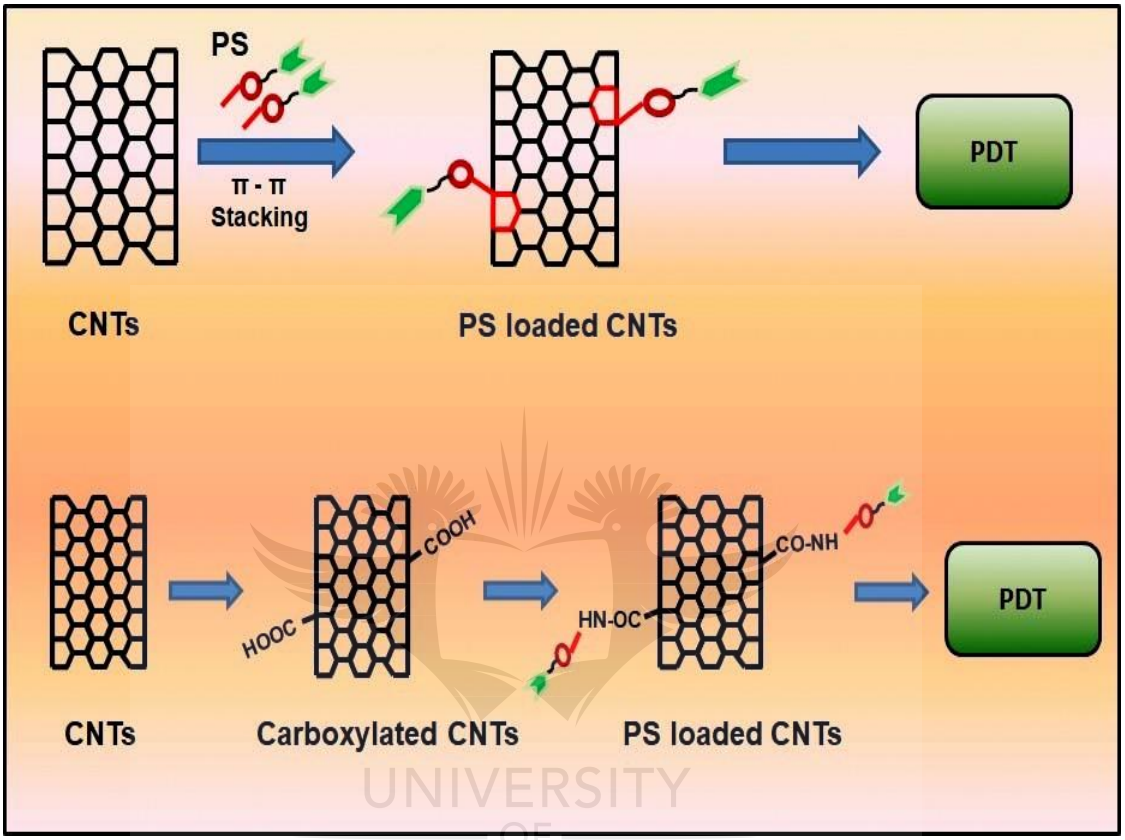

Figure 2. 11 Loading mechanism of PS on SWCNTs. (The attachment of the PS molecule on aromatic rings of CNTs by π–π stacking, and the carboxyl group into amide formation of PS on the walls of CNTs, followed by the molecules being subjected to PDT. (CNTs-carbon nanotubes, PS-photosensitizers, PDT-photodynamic therapy, COOH-carboxyl group, CONH-amide group). (Sundaram et al., 2020b).

2.5. Combined Effects of Nanotubes and Photodynamic Therapy

The cancer nanomedicine has both positive and negative response in terms of overcome the barriers in clinical translation. In drug delivery systems, the fundamentals of nanoparticles interaction with biological substances are not clearly reported (Editors, 2019). PDT widely used in various cancer types with minimal invasive and non-invasive treatment, and then low cumulative toxicity and no drug resistance. PDT application has some challenges to achieve complete side effects free treatment, they are long-enduring photoactivities of PS

molecule could cause photosensitization on skin, after treatment patients must stay in dark for several weeks, lack of tumour selectivity and accumulate in normal tissues leads to toxic effects (Dolmans et al., 2003; Li et al., 2018).
Nanomedicine offers potential benefits in drug delivery systems such as bioavailability, protect drug degradation, and improve targeting the cells, regulated drug release at specific site, therapeutic efficacy with minimum side effects (Singh et al., 2020). Combined effects of nanomedicine and PDT mainly focused to overcome the side effects of the cancer treatments

In recent study, PS coupled SWCNTs reported increased cytotoxic effect on breast cancer MCF-7 cell line and the combination therapy proved to be an effective therapy to treat breast cancer with reduced side effects (Ogbodu et al., 2015a). The SWCNTs molecules are covalently carboxyl amine linking with anti-CD133 markers to target the Glioblastoma stem-like cells, the photothermal effects of SWCNTs at 808 nm can effectively kill the targeted cells (Wang et al., 2011). Very few studies have been performed using SWCNTs in the PDT listed in table 2.7.

Table 2. 7 Application of PDT using SWCNTs.

Nanotubes	**photosensitizers**	**Therapy**	**Cancer**	**Ref**
SWCNTs	Zincmonoamino Phthalocyanine	PDT	Melanoma (A375 cells)	(Ogbodu et al., 2015b)
SWCNTs	Zinc phthalocyanine	PDT	Breast cancer (MCF7 cells)	(Ogbodu et al., 2015c)
SWCNTs	PEI PVPk30	PDT	Mus musculus skin melanoma cells (B16-F10 cells)	(Lei et al., 2014)
SWCNTs	Chlorin e6	PDT	Cervical cancer (HeLa cells)	(Xie et al., 2016)

SWCNTs	Chlorin e6	PDT	Colon cancer (Caco-2 cells)	(Sundaram et al., 2020a)

In this study, nanobiocomposite was prepared using SWCNTs functionalised HA to target CD44 receptors and coupled with Ce6 molecule for photodynamic effects to treat CCSCs. The stability, controlled release and localisation of nanobiocomposite were analysed on isolated CCSCs using PDT effects.

CHAPTER 3 METHODOLOGY

3.1. Synthesis of Nanobiocomposite

Purchased commercially available carboxyl acid functionalised SWCNTs (Sigma Aldrich, 652490), HA (Sigma Aldrich, 40583), Ce6 (Santa Cruz biotechnology, CAS 19660-77-6).

3.1.1. Purification of SWCNTs

SWCNTs were treated using 12M Nitric acid (HNO_3) (Sigma Aldrich, 438073) to get purified form of SWCNTs, then washed thoroughly with Milli-Q water (Thermo scientific, Barnstead, smart pure) and the filtration process using Stericup quick release-GP sterile vacuum filtration system, membrane filter pore size 0.22 µm (Merck, S2GPU05RE).

3.1.2. Synthesis of Hyaluronic acid coupled SWCNTs (SWCNTs-HA)

Hyaluronic acid added into dimethyl formamide (DMF) (Sigma Aldrich, 227056) and dispersed completely by sonication (Branson 1800). To activate the amine group of HA EDC/NHS method were followed: N-ethylcarbodiimde hydrochloride (EDC.HCl) (Sigma Aldrich, E6383) and N-hydroxysuccinimide (NHS) (Sigma Aldrich,130672) added to the HA dispersed solution by stirring 30 mins at room temperature, then added triethylamine 99 % (Sigma Aldrich, T0886) drop by drop and kept cool using ice bath and the solution was stirred and kept at room temperature for 2 h, which activated the HA. The reacted product was collected in membrane filter (D9777, Sigma-Aldrich) through rinsing repeatedly with acetone. The activated HA was dialysed for 48 h to remove acetone and unreacted EDC.HCl and NHS. The SWCNTs-COOH and HA-NH2 were added into formamide, sonicated for 10 min, EDC.HCl and NHS were added, and then it was stirred at room temperature for 15 min. After that, 180 mL of triethylamine was added drop by drop in the ice bath and reacted at room temperature for 24 h. The reaction solution was cooled with excess precooled acetone and centrifuged at 10,000 rpm for 15 min. Finally, the precipitation was dissolved with water and dialyzed by a dialysis bag for 48 h to remove free HA and the synthesised products.

3.1.3. Synthesis of Chlorin e6 coated SWCNTs-HA (SWCNTs-HA-Ce6)

The non-covalent binding of Ce6 on the walls of SWCNTs was achieved by the π-π interaction technique. Ce6 and HA-SWCNFTs were dissolved in DMF. The solution was then sonicated for 10 min. The mixture was stirred overnight and kept at RT. The final product was filtered using membrane filters (0.22 µm) and rinsed with DMF solution to remove unloaded Ce6. The final solution was then rinsed with milli-Q water and acetone to remove residual DMF.

3.2. Characterisation of Newly Synthesised Nanobiocomposite

3.2.1. Solubility study

The synthesised nanobiocomposite and purchased SWCNTs were dispersed in 1 mL of milli-Q water and stirred for 15 mins at room temperature using Eppendorf stirrer. The aggregation and solubility of the samples were observed and captured in photograph.

3.2.2. Determination of activation wavelength

The absorption peak for the synthesised nanobiocomposite were measured using UV-visible spectrophotometer (Genova 7315, Life Science Spectrophotometer, JENWAY). The spectral analysis for SWCNTs, HA, Ce6 and the final compound SWCNTs-HA-Ce6 were measured against milli-Q water in 1 mL UV fused quartz cuvette, the whole experiments carried at the resolution of 1 nm from 200 to 800 nm.

3.2.3. Fourier Transformation Infra-red spectroscopy (FTIR)

The FTIR spectroscopy analysis was used to identify the chemical shifts and functional groups present in the compound. Moreover, potassium bromide (KBr) was used as well as the Hydraulic Pellet Press method to produce a thin sample of KBr pellet that was then subjected to FTIR analysis. The synthesised nanobiocomposites, SWCNTs, HA, Ce6 and SWCNTs-HA were added on the surface of pelleted KBr to measure FTIR spectroscopy. The frequency range was measured as wave numbers, typically over the range 4000–500 cm^{-1} using the JASCO FT/IR-6300 Series, Japan.

3.2.4. X-Ray Diffraction (XRD)

The X-ray diffraction measures structures of crystalline compounds and surface chemistry. The XRD patterns were determined using a diffractometer equipped with a rotating target X-ray tube and a wide-angle goniometer. The X-ray source were Kα radiated from a copper target with a graphite monochromator. The X-ray tube was operated at a potential of 45 kV and a current of 40 mA. The range (2 θ) of scans was performed from 10to 80 at a speed of 4 per min at increments of 0.05. The XRD pattern were analysed for SWCNTs and SWCNTs-HA-Ce6 using the Rigaku Ultima lV instrument and the data were collected from PDXL analysis software (Tokyo, Japan).

3.2.5. Particle size and zeta potential

The synthesised nanobiocomposite size distribution (hydrodynamic diameter) and Zeta potential were studied by the dynamic light scattering (DLS) method (Zeta sizer ver. 7.10, Malvern Instruments Ltd., Malvern, UK). The scattering intensity was adjusted in the range of 50-500 kcps and the samples were diluted using Millipore water, measurements were carried out using disposable cuvettes (DT S0012) in triplicate. For the light method, samples were measured at a fixed angle of 90° at 25 °C.

3.2.6. High resolution transmission electron microscope (HR-TEM)

Morphological evaluation of the synthesised nanobiocomposite done by HR-TEM. SWCNTs, SWCNTs-HA and SWCNTs-HA-Ce6 samples were measured about 10 µg and dispersed in ethanol, then sonicated in ultrasonic bath for 15mins. Prepared samples were drop-casted separately on carbon-coated copper TEM grid dried it for 10 mins. HR-TEM images recorded on JEOL JEM 2100F operated at an accelerating voltage of 200 kV.

3.3. Stability Study

The stability of the newly synthesised nanobiocomposite was determined using the two different pH (5.5 & 7.4) of PBS solution at room temperature. Ce6 and SWCNTs-HA-Ce6 was measured 1 mg/mL in the eppendorf tubes and dispersed in PBS solution, maintained in shaker at 37 °C. In various physiological conditions the stability of the nanobiocomposite at different time interval the samples were measured using the UV-visible spectrophotometer.

3.4. Photosensitizer Ce6 Loading and *In Vitro* Release Study

The photosensitizer loading efficiency on the SWCNTs-HA were calculated using the amount of unbound Ce6 from the synthesis process. The final solution of the synthesis process collected and unbound Ce6 determined using UV-visible spectrophotometer measured the absorbance at 660 nm. The measured values are calculated using the formulae

$$PLE\ (\%) = \frac{weight\ of\ loaded\ PS}{weight\ of\ PS\ infeed} \times 100$$

The photosensitizer release study was carried out using the dialysis technique, the release behaviour of the Ce6 from SWCNTs-HA-Ce6. The newly synthesised nanobiocomposite dispersed in phosphate buffer saline (PBS) pH 7.4 and pH 5.5 and then the solution transferred into the dialysis membrane tubes. The dialysis membrane tubes were submerged in 200 mL of PBS with 0.1 % (W/V) tween80 (P1754, Sigma-Aldrich) and kept in gentle shaker at 37 °C. To analysis the released Ce6 from the dialysis bag 1 mL of the release medium taken in the new eppendorf tubes in predetermined time and replaced by 1 mL of fresh medium each time. The amount of released Ce6 from SWCNTs-HA-Ce6 measured using UV-visible spectrophotometer. The dialysis bag unit shown in Figure 3.1.

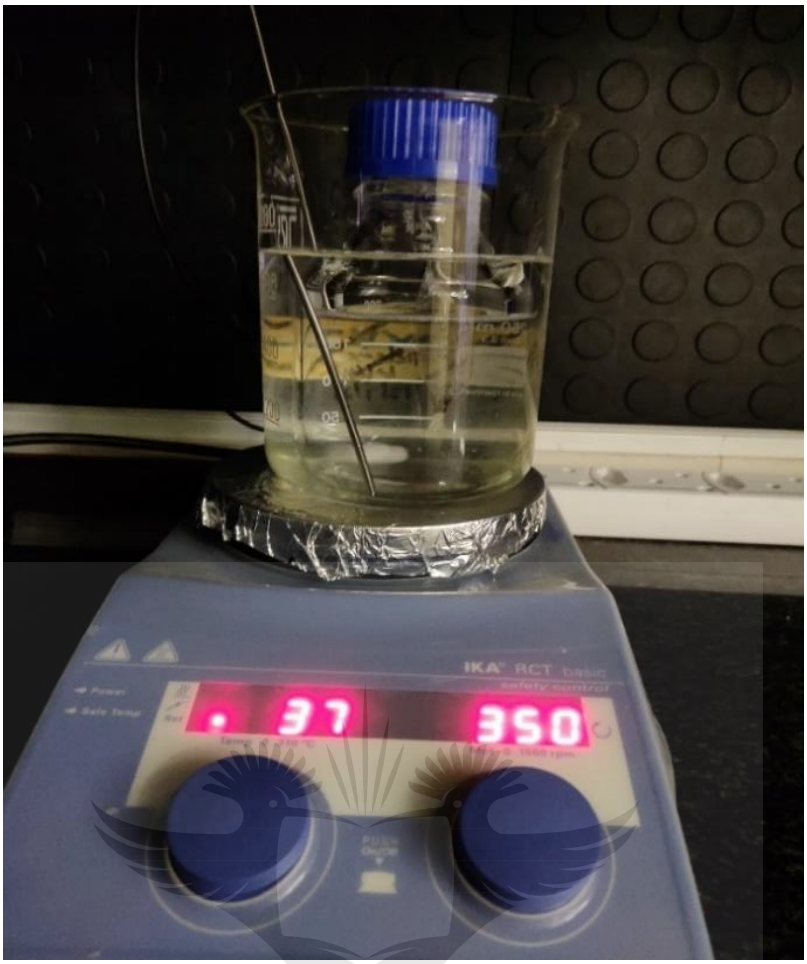

Figure 3. 1 Dialysis bag unit for drug release study.

The *in vitro* release studies data was analyzed using different mathematical models to study the mechanism of release. The studied mathematical models are Zero order kinetic (Eq.1), First order kinetic (Eq. 2), Higuchi kinetic (Eq.3), and Korsmeyer-Peppas model (Eq. 4).

$$Q_t = K0\,t \quad \text{---------- (1)}$$

$$\text{Log Qt} = \text{Log Q0} + \frac{K1t}{2.303} \quad \text{---------- (2)}$$

$$Q_t = KH\,t^{1/2} \quad \text{---------- (3)}$$

$$\frac{M_t}{M_\alpha} = K_p t^n \quad \text{---------- (4)}$$

The plots were made of percentage of drug release, Qt Vs time (zero order kinetic model), log percentage drug remaining Vs time (first-order kinetic model), percentage of drug release, Qt Vs square root of time (Higuchi model) and Log cumulative percentage drug released Vs Log Time (Korsmeyer-Peppas model) (Gouda et al., 2017).

where Qt is the percent of drug released at time t, Q0 is the initial amount of drug present in the nanotubes, Mt is the fraction of drug released at time, t and n is the diffusional exponent for drug release, K0, K1, K H and KP the rate constants of the equations 1,2, 3 and 4 respectively.

3.5. Cell Culture

Colon cancer cell line Caco-2 was purchased from ATCC®, HTB-37™ and cultured in Dulbecco's modified eagle's medium (DMEM) (sigma-Aldrich) supplemented with 10 % (v/v) foetal bovine serum (FBS) (F9665-Sigma-Aldrich), 2 mM L-glutamate (G7513, Sigma-Aldrich). Cultured cells were incubated at 37 °C in 5% CO_2 and 85 % humidity in tissue culture flasks. When the cells are reached 90 % confluence, cells were washed twice with Hank's balanced salt solution (HBSS) (14065-056, Gibco) and to detach the cells from cultured flask TrypLE Express (12604, Gibco) was used.

3.5.1. Viability of cells using trypan blue assay

It is essential to quantify the number of cells and check their viability before conducting all the experiments. An automated cell counter, Countess® II (Invitrogen) was used for this purpose. The machine counts and differentiates live from dead cell by trypan blue exclusion test which is based on the principle that viable cells do not take up impermeable dyes (like Trypan Blue), but dead cells are due to damaged membranes, take up the dye. A 1 mL cell suspension as described previously was mixed properly using a vortex shaker. 10µLof the well mixed cell suspension was added to an equal volume of 0.4% trypan blue solution (Sigma Aldrich.) in a 1 mL test tube. The mixture could stain for 5 min at room temperature in the dark to avoid photo-bleaching of the dye. After staining, each chamber of the Countess® cell counting slide was loaded with 10 µL of the

sample mixture. Upon insertion of the slide unto to the slide reader, the instrument automatically illuminates the sample and focuses the cells. After the cells were fully focused, automatically and manually when necessary, the capture button was pressed to read the measurement. The instrument captures the image and displays the results including the total cells concentration per mL, and the percentage of live and dead cells with their concentration per mL. Both sides of the slide were analyzed and the average of the two counts was used as the cell count.

3.6. Intracellular Localisation of SWCNTs-HA-Ce6

To localize the newly synthesised nanobiocomposite using sub-cellular trackers. 5×10^5 Caco-2 cells were cultured on the sterile glass cover slips (0895202, MARIENFELD) with complete medium in treated culture dishes (45 CLS430588, Sigma), after attachment of cells SWCNTs-HA-Ce6 was added into the medium and incubated at 37 °C in 5% CO_2 and 85 % humidity. After 12 h the cells were thrice rinsed using HBSS to remove unbound Ce6 and SWCNTs-HA-Ce6. Added 500 µL of 4 % paraformaldehyde (P6148, Sigma-Aldrich) on the cells and incubated for 20 mins at 37 °C to fix the cells, then rinsed twice using HBSS. For permeabilization 200 µL of 0.2 % triton X-100 (Sigma Aldrich, T9284) added on the cells and incubated for 10 mins at 37 °C, then rinsed twice using HBSS. Prewarmed staining solution of mito tracker 100 nM (M7514, Invitrogen) and lyso tracker 50 nM (L7526, Invitrogen) were added on the cells and incubated for 30 mins at 37 °C, then rinsed twice using HBSS. For counter staining 300 nM 4', 6-Diamidino-2-Phenylindole, Dihydrochloride (DAPI) (D1306, Invitrogen) was added and incubated for 20 mins at 37 °C, then washed twice using PBS. The glass cover slip was taken out and dried for 5 mins using Fluoromount™ Aqueous Mounting Medium (F4680, Sigma-Aldrich) the cover slip mounted on the glass slide (GLAS4S22M3000F, Lasec) and visualized using Carl Zeiss live imaging microscope (Axio Observer Z1).

3.7. PDT Effect of Swcnts-HA-Ce6 on Colon Cancer Cell Lines

The red-light lasers were obtained from the National Laser Centre of South Africa. The laser output was measured using a FeildMate Laser Power Meter

(FieldMate, Coherent, Power sens detector) and the laser parameters are tabulated in table 3.1. The cells were cultured in a 3.4 cm petri dish where the laser spot size covers the monolayer of cells. The height of the light source was 8 cm above the cells. To treat the cancer cells, red light lasers were used at the wavelength of 660 nm, which is the excited range of the Ce6 photosensitizer. The cells were divided into three groups: group 1: cells alone and cells with SWCNTs, Ce6 and SWCNTs-HA-Ce6 without treatment; group 2: cells alone and cells with SWCNTs, Ce6 and SWCNTs-HA-Ce6 with treatment of fluence 5 J/cm^2; group 3: cells alone and cells with SWCNTs, Ce6 and SWCNTs-HA-Ce6 with treatment of fluence 10 J/cm^2.

3.7.1. Morphology

The live and dead cell morphology before and after irradiation was viewed under a CKX41 inverted light microscope (Olympus, Wirsam) connected to a camera with analysis getIT software.

3.7.2. Cytotoxicity

The cytotoxicity level of the samples was estimated using Cyto Tox 96® Non-Radioactive cytotoxicity assay. The CytoTox 96® assay quantitatively measures the lactate dehydrogenase (LDH), which was released from cells during lysis. Fifty microliters of control and test samples were added in a 96 well plate and the same amount of LDH reagent was added in the wells, then incubated in the dark at room temperature for 30 min. The colorimetric compound was measured spectrophotometrically at 490 nm using a multilabel Counter (Perkin Elmer, VICTOR3— Multilabel Plate Reader, 1420). We adopted the same methodology to find out the IC50 concentrations of synthesized nanobiocomposite.

3.7.3. Cell Death

The assay uses Annexin V–fluorescein isothiocyanate (FITC) and propidium iodide (PI) (556547, BD Biosciences) to identify phosphatidyl serine sites on the membrane of apoptotic cells, as well as sites of membrane damage in necrotic cells, respectively. The assay was done according to the manufacturer's instructions and analysed on the BD Accuri™ C6 flow cytometer. Annexin V–

FITC was detected as green fluorescence and PI as red. After treatment and incubation, the cells from all groups were detached and washed with Hanks Balanced Salt Solution. Cells were resuspended in the 1X binding buffer at a concentration of 10^6 cells/mL, and 100 µL of the cell suspension was transferred into flow cytometry tubes. Five microliters each of the Annexin V–FITC and PI reagents were added, and the tubes were thoroughly mixed and incubated for 10 min at RT in the dark. Flow cytometric analysis was performed within one hour at a rate of 400 events per second with a limit of 350 µL for each sample. Data acquisition proceeded until 10,000 events were obtained for every sample. Data was analysed on the BD C Sampler software.

3.8. Isolation of Colon Cancer Stem Cells

Colon cancer stem cells also known as side population of colon cancer cell lines, CCSCs were isolated from Caco-2 cell lines using magnetic activated cell sorting MACS (Miltenyi Biotec). CD133 (130-050-801, microbead kit, Miltenyi Biotec), CD44 (130-095-194, microbead kit, Miltenyi Biotec) and CD24 (130-095-951, microbead kit, Miltenyi Biotec) markers are used to isolate the side population from the Caco-2 cell line. The positive selection of CD133+, CD44+ and CD24+ cells was separated using QuadroMACS™ based on the principle of monoclonal antibody and specific antigen interactions.

Caco-2 cells was cultured in 175 cm^2 T-flask incubated at 37 °C in 5% CO_2 and 85 % humidity, when it reached 80 % confluence, the cells were washed twice using HBSS and detached using TrypLE express. The detached cell number and viability were determine using trypan blue stain, 0.4% (T10282, Invitrogen™) and measured on a Countess™ II automated cell counter (AMQAX1000, ThermoFischer). According to the MACS protocol cells were resuspended to the concentration 1×10^7 cells and centrifuged at 3000 rpm for 10 mins. The supernant was discarded and the cell pellet was resuspended in isolation buffer (PBS 7.2, 0.5% BSA, 2mM EDTA).

Fragment crystallizable receptor (FcR) blocking buffer to avoid unwanted binding of antibodies, 80 µL of FcR buffer was added on each tube and gently mixed by vortex. CD 133, CD44 and CD24 MACS microbeads were added on the cell

suspension mixed well and incubated on ice for 30 mins at dark condition on a shaker. After exposure to antibodies, the cells were washed using buffer solution and centrifuged at 3000 rpm for 10 mins, the supernatant aspirated completely, and the cells resuspended with buffer solution.

Isolation of SCs, MACS LS columns were used. LS columns were placed on the magnetic field of the QaudroMACS™ Separator, to rinse the LS column initially 3 mL of buffer run through the LS columns and the cell suspension was added onto the column left undisturbed. $CD133^+$ cells attached on the walls of LS column and unbound cells washed with buffer solution and collected in empty vials. For positive cells using a LS column plunger 3 mL of buffer solution added on the LS column then flushed out by pushing the plunger into the LS column. Positive selected cells were cultivated using ultra-low attachment flasks to maintain the spheroids and prevents differentiation of CSCs. To grow the CCSCs complete stem cell media DMEM-F12 supplemented with 0.4% FBS, 20 ng/mL epidermal growth factor (EGF), 20 ng/mL basic fibroblasts growth factor (bFGF) was used.

3.9. Characterisation of Isolated Colon Cancer Stem Cells

3.9.1. Spheroid formation

The isolated were incubated in complete stem cell medium at 37 °C in 5% CO2 and 85 % humidity in ultra-low attachment flask. The flask was viewed under light microscope in time interval and captured the spheroid formation images.

3.9.2. Flow cytometry

To confirm the isolated side population, were origin of CSCs using fluorescently labelled antibodies conjugation method identified by flow cytometry. The cultivated cells were rinsed twice with HBSS and detached using TrypLE express and then washed twice using washing buffer then incubated with blocking buffer for 1 hr at 37°C after that washed twice using washing buffer. Primary antibodies mouse anti human CD44 (MABF425, human/mouse, PE-Cy5, clone IM7, Sigma-Aldrich), CD133 (130-133-673, AC133, Vio® Bright FTIC, Miltenyi Biotec) are fluorochrome conjugated so direct immunofluorescence method and CD24 (#

555426, human/mouse, clone ML5, BD Biosciences) indirect immunofluorescence method.

The antibodies were diluted using working buffer and added into the cell suspension was incubated for 1 hr at 4°C under dark condition, then the cell suspension was washed trice using washing buffer. For CD24 alone fluorochrome conjugated secondary antibodies Cy5 goat anti-mouse (Novus Bio, NB7602) were added into the working buffer incubated for 30 mins at 4°C under dark condition, then cell suspension washed trice using washing buffer. Finally, the cell suspension subjected to analyse using C6 flow cytometer (BD Biosciences, BD ACCURI C6 PLUS) which detect the fluorescent probes on the cell surface. These results indicate the positive and negative selection of CD44, CD133 and CD24 markers on the surface of isolated CCSCs.

3.9.3. Immunofluorescence (IFL)

The isolated CCSCs was characterised using direct and indirect immunofluorescence method. In direct IFL, the primary antibody conjugated with fluorochromes to visualise CCSCs. In-direct IFL CCSCs are labelled using primary antibodies to target specific antigen and fluorochromes conjugated secondary antibodies directed towards primary antibodies, this fluorescence visualized under live microscope. CCSCs were cultured on sterile coverslips placed in culture dishes, at a concentration of 5×10^5 cells in complete stem cell media.

Once the cells reached confluence discarded the media and rinsed twice with ice-cold washing buffer (PBS, 0.1% BSA, 0.01% Sodium azide). For fixation of cells 4% paraformaldehyde was added and incubated for 20 mins at 37 °C, then rinsed twice using washing buffer. After fixing the cells, to permeabilize the cells 0.1 % Trixton X-100 was added and incubated for 10 mins at 37°C, then rinsed twice using washing buffer. Blocking buffer (10% BSA) was added and incubated for 1 hr at 37°C and washed twice using washing buffer.

Cells were then incubated with 100 µL of primary antibodies anti human CD44 (MABF425,human/mouse, PE-Cy5, clone IM7, Sigma-Aldrich) CD133 (ZRB

1013, human/rabbit, clone F8, ZooAb, Merck) and CD24 (# 555426, human/mouse, clone ML5, BD Biosciences) in working buffer (PBS, 2% BSA, 0.01% Sodium azide) overnight incubation at 4°C, to protect from dryness the petri dishes are placed on wet bed and maintained dark condition. The cells were then washed trice using washing buffer.

The washed cells were incubated with 100 µL of secondary antibodies FTIC (Santa Cruz biotechnology, mouse anti-rabbit IgG, Sc 2359), Cy5 (Novus Bio, NB7602) goat anti mouse antibodies in working buffer for 1 hr at 4°C maintain dark condition and the cells were washed twice using washing buffer. CD 44 was direct IFL process so that skipped the introduction of secondary antibody into the plates. To counter staining 300 nM DAPI was added and incubated for 20 mins at 37°C, then washed trice using washing buffer. Finally, the coverslips were taken from the plates using tweezers, dipped in distilled water to remove residual and mounted on the microscope slides using mounting media. The slides were visualized under Carl Zeiss Axio Z1 microscope.

3.10. Targeted Delivery of SWCNTs-HA-Ce6

The isolated CCSCs were cultured on glass cover slip containing petri dish and incubated at 37 °C in 5% CO_2 and 85 % humidity. As control cells CD44 negative SK-UT-1 (ATCC ® HTB 114™) cells also cultured with MEM complete medium. Once the cells reached confluency incubated with SWCNTs-HA-Ce6 for 4 h and thrice rinsed using HBSS to remove unbound SWCNTs-HA-Ce6. Added 500 µL of 4 % paraformaldehyde (P6148, Sigma-Aldrich) on the cells and incubated for 20 mins at 37 °C to fix the cells, then rinsed twice using HBSS. For permeabilization 200 µL of 0.2 % triton X-100 (Sigma Aldrich, T9284) added on the cells and incubated for 10 mins at 37 °C, then rinsed twice using HBSS. Prewarmed staining solution of mito tracker 100 nM (M7514, Invitrogen) were added on the cells and incubated for 30 mins at 37 °C, then rinsed twice using HBSS. For counter staining 300 nM 4', 6-Diamidino-2-Phenylindole, Dihydrochloride (DAPI) was added and incubated for 20 mins at 37 °C, then washed twice using PBS. The glass cover slip was taken out and dried for 5 mins

using Fluoromount™ Aqueous Mounting Medium the cover slip mounted on the glass slide and visualized using Carl Zeiss live imaging microscope.

3.11. Photodynamic Therapy on Isolated CCSCs

The red light-lasers were purchased from the National Laser Centre of South Africa (NLC). The laser output power was measured using a FeidMate Laser Power Meter (Coherent, 1098297) and a high-sensitivity thermopile sensor PM3 (Coherent, 1098336). Based on the measured power and selected fluence using the below formulae time of irradiation was calculated.

$$\frac{mW}{cm^2} = \frac{mW \times 4}{\pi \times 3.4^2}$$

$$\frac{W}{cm^2} = \frac{mW/cm^2}{1000}$$

$$Time\ (s) = \frac{J/\ cm^2}{W/cm^2}$$

The isolated CCSCs were cultured in a small petri dish (3.4 cm) and incorporated with newly synthesised nanobiocomposite after attachment of cells. The treated laser parameters are summarized in Table 3.1

Table 3. 1 Laser parameters.

Parameters	
Laser type	Semiconductor diode
Wavelength (nm)	660
Emission	Continuous wave
Fluences (J/cm^2)	5 and 10
Irradiation time	7 min 16 s
	14 min 32 s
Photosensitizer	Chlorin e6
Height of laser	8 cm

When the cells reached confluency, treated with red light lasers at 660 nm which is the excited range of Ce6, the whole treatment was carried at dark condition. The cells where divided into groups explained in Table 3.2

Table 3. 2 Experimental groups used in the present study.

Groups	Description	Number of plates
Group A	0J/cm^2	Only cells
		Ce6 alone
		SWCNTs-HA-Ce6
Group B	5J/cm^2	Only cells
		Ce6 alone
		SWCNTs-HA-Ce6
Group C	10J/cm^2	Only cells
		Ce6 alone
		SWCNTs-HA-Ce6

3.11.1. Morphology studies

The treated cells morphology was visualized using CKX41 inverted light microscope (Olympus, Wirsam) connected to a camera with getIT software. After PDT 0 h, 24 h and 48 h morphology (live and dead cells) of each plate were captured.

3.11.2. Cytotoxicity assay using lactate dehydrogenase (LDH) assay

To measure the cytotoxicity range of synthesised nanobiocomposite under PDT treatment using LDH assay. when the cell membrane damaged induces to leakage of LDH through plasma membrane rapidly released into the cell culture medium. CytoTox 96® Non-Radioactive Cytotoxicity colourimetric assay (G1780, Promega), LDH reacts to convert a tetrazolium salt (in the reconstituted reagent, oxidised form) into a quantifiable red formazan product (reduced form) in a NADH dependent reaction.

The PDT treated cells were incubated for 24 hrs and 48 hrs at 37 °C in 5% CO_2 and 85 % humidity, then the 50 µL of medium from cells and 50 µL of reconstituted reagent mixed together in flat bottom 96 well clear polystyrene microplate (CLS3370, Corning®, Merck). The microplate was incubated for 30 mins at room temperature in the wave motion mixer and the compound measured using VICTOR3 multilabel plate counter.

3.11.3. Flow cytometry Annexin V–fluorescein isothiocyanate (FITC) and Propidium Iodide (PI)

To measure the cell death events and cell populations (normal or dying cells) FTIC Annexin V Apoptosis detection kit I (556547, BD Pharmingen™) was used. After 24 hrs and 48 hrs post irradiation the cell death was measured using flow cytometry to identify phosphatidyl serine sites on the membrane of apoptotic cells or membrane damage in necrotic cells. The treated cells were rinsed with HBSS and detached using TrypLE express, cells suspension was transferred into flow cytometry tubes and resuspended with 1X binding buffer. 5 µL of Annexin V-FTIC and PI reagents added into the cell suspension and mixed thoroughly incubated for 10 mins at room temperature under dark condition. Finally, the C6 flow cytometric analysis was performed to detect the FTIC green and PI red fluorescence respectively.

3.11.4. Determination of metabolic activity of cells using Adenosine Triphosphate (ATP) luminescence assay

The PDT treated cells incubated for 24 hrs and 48 hrs at 37 °C in 5% CO_2 and 85 % humidity and to quantify the amount of ATP presence in the cells using CellTiter-Glo® 2.0 ATP luminescence assay (Promega, G9241). ATP luminescence assay was homogenous method to determine the amount of ATP in the cultured cells is directly proportional to the viable cells.

PDT treated cells were rinsed with HBSS and detached using TrypLE express, then centrifuged at 3000 rpm for 5 mins and collected pellets. In white polystyrene 96well plate (CLS3912, Corning®, Merck) 50 µL of cell suspension and 50 µL of CellTiter-Glo® reagent was added and mixed slowly in wave motion mixer

(Polymax 1040, Heidoplh) for 2 mins to induce cell lysis and incubated for 10 mins at 37°C under dark condition, for baseline control complete media was added to test. The luminescent signal was measured in relative light units (RLUs) using multilabel plate counter (1420, VICTOR3™, Perkin Elmer).

3.11.5. Nuclear damage study

To determine the nuclear damage of the treated cells was measured using live cell fluorescent microscope using Hoechst dye 33342 (H357, Invitrogen). CCSCs were cultured on sterile coverslips placed in culture dishes, at a concentration of 5×10^5 cells in complete stem cell media. After attachment of cells, newly synthesised nanobiocomposite was incorporated into the cells and irradiated at 660 nm and incubated for 48 hrs at 37 °C in 5% CO_2 and 85 % humidity. The incubated cells were rinsed twice with HBSS and added 500 µL of 4% paraformaldehyde incubated for 20 mins at 37 °C then washed twice using PBS solution. Cells were incubated with 1 µg/mL of Hoechst dye for 10 mins at 37 °C under dark condition, after incubation period cells were washed twice using PBS solution. For counter staining PI was added and incubated for 15 mins at 37 °C under dark condition, then washed with PBS solution. The coverslip was mounted on the glass slip using Fluoromount media and visualised under live cell microscope.

3.11.6. Intracellular reactive oxygen species detection

To determine the production of ROS using fluorometric intracellular ROS kit (MAK142, Sigma-Aldrich). It is one step fluorometric assay to detect free radicals' superoxide and hydroxyl in live cells. ROS reacts with a fluorogenic sensor localised to the cytoplasm and produce the fluorescence is proportional to the amount of ROS present. CCSCs were cultured on sterile coverslips placed in culture dishes, at a concentration of 5×10^5 cells in complete stem cell media. After attachment of cells, newly synthesised nanobiocomposite was incorporated into the cells and irradiated at 660 nm and incubated for 1 hr at 37 °C in 5% CO_2 and 85 % humidity.

Cells were rinsed with HBSS and ROS master mix 100 µL was added into the cells incubated for 30 mins at 37 °C. After incubation time cells washed with PBS

and 300 nM DAPI was added into the cells incubated for 20 mins at 37 °C. The coverslip mounted on the glass slide using fluoromount and visualised using live cell microscope.

3.12. Statistical Analysis

The results were obtained, processed for graphic presentation, and data analysis was done with Origin Pro 8 SRO (v8.0724) and BD CSampler™ software. All experiments were done in triplicate to monitor for the reproducibility of the results, and all data is expressed as the mean ± standard deviation. Difference between groups were determined using the one-tailed student t-test**.**

CHAPTER 4 RESULTS AND DISCUSSION

4.1. Synthesis of Nanobiocomposite Using SWCNTs, HA and Ce6

SWCNTs were recently introduced as nanocarrier for biomedical applications, due to the physicochemical characteristics, wide surface area and excretion from body through urine without damaging any cells and tissues (He et al., 2013). In this work, we successfully synthesized functionalized nanobiocomposite (SWCNTs-HA-Ce6) using carboxylated SWCNTs and biopolymer HA, and natural PS molecule Ce6. The carboxyl group of SWCNTs and amine activated HA chemically attached by strong carbonyl bond. Carboxylated SWCNTs were successfully coupled with HA by covalent bonding mechanism of carboxyl amine cross-linking (Hou et al., 2015). When the CNTs are coupled with polymers or proteins, it shows excellent water dispersibility, biocompatibility and sustained stability, those are some of good qualities of nanocarrier (Xu et al., 2008).

SWCNTs-HA molecule non covalently coated with naturally derived PS molecule Ce6 by π-π interaction. It is well-known that electron rich molecules easily form π-π interaction with another electron rich compound, those bonding were very strong in nature (Liu et al., 2019). Ce6 molecule is hydrophobic and electron rich molecule like SWCNTs easily bind by π-π interaction (Xiao et al., 2012). The newly synthesised nanobiocomposite were confirmed by various physicochemical characterisation techniques as discussed in section 4.2.

4.2. Physicochemical Characterisation of Newly Synthesised Nanobiocomposite

4.2.1. Dispersibility analysis of newly synthesised nanobiocomposite

Dispersibility studies for all the samples were performed by dissolving 1 mg of SWCNTs and 1 mg of SWCNTs-HA-Ce6 with 1 mL of Millipore water separately and mixing it vigorously using vortex mixer, and the images of SWCNTs alone and SWCNTs-HA-Ce6 are illustrated in Figure 4.1. The SWCNTs and Ce6 are hydrophobic in nature, while the synthesised nanobiocomposite showed excellent dispersibility due to the coupling of HA molecules.

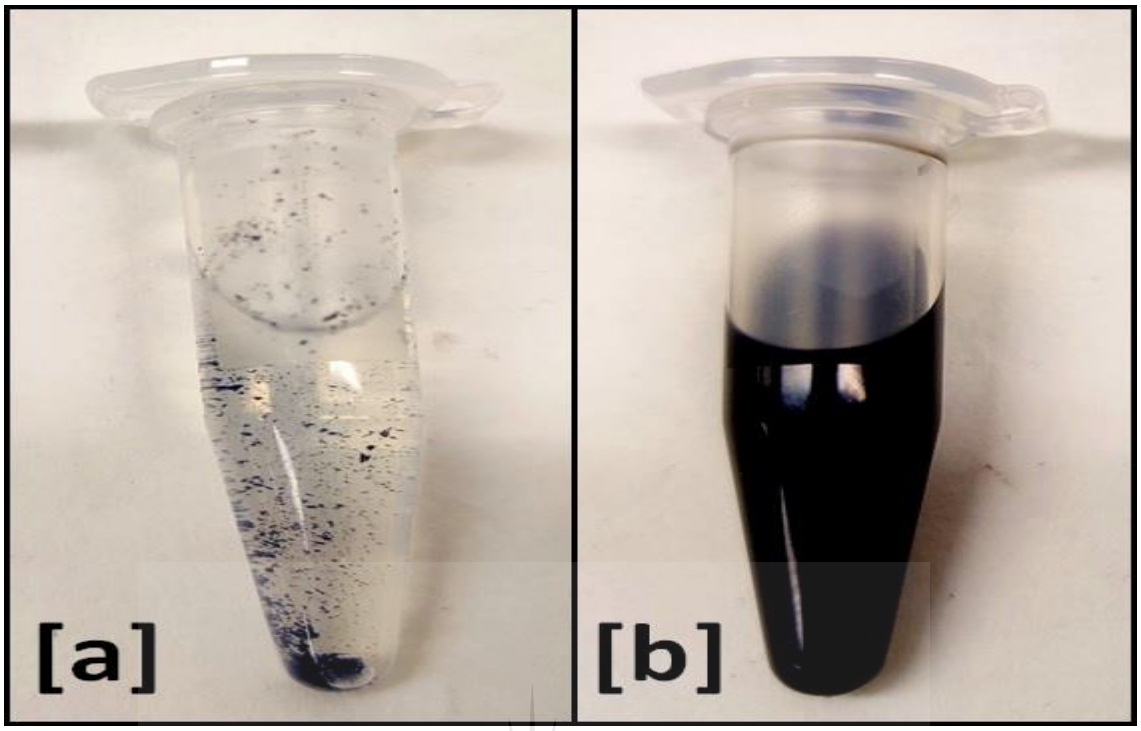

Figure 4. 1 Dispersibility analysis of nanobiocomposite. [a] SWCNTs, [b] SWCNTs-HA-Ce6.

4.2.2. UV Spectrophotometer study

4.2.2.1. Spectrum analysis of different concentration of Ce6

In order to find out the maximum absorbance peak for Ce6, the different concentration of Ce6 compound was taken and dissolved into the DMF solvent. The UV spectral analysis of Ce6 showed three characteristics peaks at 405 nm, 503 nm and 664 nm and this result correlate with reported studies by Xiao et al., 2012. The different concentration of Ce6 spectrum analysis are given in the Figure 4.2

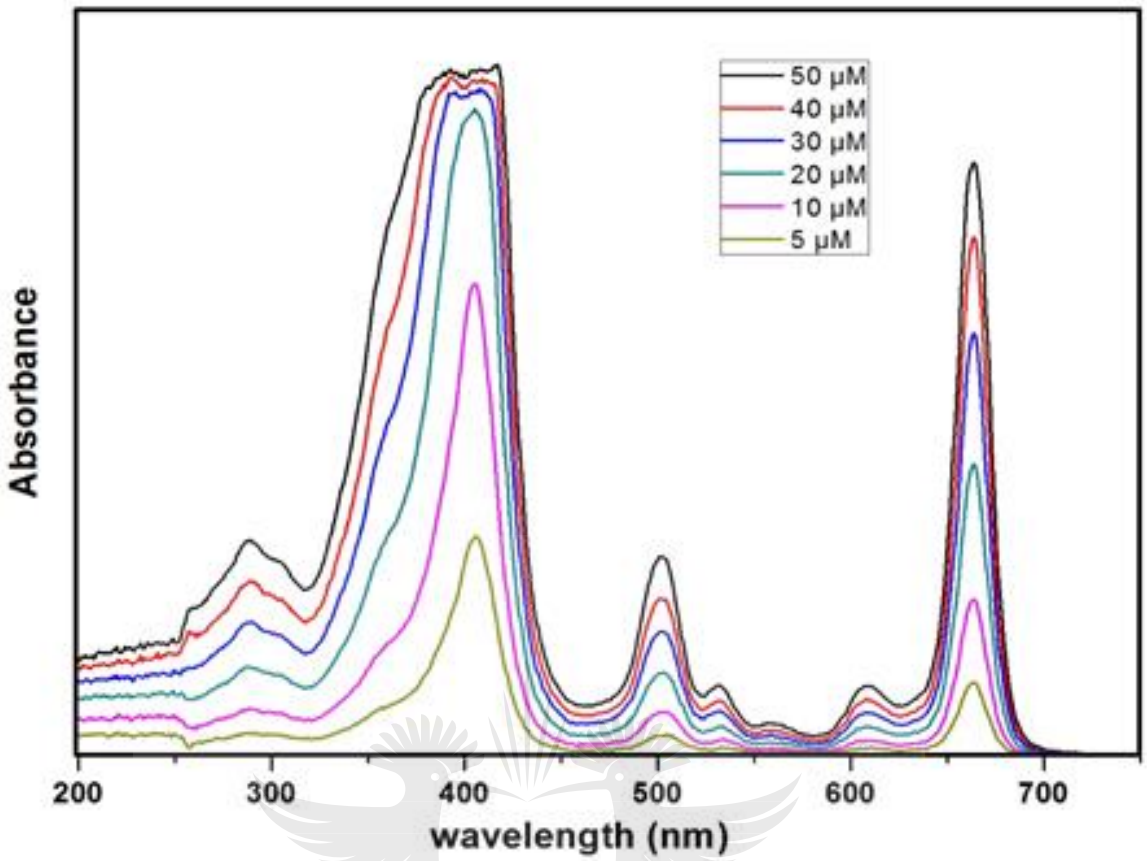

Figure 4. 2 Spectrum analysis of Ce6 at different concentration.

4.2.2.2. Spectrum analysis of SWCNTs, HA, Ce6 and SWCNTs-HA-Ce6

The spectrum analysis was carried out for SWCNTs, HA, Ce6 and SWCNTs-HA-Ce6, and the major absorbance peak was measured using UV spectrophotometer. The UV major absorption peaks of SWCNTs, HA, Ce6 and SWCNTs-HA-Ce6 compounds are shown in the Figure 4.3. The absorbance peak of SWCNTs, HA, Ce6 and SWCNTs-HA-Ce6 were recorded from 200-800 nm wavelengths. DMF solution was kept as a blank, since all the samples (SWCNTs, HA and Ce6) were dissolved in DMF solution. We observed the the maximum absorbance peak of SWCNTs was recorded at 268 nm (De Adhikari et al., 2009). The UV spectrum analysis for HA showed no characteristics peak in the absorbed ranges of 200-800 nm (Hou et al., 2015).

The final synthesised compound SWCNTs-HA-Ce6 was dispersed in Millipore water, and the UV spectrum analysis was carried out from 200-800nm

wavelengths. Here, Millipore water was used as a blank. The characteristics and major absorption peaks of SWCNTs (268 nm) and Ce6 molecule (405, 503, and 664 nm) were observed in the SWCNTs-HA-Ce6 compound. These results indicate the successful bonding of HA and Ce6 on the SWCNTs-HA-Ce6.

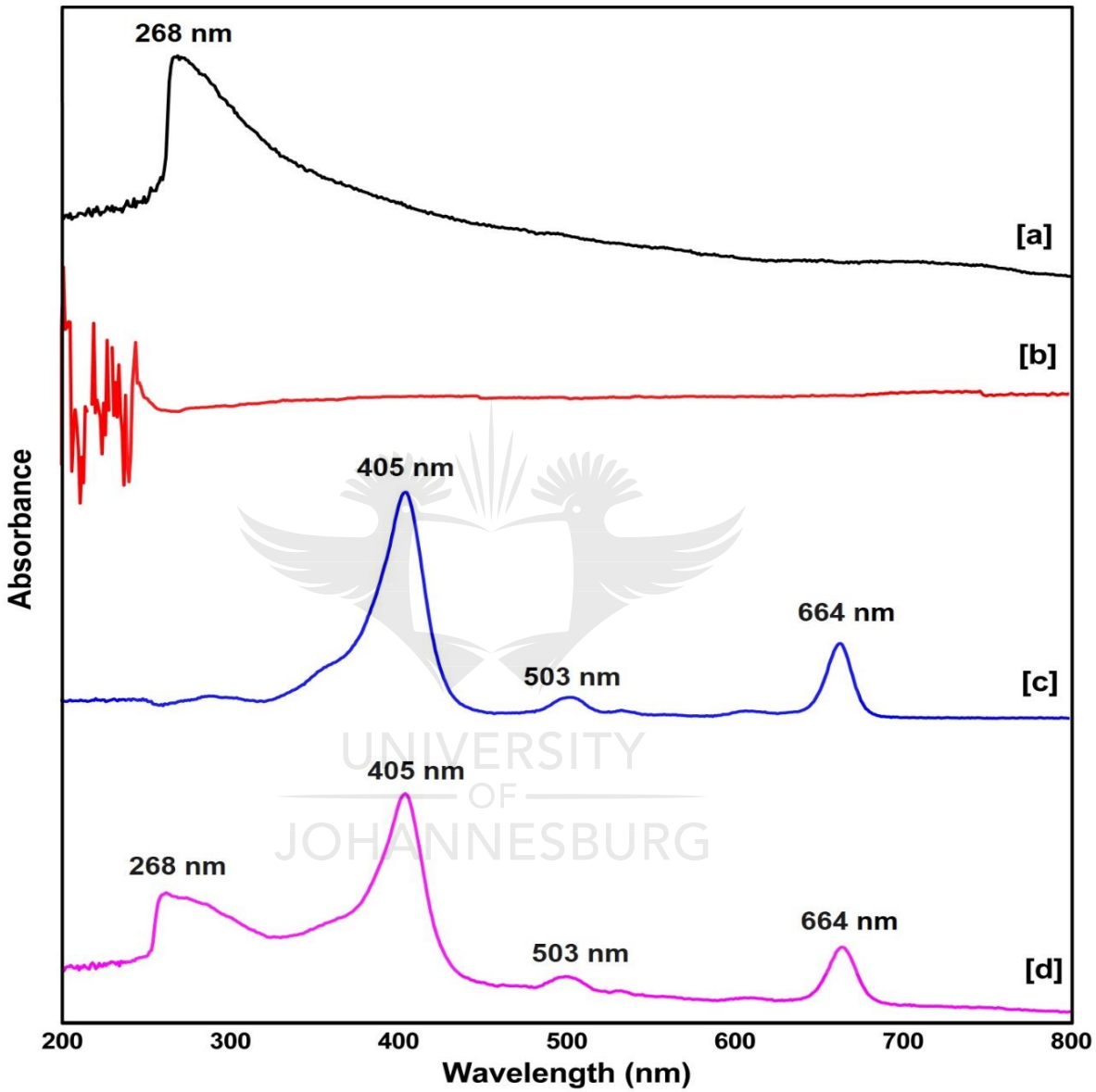

Figure 4. 3 UV spectrophotometer of [a] SWCNTs, [b] HA, [c] Ce6, [d] SWCNTs-HA-Ce6.

4.2.3. Fourier transform infrared (FTIR) spectroscopy of the newly synthesised nanobiocomposite

FTIR spectroscopy is an important and popular tool to examine the surface chemistry of the samples. Compound identification was performed based on the

absorption frequency ranges, functional group and their bond shifting in FTIR spectrum. SWCNTs, HA, Ce6 and SWCNTs-HA-Ce6 were analysed using FTIR spectroscopy and the spectrum peaks were recorded from 500-4000 cm^{-1}.

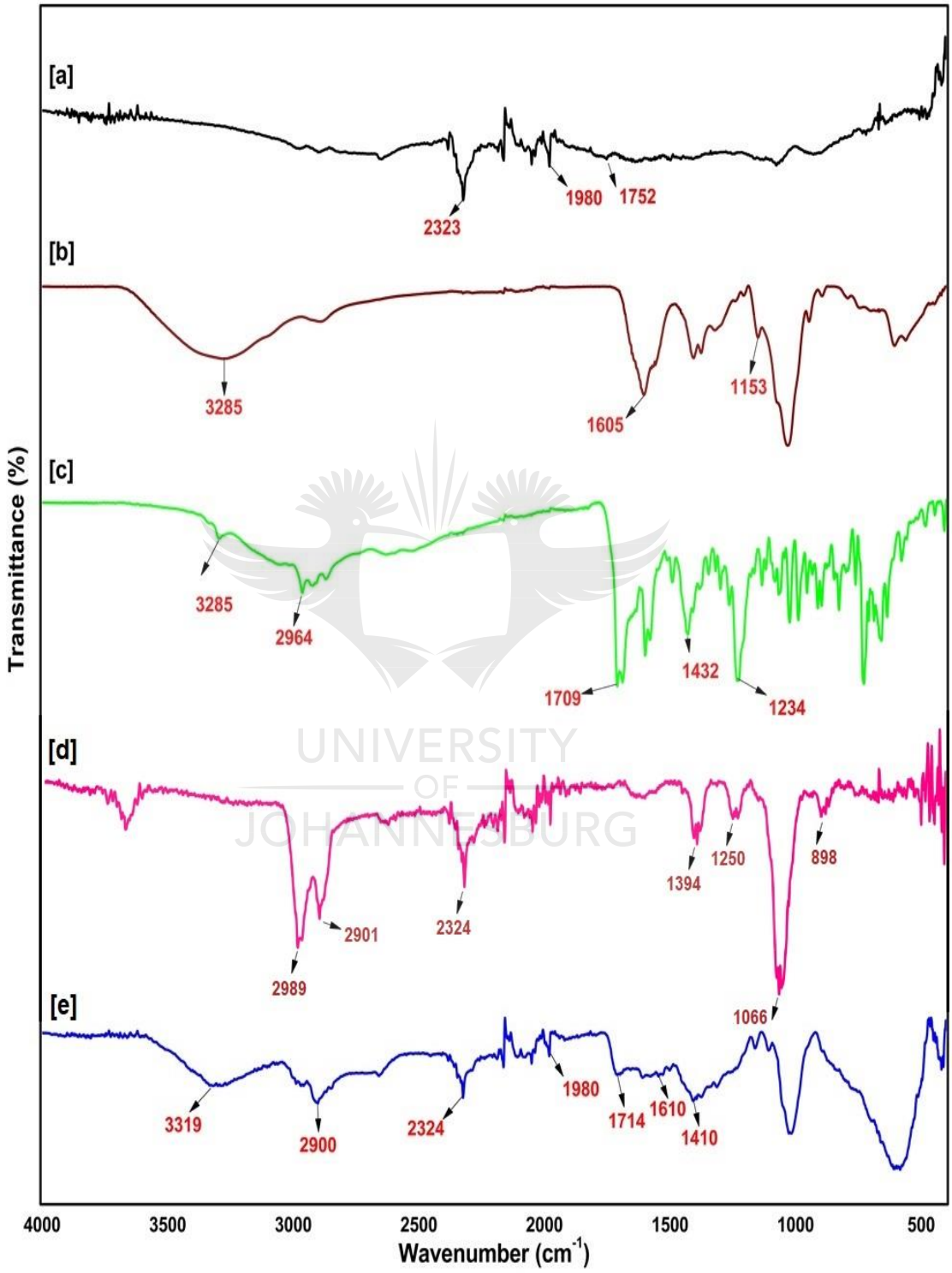

Figure 4. 4 Fourier transform infra-red spectroscopy spectrum of [a] SWCNTs [b] HA [c] Ce6 [d] SWCNTs-HA [e] SWCNTs-HA-Ce6.

The FTIR spectra of SWCNTs, depicted as a black line spectrum from Figure 4.4, showed a strong carbon absorption bond peak of C=C at 2323 cm^{-1}, =C–H at 1980 cm^{-1}, and carboxyl bond stretching C=O at 1752 cm^{-1} (Bagheri et al., 2017). In the brown line spectra, the board 3285 cm^{-1} stretching represents the amide bond and medium peaks at 1605 $cm^{-1}$and 608 cm^{-1}, the C–N minor stretching band observed at 1153 cm^{-1} (Hou et al., 2015) and 1040 cm^{-1} represents the functional group of C-O-C of HA. The Ce6 spectrum depicted as a green line shows a strong stretching vibration peak of the carboxyl group at 1709 cm^{-1} (Gladkova et al., 2010), characteristics of O–H bands were observed at 3285 cm^{-1} and 1234 cm^{-1}, and the band range of 2964 $cm^{-1}$and 1432 cm^{-1} indicates the C–H bond.

The FTIR spectrum (pink line) of SWCNTs-HA illustrates peaks at 2323 cm^{-1} (C=C) that confirm the presence of basic functional units of a strong carbon absorption bond peak of SWCNTs, and the peaks at 1066 cm^{-1} confirm the presence of the COC functional group of HA (Kumar et al., 2015). The synthesised nanobiocomposite spectrum was depicted as a blue line; it showed the characteristic peaks of SWCNTs, HA and Ce6 with minor band shifts due to the functionalisation process. These results indicated the presence of the functional groups, the carboxyl amide bonds spectrum vibrations of SWCNTs, HA, and Ce6 were seen in the synthesised nanobiocomposite.

4.2.4. X-ray diffraction analysis

The crystallinity and structural properties of the nanosized particles were analysed using X-ray diffraction study. The obtained XRD results were compared with Joint Committee on Power Diffraction Standards (JCPDS) numbers. Both SWCNTs and SWCNTs-HA-Ce6 were deposited on a crystal silicon wafer for XRD analysis. The XRD patterns of the SWCNTs are shown in Figure 4.5 and indicate that the characteristic peak at 26.3° corresponds to C (002) planes, according to JCPDS # 751621 reflecting graphite.

The plane 002 indicates the presence of SP^2 bonded carbon arrangements of SWCNTs (Kumar et al., 2018). For the synthesised nanobiocomposite, there was a mild shift at 25.8° and the intensity of peak was less characteristic in the plane

002. This may be due to the coupling of HA and Ce6 on the surface of SWCNTs, and there were changes observed in the crystalline nature of the nanobiocomposite. These results confirm the addition of HA and Ce6 on the SWCNTs.

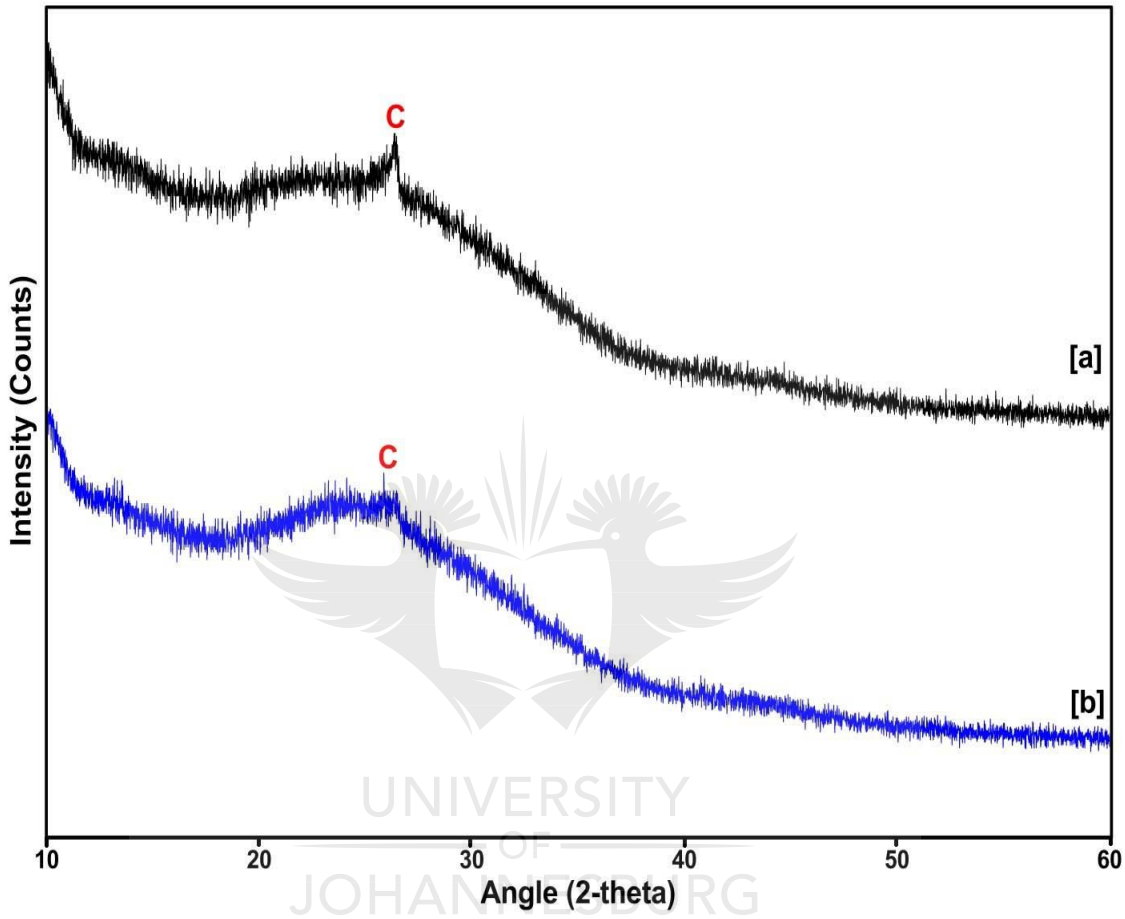

Figure 4. 5 X-ray diffraction pattern of [a] SWCNTs, [b] SWCNTs-HA-Ce6.

4.2.5. Zeta potential and particle size analysis by DLS method

The zeta potential and particle size distribution were studied using the dynamic laser scattering technique (DLS) and the results are presented in Figure 4.6. Zeta potential measurements were used to characterise the surface charge and physical stability of the system. Particle size distribution was used to measure the size of the newly synthesised nanobiocomposite and in this study we compared the initial size of SWCNTs to the synthesised SWCNTs-HA-Ce6.

The average size of the particles recorded was approximately 191 ± 4.6 nm for SWCNTs and 203 ± 6.6 nm for SWCNTs-HA-Ce6. The size of the

nanobiocomposite increased due the coupling of HA and Ce6 molecules. The zeta potential analysis for SWCNTs was −17.8 ± 1.2 mV and for SWCNTs-HA-Ce6, it was −18.9 ± 1 mV. These results indicate that the SWCNTs and synthesized nanobiocomposite is stable. The stability of the nanoparticles is a crucial part of newly synthesised drug delivery systems, the zeta potential results strongly indicating the stability of SWCNTs-HA-Ce6.

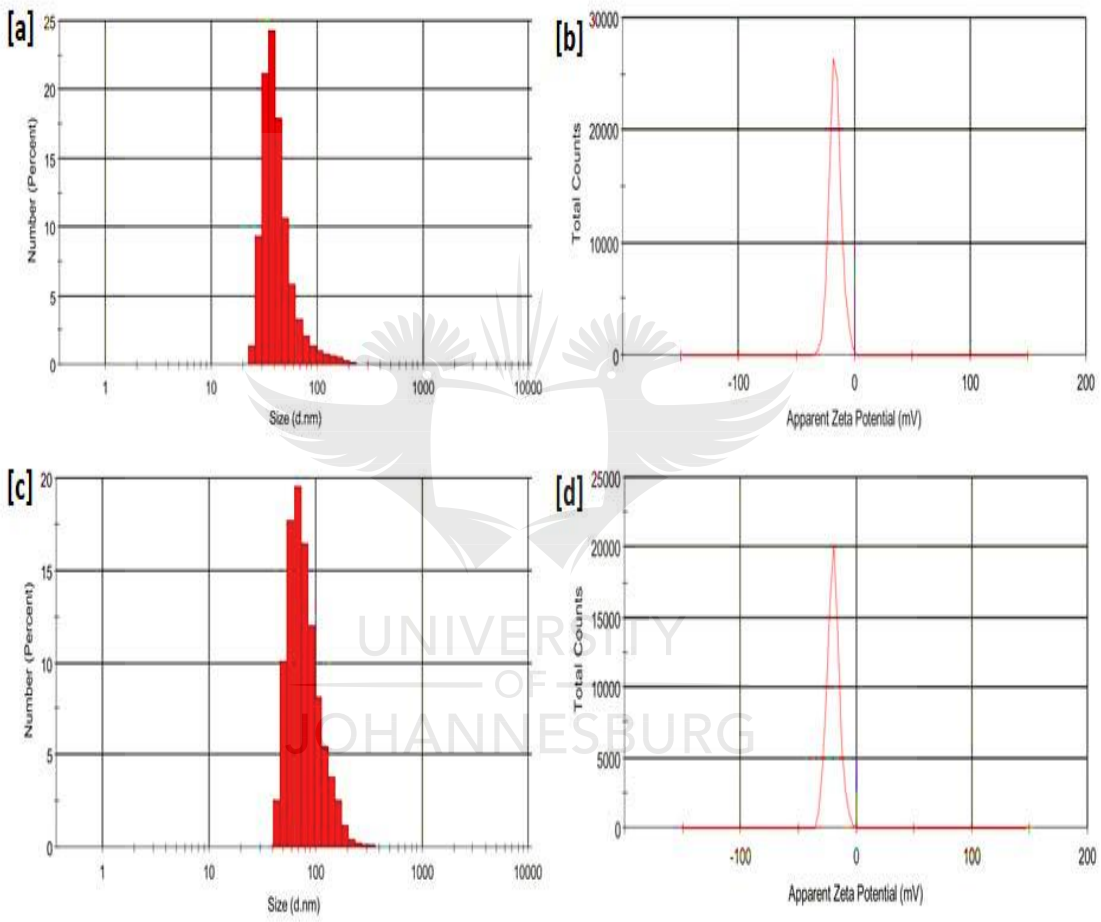

Figure 4. 6 Dynamic laser scattering technique for SWCNTs and SWCNTs-HA-Ce6. [a] particle size for SWCNTs [b] zeta potential for SWCNTs [c] particle size for SWCNTs-HA-Ce6 [d] zeta potential for SWCNTs-HA-Ce6.

4.2.6. High-resolution transmission electron microscope (HR-TEM)

High-resolution transmission electron microscope technique reveals the structure of nanosized particles, by passing the electron beam on the specimen to form the image of the object. Figure 4.7 shows the HRTEM images of SWCNTs, HA and synthesised SWCNTs-HA-Ce6.

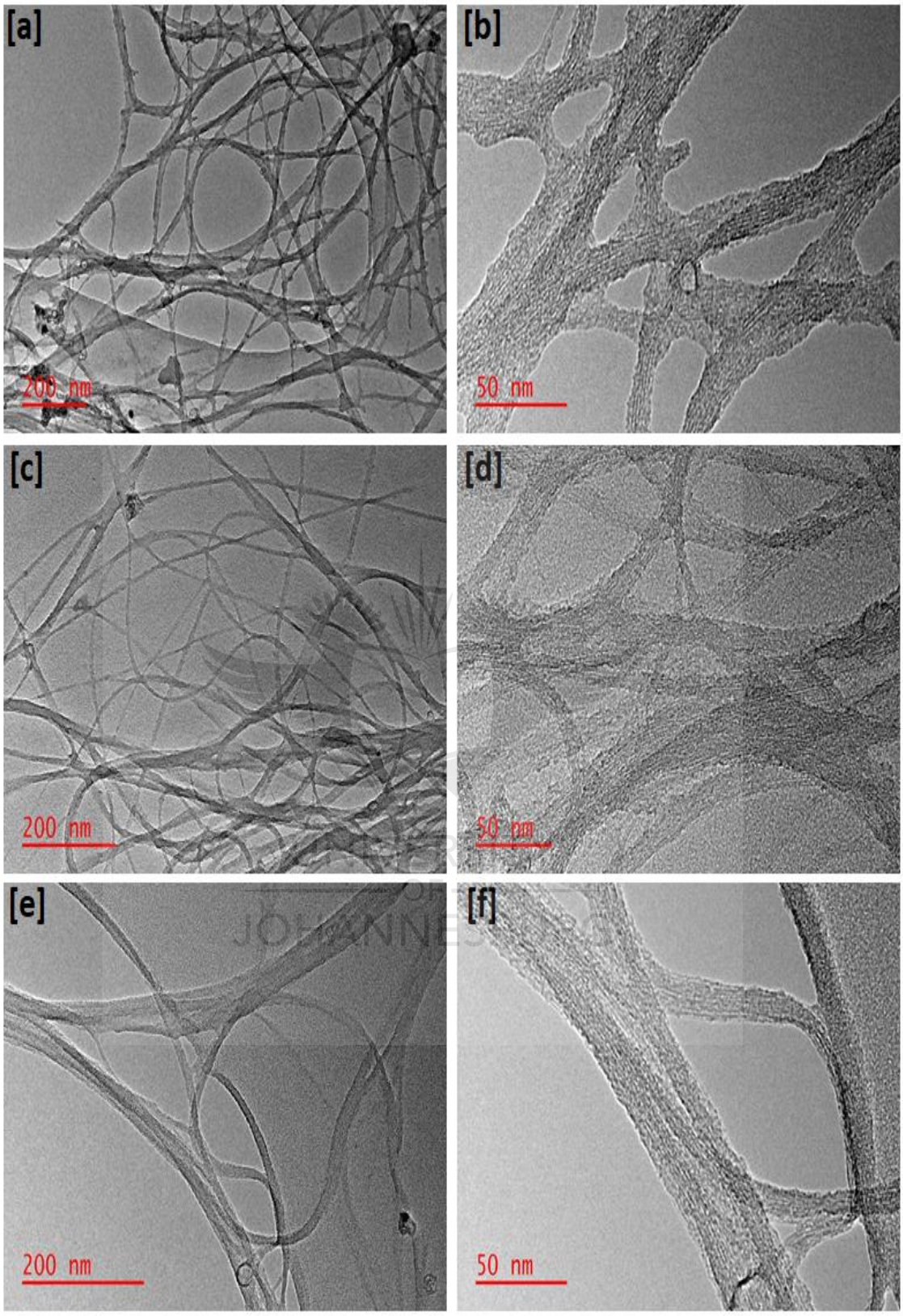

Figure 4. 7 Transmission electron microscope (TEM) images of [a] SWCNTs at 200 nm [b] SWCNTs at 50 nm [c] SWCNTs-HA at 200 nm [d] SWCNTs -HA 50 nm [e] SWCNTs-HA-Ce6 at 200 nm [f] SWCNTs-HA-Ce6 at 50 nm.

Figure 4.7a and c showed HRTEM images of SWCNTs at low and higher magnifications as can be seen by the scale bar of 200 nm and 50 nm, respectively. It shows that the SWCNTs were looks mostly smooth in surface, nanotubes were clumped together, and the sidewalls of the nanotubes are distinctly visible and free from aggregation (Xiao et al., 2012). Figure 4.7c & d showed the HRTEM images of SWCNTs-HA at low and higher magnifications respectively and Figure 4.7 e & f showed the HRTEM images of SWCNTs-HA-Ce6 at low and higher magnifications respectively. In Figure 4.7 d and f, the surface of the nanotubes looks rough and the size of the sidewalls of the nanotubes were showed slightly larger than the plain SWCNTs (Figure 4.7b) and it may be due to the attachment of HA and Ce6 particles. The rougher surface morphology due to the attachment of HA molecule on the outer layer of SWCNTs. Then the Ce6 coated on the SWCNTs by π-π interactions on the walls of the SWCNTs. The structural form of SWCNTs-HA-Ce6 (Figure 4.7 e and f) morphology showed almost similar structure of SWCNTs (Figure 4.7 a and b) and no breaking or defects in the nanotubes. It elucidates that the structural morphology of SWCNTs are maintained throughout the synthesis process (Yao et al., 2014).

4.3. Stability Analysis of Synthesised Nanobiocomposite

The stability of Ce6 loaded nanobiocomposite in physiological environment (pH 7.4) is considered as an important criterion in drug delivery studies. Similarly, the stability potential of released Ce6 from the nanobiocomposite in the intracellular environment (pH 5.5) facilitate the higher therapeutic activity of photodynamic therapy (Yang et al., 2019). The comparative stability of both free Ce6 and Ce6 loaded nanobiocomposite under both physiological and intracellular pH conditions for 24 h was studied. The results are displayed in Figure 4.8 in pH 5.5, the stability free Ce6 was extensively reduced to 66.47 ± 4.53% in 2 h which continuously declined to 0.67 ± 2.2% at the end of the experiment, whereas the SWCNTs-HA-Ce6 was reduced to 88.43 ± 2.87 % in 2 h and showed 54.13 ± 1.3% stable at the end of the experiment. In pH 7.4, the stability of free Ce6 was around 91.7 ± 0.63 % in 2 h and it was rapidly declined to 9.13 ± 5.34 % at the end of the experiment whereas the SWCNTs-HA-Ce6 showed 92.2 ± 3.62 % in

2 h and it considerably stable around 72.5 ± 2.89 % at the end of the experiment. These results suggested that the synthesized SWCNTs-HA-Ce6 was capable of protecting the stability of loaded Ce6 in both physiological and intracellular pH conditions.

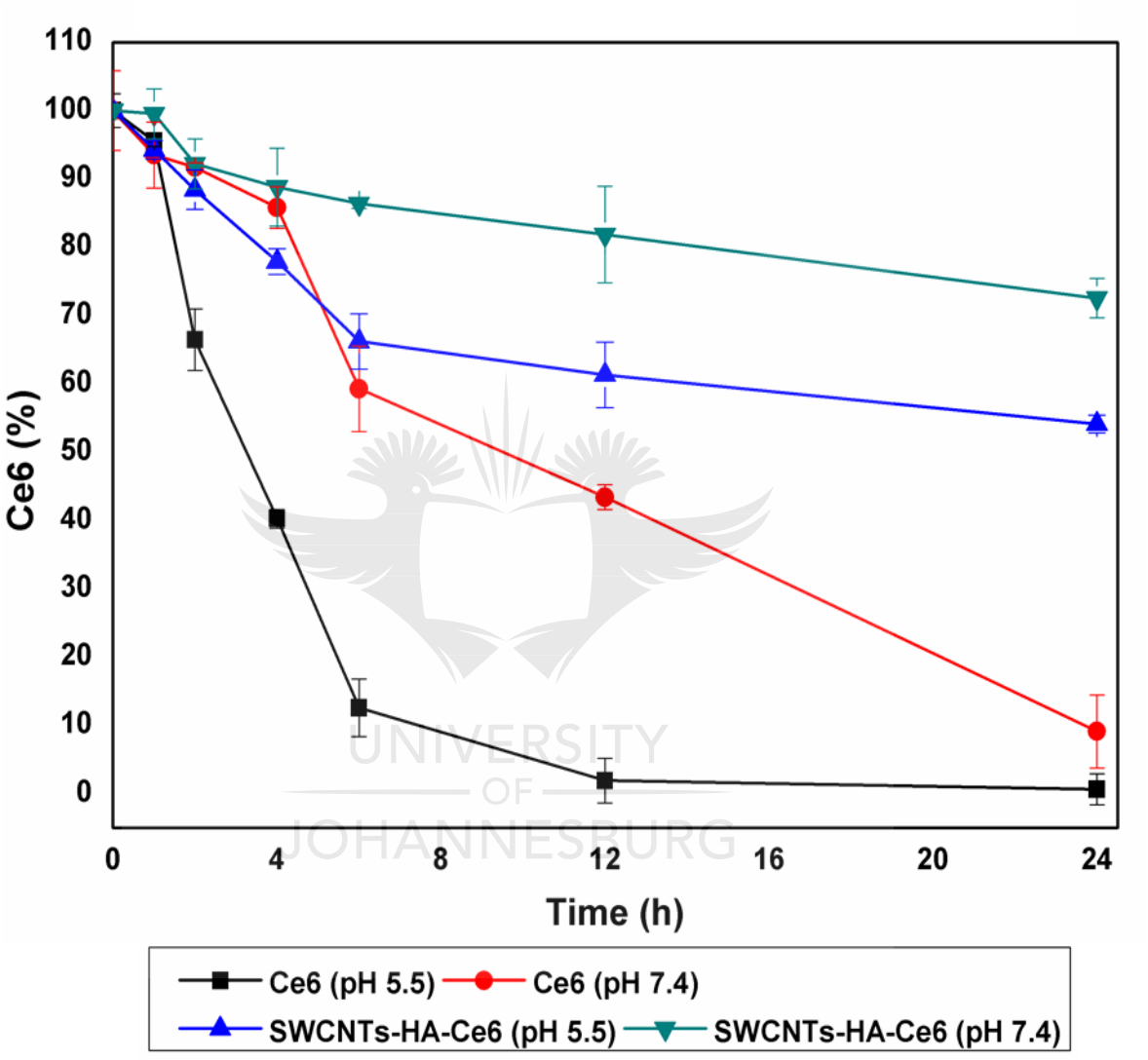

Figure 4. 8 Stability studies of free Ce6 and SWCNTs-HA-Ce6 in two different pH conditions (pH 5.5 & 7.4).

4.4. Ce6 Loading and *In Vitro* Ce6 Release Study

The loading efficiency of Ce6 on SWCNTs-HA were calculated using UV-vis spectroscopy. The non-covalent bonding of Ce6 due to π-π interaction of both

molecules. SWCNTs has large surface area, loading efficiency of Ce6 achieved at 70% calculated using the PS loading efficiency formulae mentioned in 3.3 (Sundaram et al., 2020a). The results of in vitro Ce6 release studies in both intracellular (pH 5.5) and physiological (pH 7.4) conditions are shown in Figure 4.9. The release behaviour of Ce6 was observed over a period of 4 days (96 hours) at different time intervals. The results revealed that the Ce6 release behaviour in pH 5.5 was faster as compared to pH 7.4. The burst release of Ce6 in pH 5.5 was observed around 33.8 ± 4.0 % for initial 6 h whereas it was only 13.6 ± 0.69 % in pH 7.4. The slow and sustained release pattern of Ce6 from SWCNTs-HA-Ce6 was observed in the remaining hours. The release percentage of Ce6 was 76.8 ± 2.58 % in pH 5.5, whereas it was 34.8 ± 7.45 in pH 7.4 at the end of the experiment.

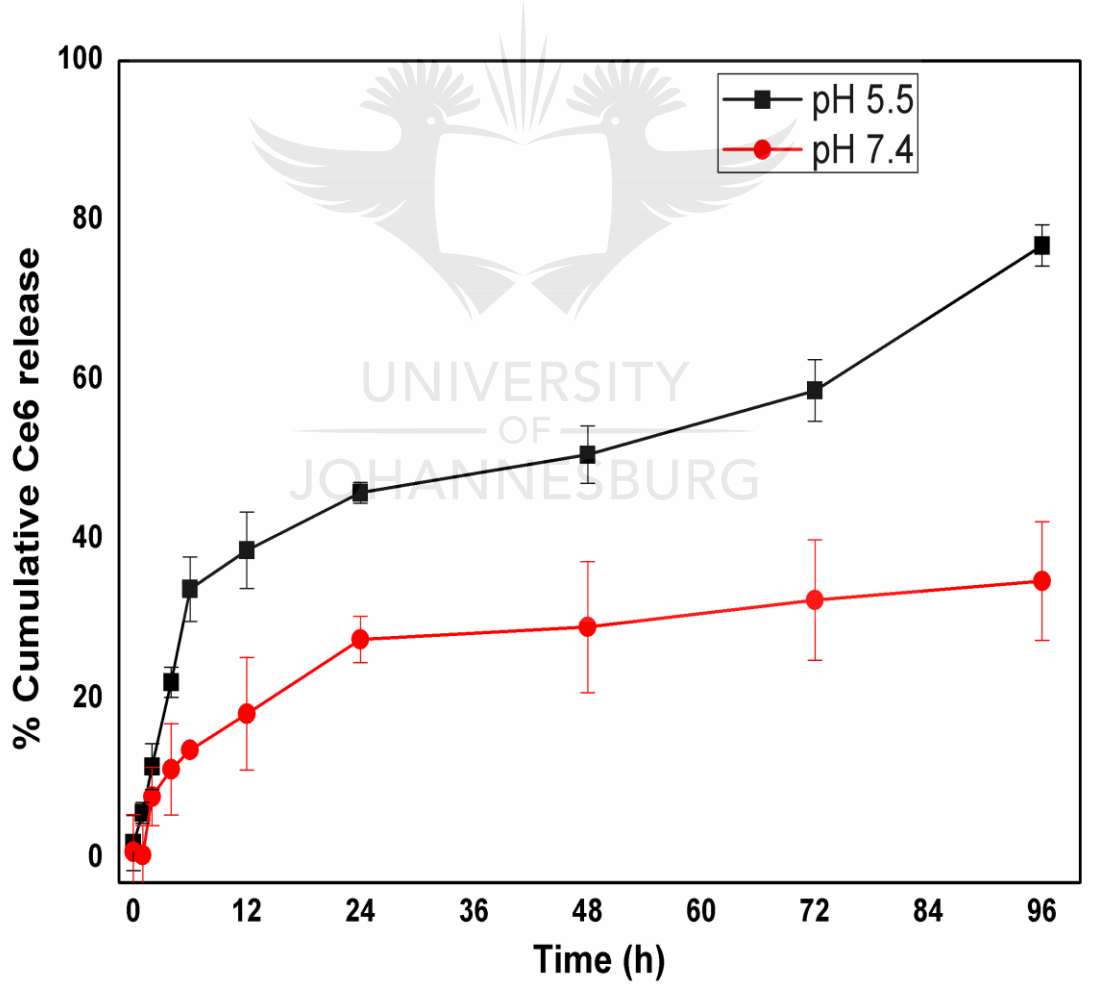

Figure 4. 9 *In vitro* release of Ce6 from nanobiocomposite (SWCNTs-HA-Ce6) in PBS at pH 7.4 & 5.5.

To study the mechanism of release behaviour, the release study results from both pH 5.5 and 7.4 were substituted separately in different mathematical model equations and the obtained results are illustrated in Figure 4.10 and 4.11. In both pH 5.5 and 7.4 the higher R2 value was observed around 0.90855 and 0.90047 respectively in Higuchi models than compared to other studied models.

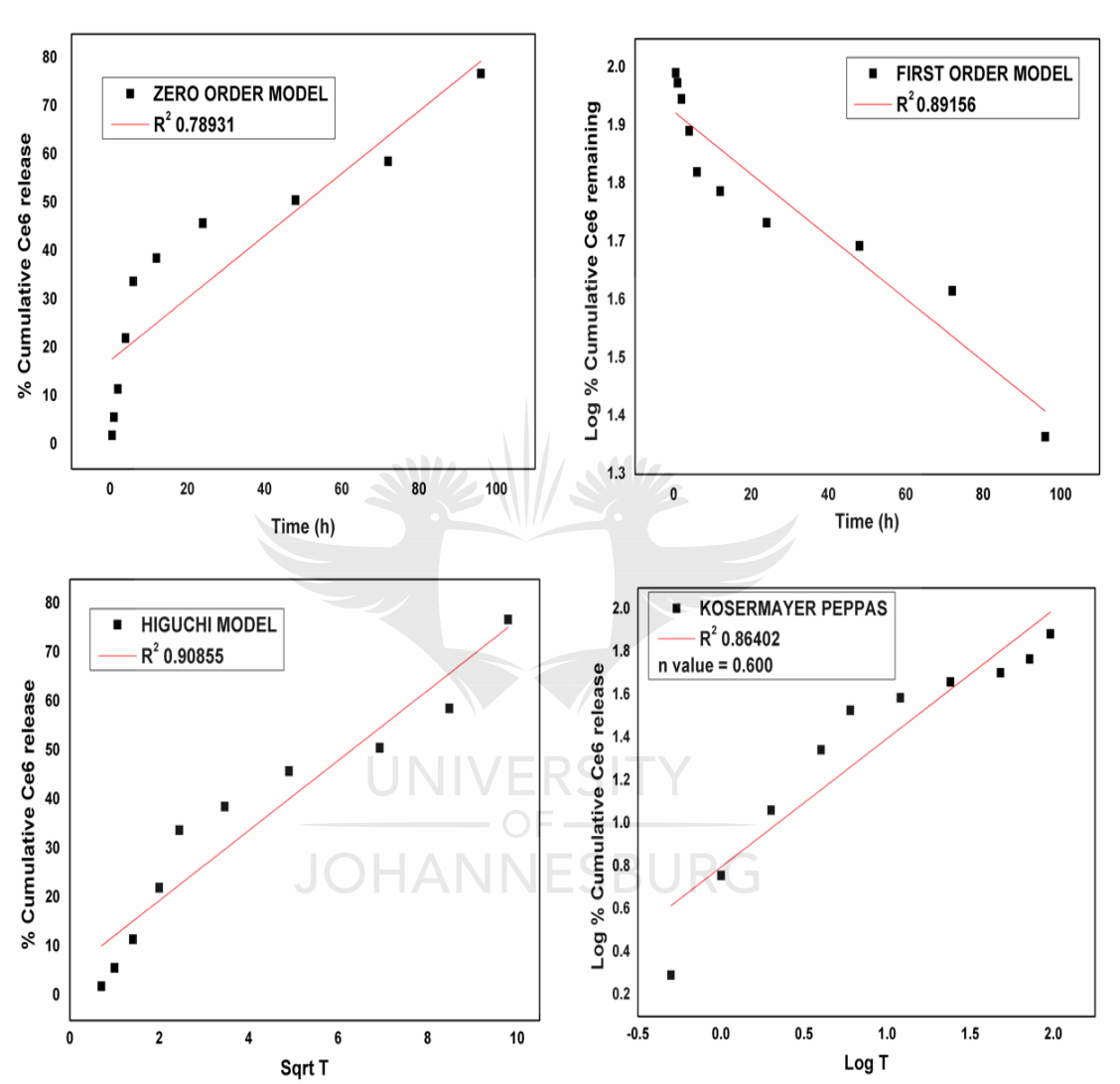

Figure 4. 10 Release kinetic profiles obtained for SWCNTs-HA-Ce6 in pH 5.5. [a] Zero order model, [b] First order model, [c] Higuchi model, and [d] Korsmeyer-Peppas model.

It indicates that the Ce6 release pattern from the SWCNTs-HA-Ce6 followed Higuchi kinetic release. In order to understand the mechanism of Ce6 release, we have applied the Korsmeyer-Peppas equation and the observed release exponent ‘n’ value was found to be 0.600 (in pH 5.5) and 0.742 (in pH 7.4). According to Korsmeyer-Peppas equation, the exponent ‘n’ value is used to study

the different release mechanisms. If the ‘n’ value is 0.5, it indicate Fickian diffusion; if the ‘n’ value is in between 0.45<=0.89, it indicate Non-Fickian transport; if the ‘n’ value is 0.89, it indicate case II transport and the ‘n’ value is higher than 0.89, it indicate super case II transport (Gouda et al., 2017). In our study, the observed release exponent value of ‘n’ occurred between the range of >0.45 and <0.89 in both pH 5.5 and 7.4. It indicate that the Ce6 release mechanism was followed by Non-Fickian transport mechanism. Briefly, it was controlled by more than one process, it may be the coupling of fickian diffusion and polymer matrix relaxation (Chouhan et al., 2009).

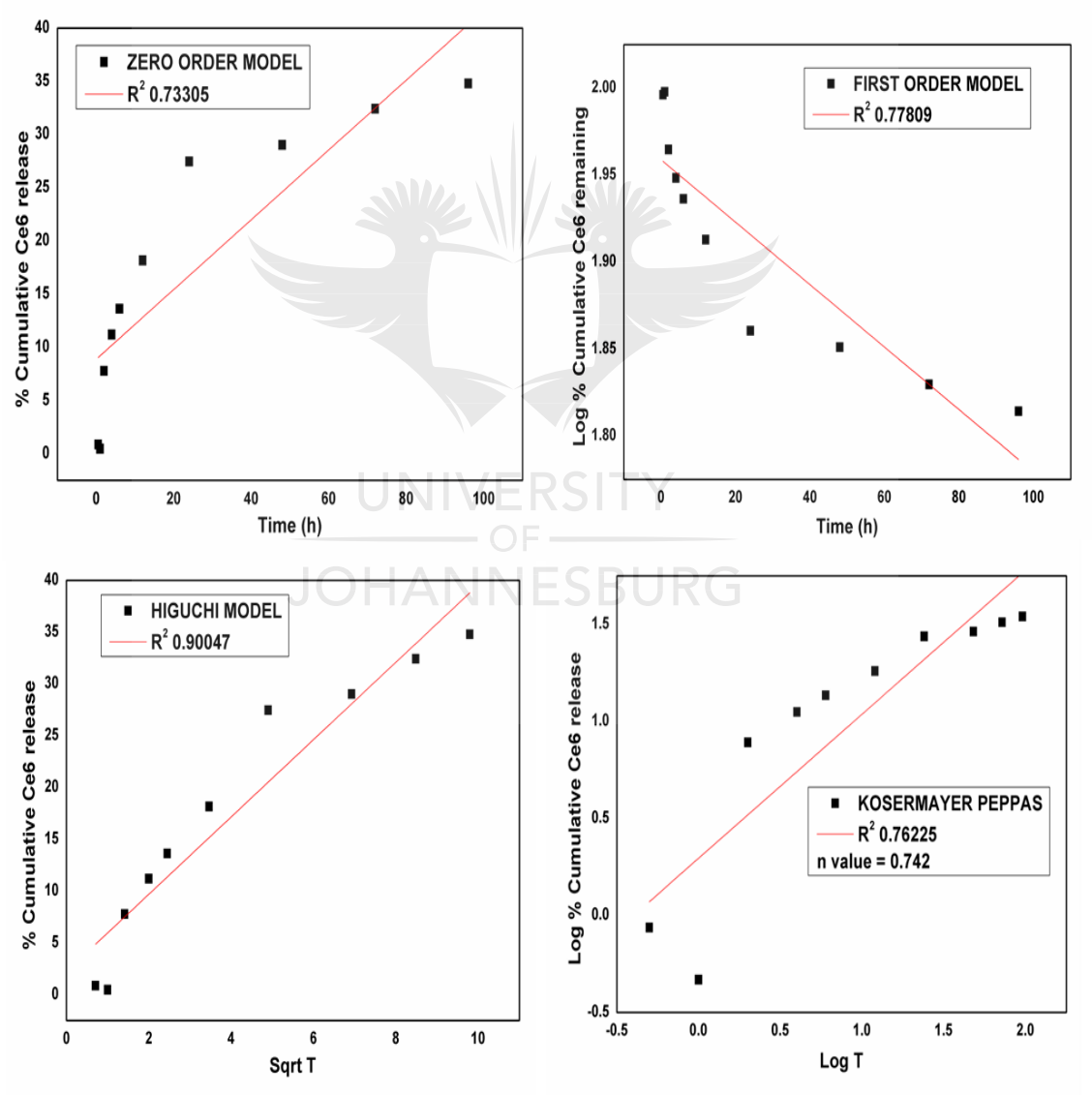

Figure 4. 11 Release kinetic profiles obtained for SWCNTs-HA-Ce6 in pH 7.4. [a] Zero order model, [b] First order model, [c] Higuchi model, and [d] Korsmeyer-Peppas model.

4.5. Intracellular Localisation of SWCNTs-HA-Ce6 on Colon Cancer Cell Lines

Cellular localisation of synthesised SWCNTs-HA-Ce6 on Caco-2 cells were analysed using MitoTracker™ green FM and LysoTracker™ green, the autofluorescence of Ce6 and DAPI used as nuclei counter staining viewed under Zeiss Carl fluorescence microscope. Cellular localization was performed to investigate the cause and efficacy of SWCNTs-HA-Ce6 and their photo-induced cell death on colon cancer cell lines. The intensity of fluorescence was gradually increased based on the incubation time (Luo et al., 2015). The fluorescence intensity and distribution of SWCNTs-HA-Ce6 inside the Caco-2 cells were imaged after 12 h of incubation.

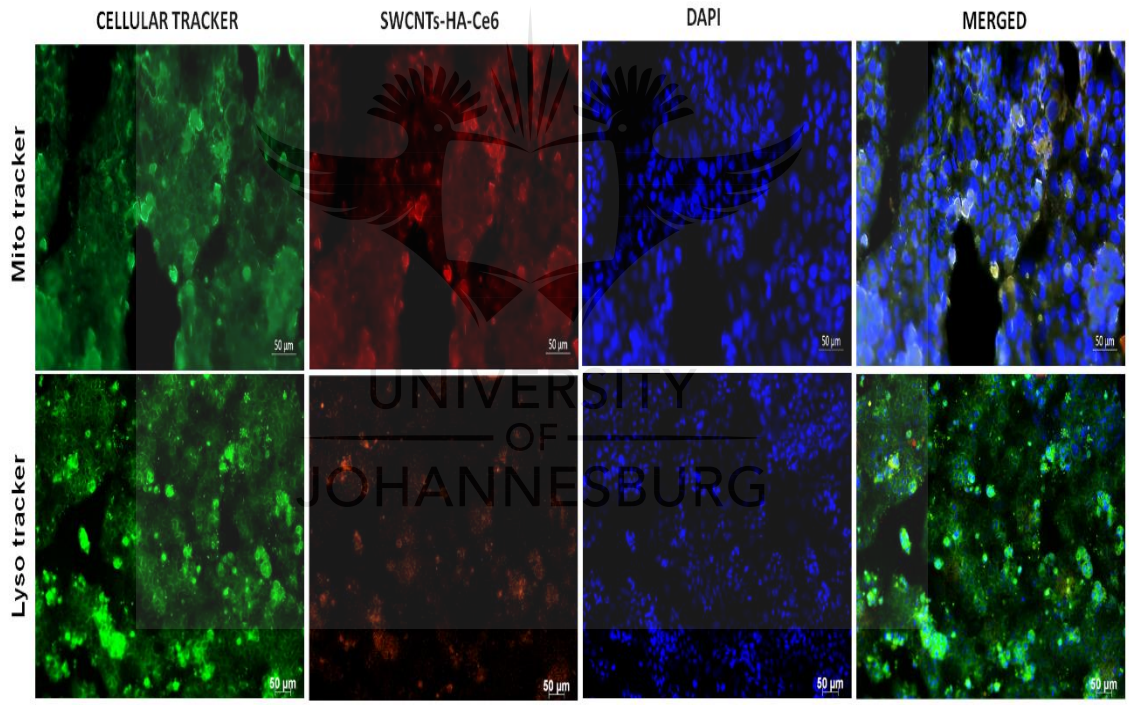

Figure 4. 12 Intracellular localisation of SWCNTs-HA-Ce6 using mito and lysotracker. Scale bar 50 µm.

Cellular localisation of Ce6 was observed in red fluorescence, the nucleus was observed in blue fluorescence, and the mitochondrial and lysosome tracker were observed in green fluorescence. The results are shown in Figure 4.12 and the captured images clearly show that there was an increased fluorescence intensity

and distribution of Ce6 loaded nanobiocomposite was observed in the mitochondrial region compared to the lysosome region. The synthesized SWCNTs-HA-Ce6 were found within the intracellular region compared to extracellular region, and the Mito tracker staining revealed that the SWCNTs-HA-Ce6 were predominantly localized at the mitochondrial region than lysosomes. Luo et al. 2015 have previously reported the similar cellular localization of Ce6.

4.6. PDT Using SWCNTs-HA-Ce6 on Colon Cancer Cell Lines

4.6.1. Morphology

The qualitative and preliminary confirmation of cellular viability and cell death were analysed from cellular morphology using captured microscopic images. The IC50 concentration of SWCNTs-HA-Ce6 were 2.56 µg/mL and used it throughout this study (Sundaram et al, 2020a). The morphological observation of treated and untreated cells was captured using inverted light microscope for 0 h and 24 h and the images are shown in Figure 4.13. The close observation of Figure 4.13a revealed that there was a full confluence of cells at 0 and 24 h in controls and cells treated with SWCNTs, Ce6 and SWCNTs-HA-Ce6 at 0 J/cm^2. In Figure 4.13b and c revealed that there was a significant change in the cellular morphology of Caco-2 cells and pronounced more cell death was observed at 24 h in the cells treated with SWCNTs, Ce6 and SWCNTs-HA-Ce6 at both 5 and 10 J/cm^2. It was previously reported that the morphological characteristics of the apoptotic cells were shown increased vacuoles, apoptotic structure, nuclear damage, change in shapes and detachment of cells (Hacker et al., 2000).

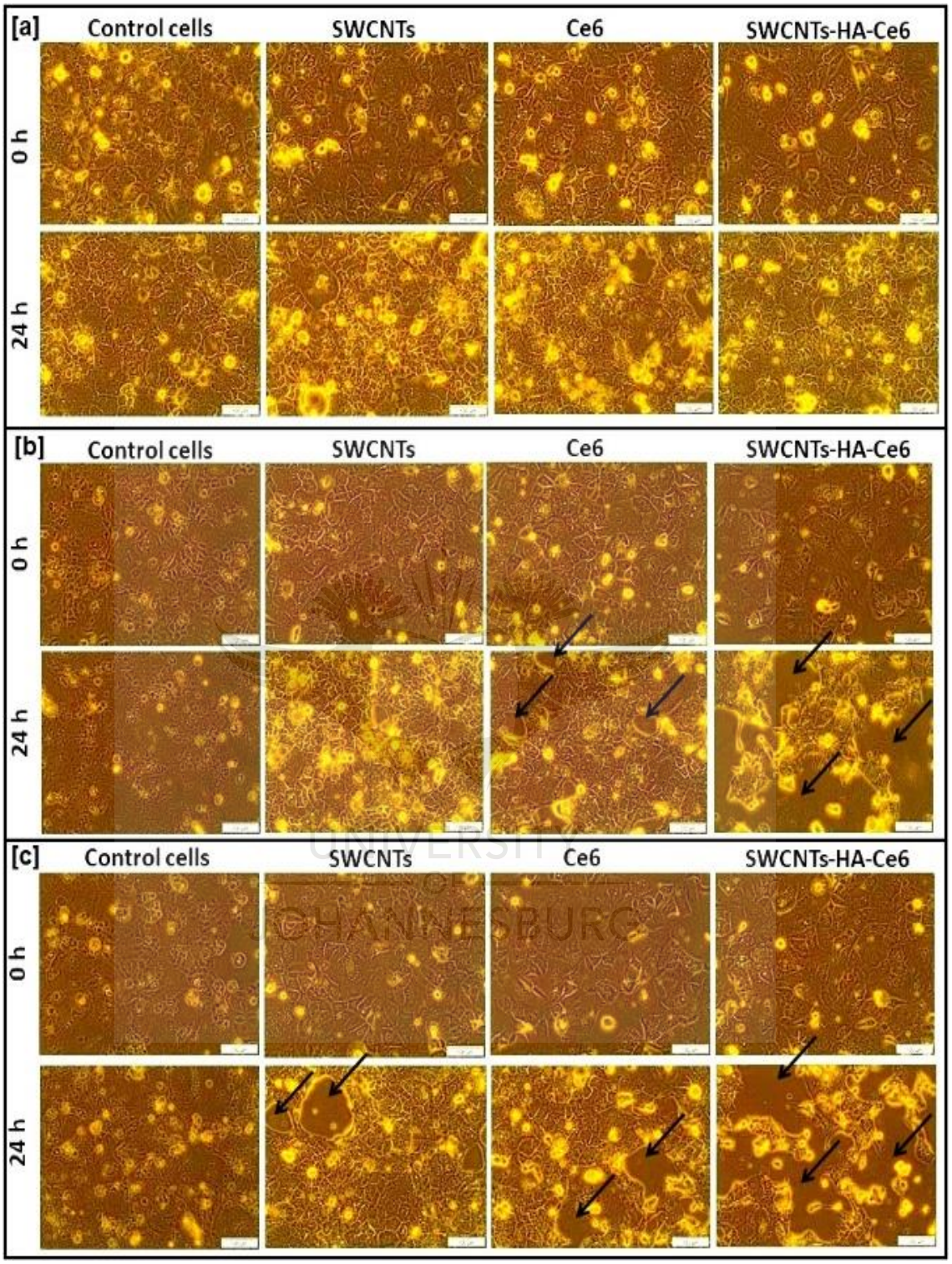

Figure 4. 13 Microscopic images of treated and untreated colon cancer cells. [a] untreated cells of 0 h and 24 h, [b] 0 h and 24 h of laser irradiated at 660 nm, 5 J/cm^2, [c] 0 h and 24 h of laser irradiated at 660 nm, 10 J/cm^2.

4.6.2 Cytotoxicity analysis using Lactate dehydrogenase assay.

The quantitative analysis of cell death was performed using LDH cytotoxicity assay kit. All the samples from 0, 5 and 10 J/cm^2 at 24h were analysed to evaluate the cytotoxic behaviour of SWCNTs, Ce6 and SWCNTs-HA-Ce6. After the successful PDT treatment, the damaged cancer cell was released LDH enzyme into the cell culture media, and these media were analysed using LDH cytotoxicity assay kit. The measured absorbance value of untreated cells was kept as a control. Cytotoxicity assay results are shown in Figure 4.14, the observed results revealed that the non-irradiated 0 J/cm^2 cells showed lower percentage of cytotoxic behaviour for SWCNTs 9%, Ce6 12% and SWCNTs-HA-Ce6 18%. SWCNTs-HA-Ce6 treated cells showed the cytotoxicity of 84.9% at 10 J/cm^2 and 77% at 5 J/cm^2. The results showed that the 10 J/cm^2 treated cells had better cytotoxic behaviour compared to 5 J/cm^2 laser treatment. In addition, the study revealed that the newly synthesised nanobiocomposite showed an improvement in cytotoxicity compared with free Ce6 treatment in both 5 J/cm^2 (63 %) and 10 J/cm^2 (72.3%).

This could be a result of the enhanced bioavailability and uptake profile of released Ce6 from nanobiocomposite, which led to the increased cytotoxic behaviour of SWCNTs-HA-Ce6 compared to free Ce6. The study also confirmed that the combined effect of laser irradiation (both 5 and 10 J/cm^2) and nanobiocomposite treatment effectively inhibits the proliferation of Caco-2 cells. A comparison between 5 and 10 J/cm^2 using the results of SWCNTs-HA-Ce6 was performed at 24 h, and even though an increase in cytotoxicity was seen, there was no statistically significant difference was observed. Furthermore, we performed a comparison between Ce6 and SWCNTs-HA-Ce6 at both 5 and 10 J/cm^2 and these results showed that no significant differences were observed at 5 J/cm^2 ($p = 0.118$), but in 10 J/cm^2 there was a significant increase in SWCNTs-HA-Ce6 compared to Ce6 ($p = 0.041$) (Sundaram et al, 2020a).

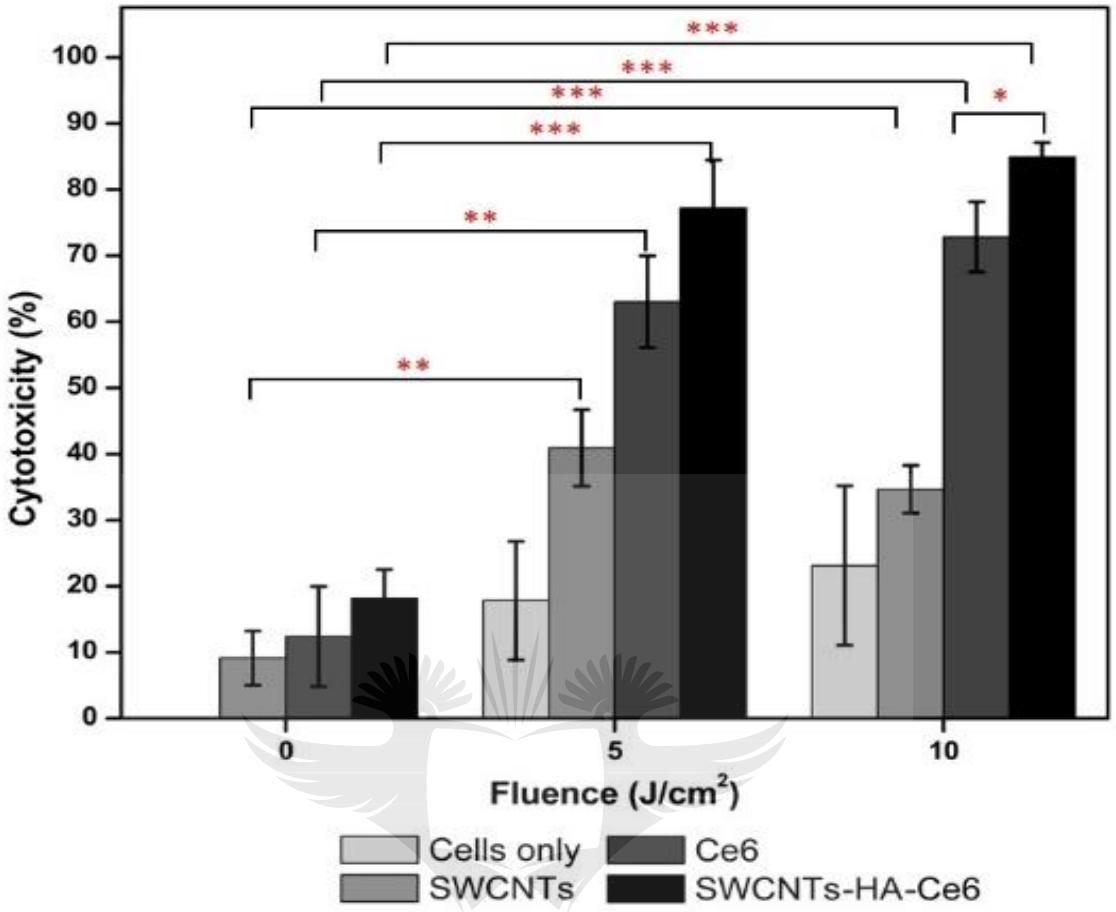

Figure 4. 14 The cytotoxicity effects of SWCNTs, Ce6, SWCNTs-HA-Ce6 on Caco-2 cells determined by LDH assay. Significance is shown as * p < 0.05; ** p < 0.01; *** p 0.001.

4.6.3 Cell death studies

The cell apoptosis profile of laser irradiated cells was analysed using flow cytometry by FITC-Annexin V and PI staining method. The apoptotic inducing efficacy of nanobiocomposite after 24 h of PDT treatment was evaluated in this study. The percentage population of live cells (bottom left), early stage of apoptosis (bottom right), late stage of apoptosis (top right) and dead cells (top left) are represented in four different quadrant and the images are illustrated in Figure 4.15. The early and late stages apoptosis from treated groups were compared to control and the p-values were calculated.

In early stage apoptotic cells, a statistical comparison between control and SWCNTs, Ce6 and SWCNTs-HA-Ce6 was performed. The 0 J/cm^2 treated samples results showed that there was a significant difference observed in Ce6 ($p = 0.018$) and SWCNTs-HA-Ce6 ($p = 0.006$), whereas there was no significant difference in SWCNTs ($p = 0.175$); the 5 J/cm^2 treated samples results showed that there was a significant differences observed in SWCNTs ($p = 0.029$) and SWCNTs-HA-Ce6 ($p = 0.022$) whereas there was no significant differences in Ce6 ($p = 0.291$); and 10 J/cm^2 treated samples results showed that there was no significant differences observed in SWCNTs ($p = 0.432$), Ce6 ($p = 0.41$) and SWCNTs-HA-Ce6 ($p = 0.076$).

Similarly, a statistical comparison was performed between control and SWCNTs, Ce6 and SWCNTs-HA-Ce6 in late stage apoptotic cells and the 0 J/cm^2 treated samples results showed that there was a significant differences observed in Ce6 ($p = 0.007$) and SWCNTs-HA-Ce6 ($p = 0.005$), whereas there was no significant differences in SWCNTs ($p = 0.207$); the 5 J/cm^2 treated samples results showed that there was a significant difference observed in SWCNTs-HA-Ce6 ($p = 0.007$), whereas there was no significant difference in SWCNTs ($p = 0.164$) and Ce6 ($p = 0.201$); and 10 J/cm^2 treated samples results showed that there was a significant difference observed in Ce6 ($p = 0.012$), whereas there was no significant difference in SWCNTs ($p = 0.137$) and SWCNTs-HA-Ce6 ($p = 0.177$).

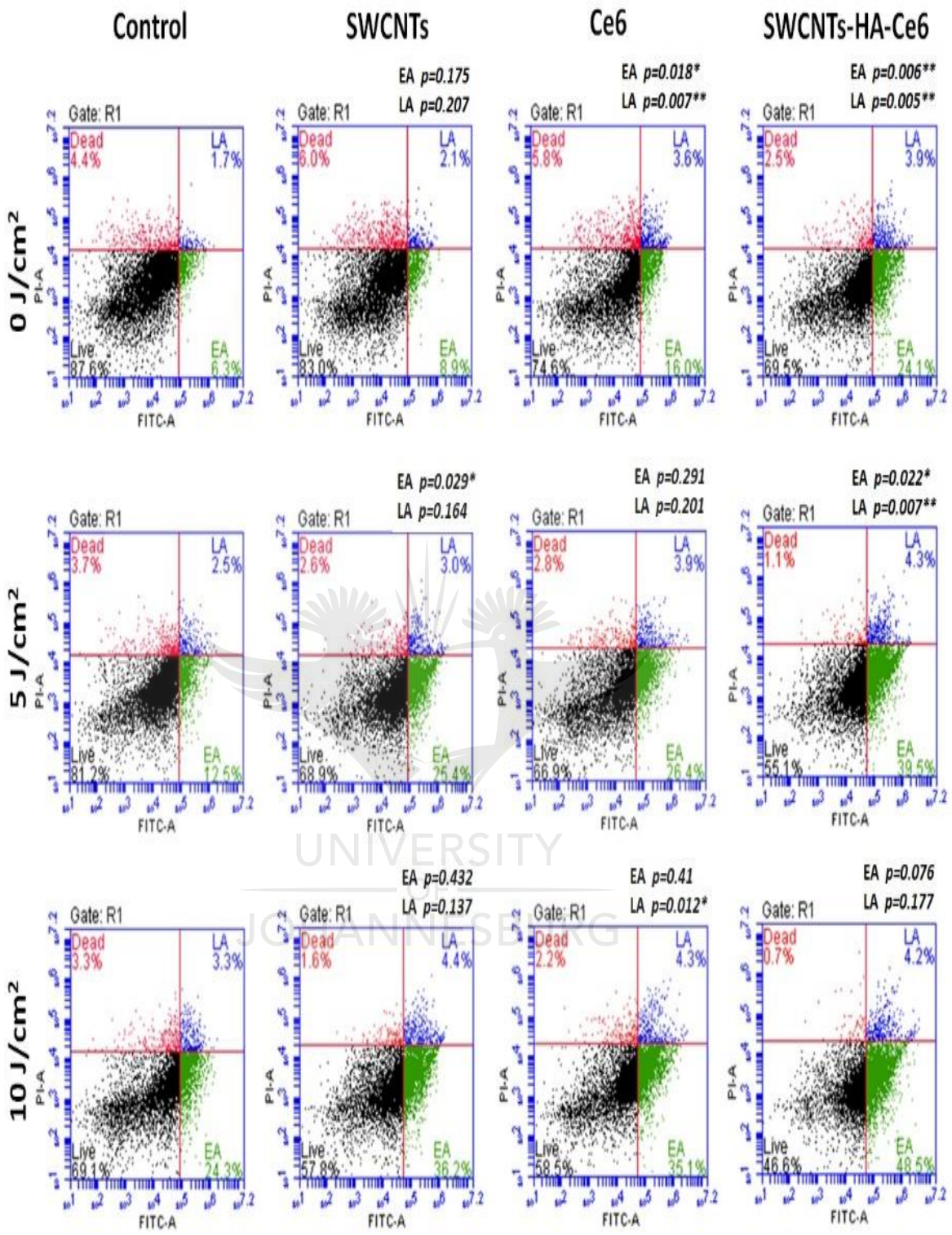

Figure 4. 15 Flow cytometry analysis using Annexin V PI for cell death, laser irradiated at 660 nm of fluence 0, 5 and 10 J/cm^2 of SWCNTs, Ce6, SWCNTs-HA-Ce6 on Caco-2 cells incubated for 24 h.

4.7 Isolation and Characterisation of Colon Cancer Stem Cells From Caco-2 Cell Lines.

The colon cancer stem cells were isolated from Caco-2 colon cancer cell lines by magnetic bead isolation technique using CD133, CD44 and CD24 cell surface markers. It has been reported that CD133+, CD44+ and CD24+ markers from colon cancer cells were tumorigenic stem cells markers (Sahlberg et al., 2014). CSCs isolated from solid tumour have the potential to initiate tumour formation as well as differentiate and it has been demonstrated in the in vivo model (Chen et al., 2013). There are different studies explained the isolation and identification of CSCs using different markers, gene expression and cell signalling pathways (Kim et al., 2017; Jaggupilli et al., 2012). The most common method for isolating CSCs is to isolation side population cells based on the protein markers or cluster of differentiation markers, expressed on the outer surface of the cells (Khan et al., 2015). In this research study, isolation of side population from Caco-2 cells using MACs magnetic microbeads technique by CD133+, CD44+ and CD24+ markers. The characterization methods used to identify the isolated side population cells including CSCs spheroid morphology through microscopy, flow cytometry and immunofluorescence staining.

4.7.1 Spheroid formation of isolated CCSCs

Magnetic separated CCSCs were cultured using complete stem cell medium, the cultured cells able to self-renewal of stem cells and CSCs. The cultured cells grown very slow in ultra-low attachment flask. The morphology of the cells captured on day 1, day 2 and day 5 under inverted light microscope are shown in Figure 4.16. The images were confirmed the spheroid formation of isolated CCSCs using CD133, CD44 and CD24 markers. This result strongly suggested that isolated cells possess the characteristics of CSCs in colon cancer cell lines Caco-2. In this study, the isolated side population cells from Caco-2 cells were identified as colon cancer stem cells, which proliferated as mammospheres in in vitro model. The primary mammospheres could be enzymatically degraded into single cell suspension to form secondary mammospheres (Yao et al, 2014).

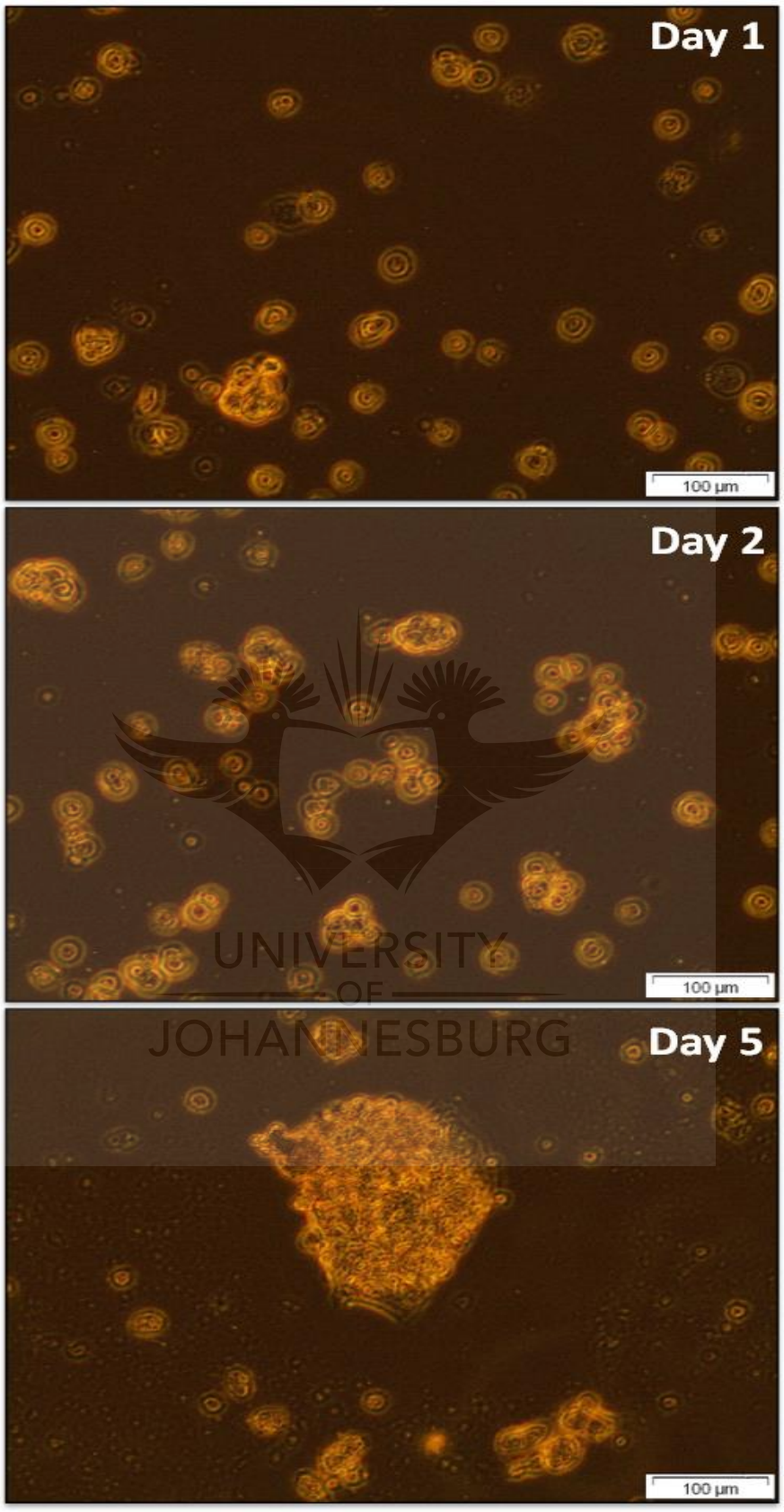

Figure 4. 16 Microscopic images of isolated CCSCs forming spheroid colonies captured on Day1, Day2 and Day 5.

4.7.2 Flow cytometry analysis

The isolated CCSCs from different markers $CD44^+$, $CD133^+$ and $CD24^+$ were analysed with BD Accuri C6 flow cytometry. The side population and non-side populations were stained using the following CD44-PE, CD133-FTIC and CD24-Cy5 antigen antibody conjugation and the details are elaborately mentioned in section 3.9.2. Initially, the primary antibodies conjugated with fluorophore were mixed with the test samples by direct or indirect method before running the flow cytometry. In this experiment, the outlying cells and debris were excluded, and peaks were generated for 10,000 cells. Fluorescence detection using flow cytometry showed that the isolated cells expressed the markers CD133, CD44 and CD24, the negative control comprising of the non-side population showed no fluorescence for all the three markers and the obtained results are given in Figure 4.17. From colorectal cancer tumours isolated side populations are widely distributed with surface antigens CD133, CD44 and CD24 markers (Chu et al., 2009; Sahlberg et al., 2014).

The isolated cells express cell surface markers CD44 were tagged with phycoerythrin (PE) yellow orange region of visible spectrum and fluorescence detected using FL-2 with a 585/40 filter, 488 nm laser, PE maximum excitation at 565 nm, emits at 573 nm. The results showed that CD 44 high expression about 68.8 % in isolated CCSCs. CD 133 were tagged with FTIC shows green region of visible spectrum and fluorescence detected using FL-1 with a 533/30 filter, 488 nm laser, FTIC maximum excitation at 494 nm, emits at 518 nm. CD 133 shows high expression on isolated CCSCs and the results showed about 53.2 %.

CD 24 was tagged with Cy5 shows red region of visible spectrum and fluorescence detected using FL-3 with a 670 LP filter and 488 nm laser used. The maximum excitation of Cy5 at 650 nm and emits at 670 nm. CD 24 markers present on the isolated CCSCs were about 19.6%. The non-side population cells are tagged with CD44-PE, CD133-FTIC and CD24-Cy5 are analysed and the results showed no positive cells. Magnetic bead isolated cells are completely attracted the positive cells, and then the negative cells were collected in the washing process. From this results, successful isolation of CCSCs from Caco-2

cells were confirmed and combination of three markers distinguish that isolated CCSCs are more tumorigenic.

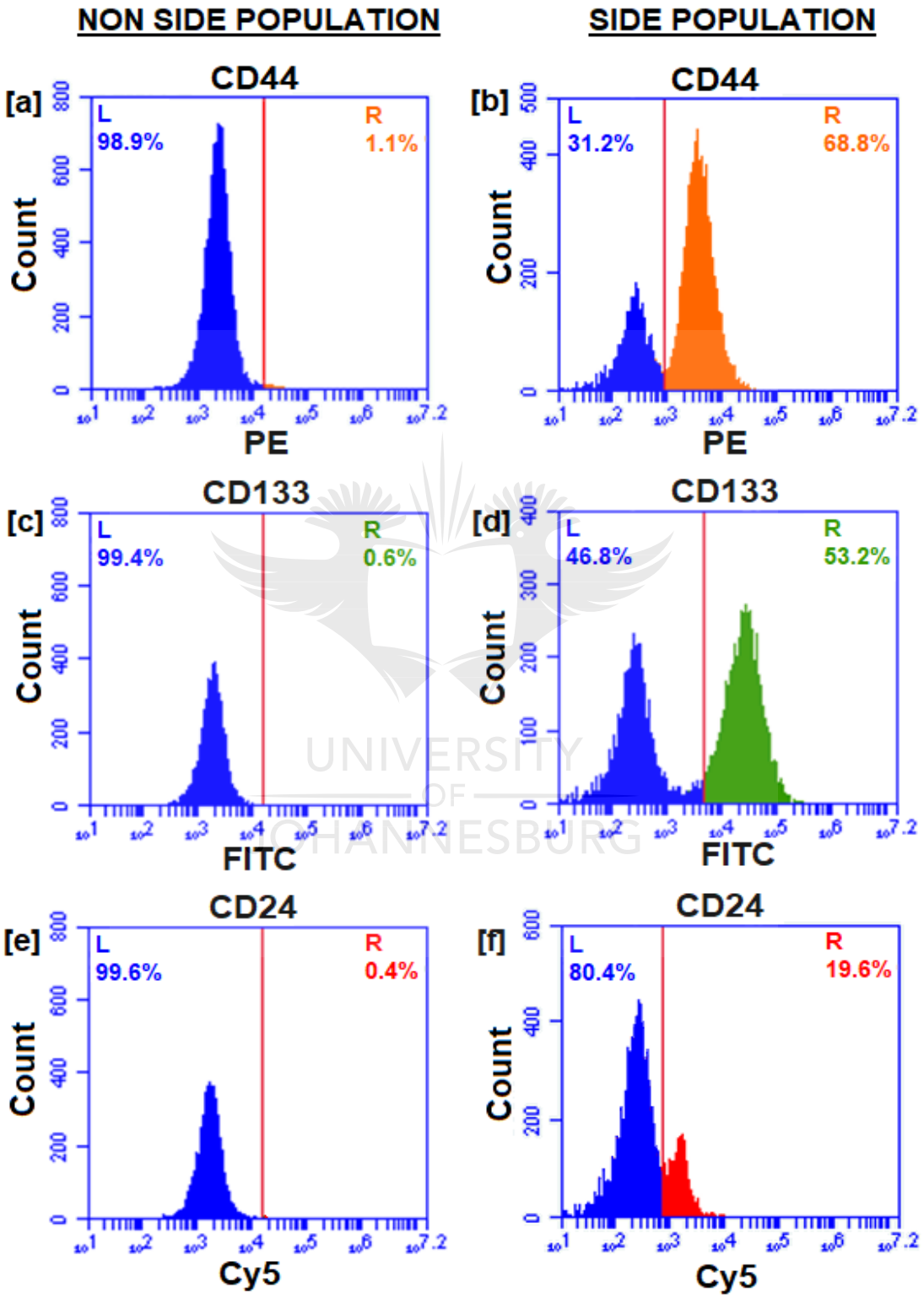

Figure 4. 17 Expression of CD44, CD133 and CD24 surface markers as observed using flow cytometry. [a, c, d- Non side population cells and b, d, f- side population cells].

4.7.3 Immunofluorescence

Immunofluorescence is a method to detect specific antigen antibody interactions to target antigen present within cell using fluorochrome attached antibodies visualised under fluorescence microscope. There are two types of immunofluorescence method: direct and indirect immunofluorescence. Direct method is a primary antibody linked with fluorophore to target specific antigen. Indirect method carried with two antibodies primary and secondary, whereas unlabelled primary antibody targets the antigen in the cell, then the fluorophore labelled secondary antibody recognise the primary antibody and binds to it (Mohan et al., 2008). In this study, we used both direct and indirect immunofluorescence.

The isolated CCSCs were cultured using complete stem cell medium. The adherent culture of isolated CCSCs showed moderate expression of CD133, CD44 and CD24 markers for immunofluorescence were shown in Figure 4.18. CCSCs nuclei were counter stained using DAPI, and the markers CD133-FITC, CD44-PE and CD24-Cy5 by direct and indirect immunofluorescence technique mention in section 3.9.1. CD133 markers are also called Promini-1 (PROM1), transmembrane glycoprotein mainly presents in plasma membrane and overexpressed in CSCs. Many studies reported that CD133 serve as independent marker for prognosis and chemoresistance in colon cancer (Ong et al., 2010; Coco et al., 2012). CD44 and CD24 markers have been widely used or putative markers to isolate CSCs (Slomianyl et al., 2009; Lee et al., 2010). Hyaluronan targeted CD44 receptors expressed on cancer cell surface and contributes to haemorrhage spreads when in contact with L- or P-selectins (Napier et al., 2007). Isolated CCSCs from Caco-2 cells showed the expression of all the three markers CD133, CD44 and CD24 clearly indicated in the presence of fluorescence Cy5, PE and FITC.

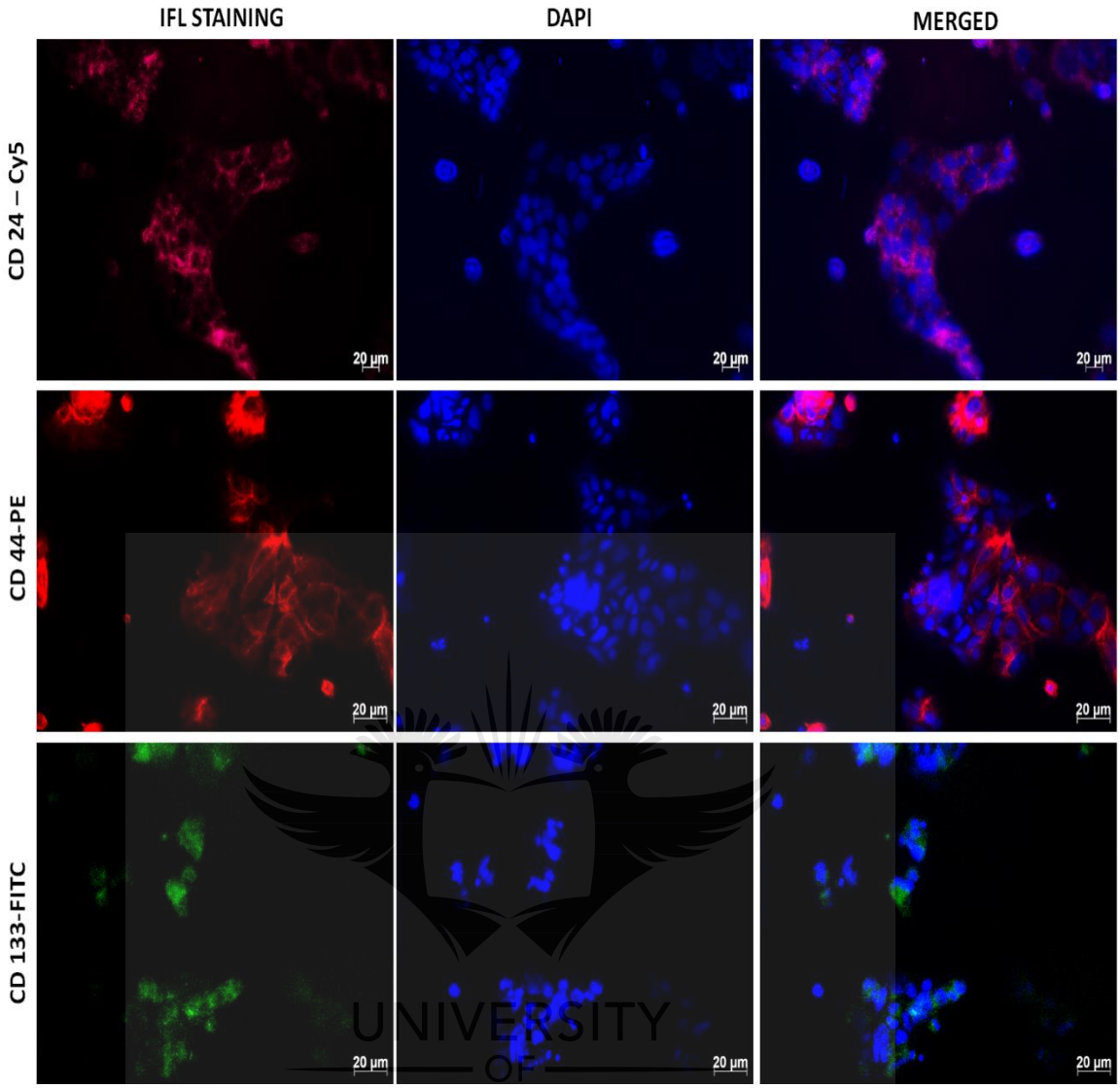

Figure 4. 18 Fluorescent antigenic detection of the surface marker CD24, CD44 and CD133 IFL staining of the isolated side population of CCSCs. DAPI nuclei counter staining. Scale bar 20 µm.

4.8 Targeted Delivery of SWCNTs-HA-Ce6 on CCSCs

The synthesised nanobiocomposite were coupled with HA to target the CD44 cell surface receptors, which is overexpressed in CCSCs. Isolated CCSCs, were cultured in petri dish with sterile glass slides and SWCNTs-HA-Ce6 were added, and SK-UT-1 cells were acted as a negative control for this study (CD44 receptor negative cells). The cells were incubated for 4 h at 37 °C in 5% CO2. The cellular imaging and targeting efficiency of SWCNTs-HA-Ce6 towards CD44 receptor was studied in both CCSCs and SK-UT-1 cells and the results are shown in

Figure 4.19. Images were taken in all three channels (Mitotracker, DAPI and Ce6), and merged to study the targeting efficiency of SWCNTs-HA-Ce6.

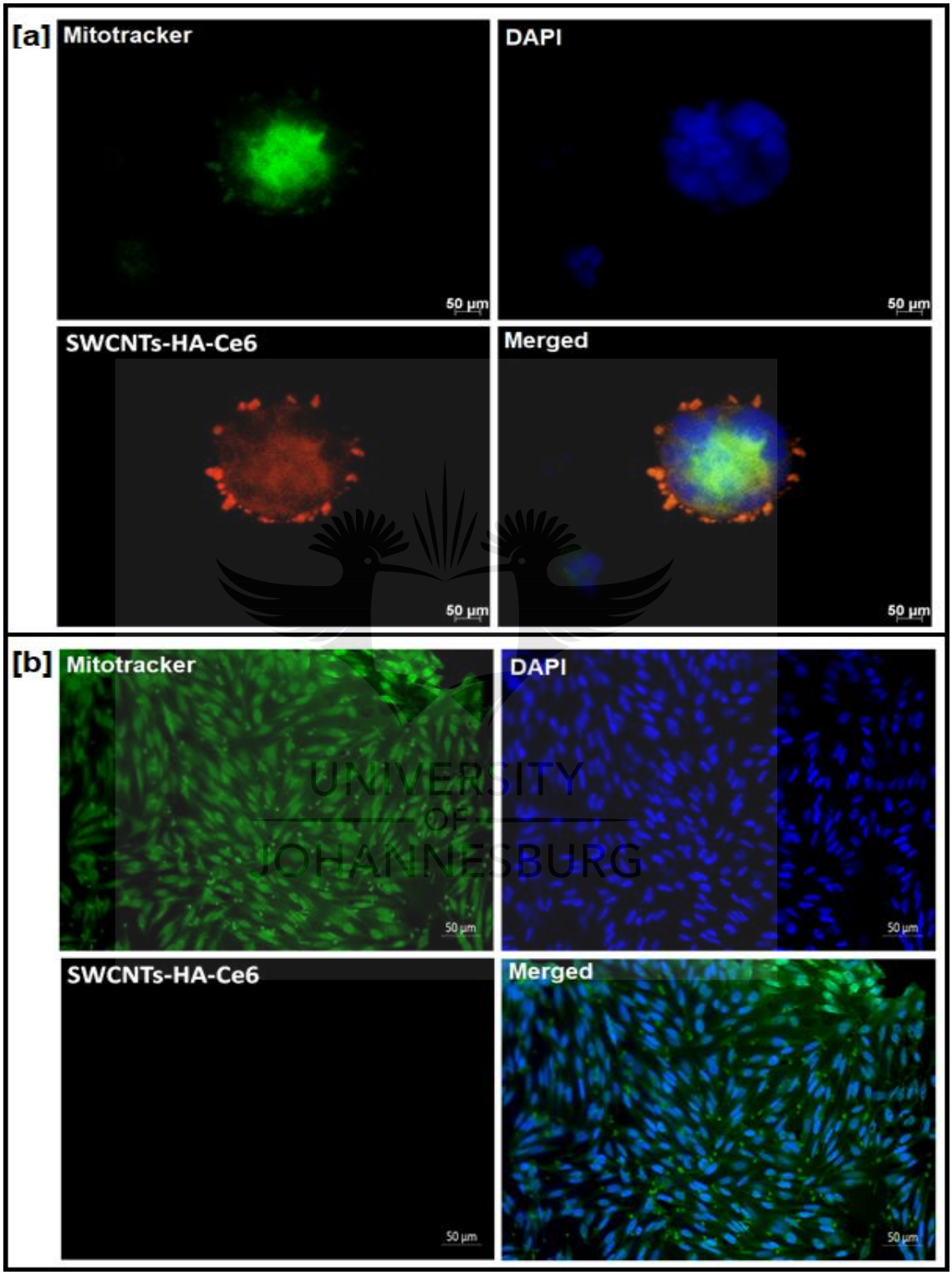

Figure 4. 19 Targeted delivery of SWCNTs-HA-Ce6. [a] Isolated CCSCs (CD44 receptor positive cells) and [b] SK-UT-1 cells (CD44 receptor negative cells). Scale bar 50 µm.

In contrast, the study performed in CCSCs (Figure 4.17a) showed the fluorescence intensity and cellular uptake of Ce6 in the SWCNTs-HA-Ce6 channel. It is further concluded that the HA functionalized SWCNTs-HA-Ce6 facilitates the targeting ability for SWCNTs-HA-Ce6 onto CD44 positive cells. The close observation of the Figure 4.19a revealed that the presence of SWCNTs-HA-Ce6 fluorescence intensity in the mitochondrial region. The results are clearly demonstrated that there is no prominent update of SWCNTs-HA-Ce6 in SK-UT-1 cells due to the absence of CD44 cell surface receptor (Figure 4.19b). Mainly the SWCNTs-HA-Ce6 molecule located in the mitochondrial region CCSCs, which leads to destroy the spheroid or clump of cells by laser radiation (Liu et al., 2014). It is further concluded that the HA functionalized SWCNTs-HA-Ce6 facilitates the targeting ability for SWCNTs-HA-Ce6 onto CD44 positive cells. From this study, the synthesised SWCNTs-HA-Ce6 could be used as a potential targeting nanomaterial to target CCSCs in cancer therapy.

4.9 Photodynamic Therapy Effect on Isolated CCSCs Using SWCNTs-HA-Ce6

4.9.1 Cell morphology study

Isolated CCSCs from Caco-2 cells were cultured on petri dishes at the population of 4×10^5 cells and the cells were further treated with laser irradiation at 660 nm fluence of 5 and 10 J/cm^2 after reaching the confluency. The morphological observation of treated and untreated cells was captured using inverted light microscope for 0 h, 24 h and 48 h and the images are shown in Figure 4.20, 4.21 and 4.22. The qualitative and preliminary confirmation of cellular viability and cell death were analysed from cellular morphology using captured microscopic images. The SWCNTs-HA-Ce6 treated and laser-irradiated (5 J/cm^2) cells revealed that significant changes in the cellular morphology at 48 h (Figure 4.21) compared to the control images. Similarly, the SWCNTs-HA-Ce6 treated and laser-irradiated (10 J/cm^2) cells morphology revealed that severe morphological changes and pronounced more cell death was observed at 48 h and the images are shown in Figure 4.22.

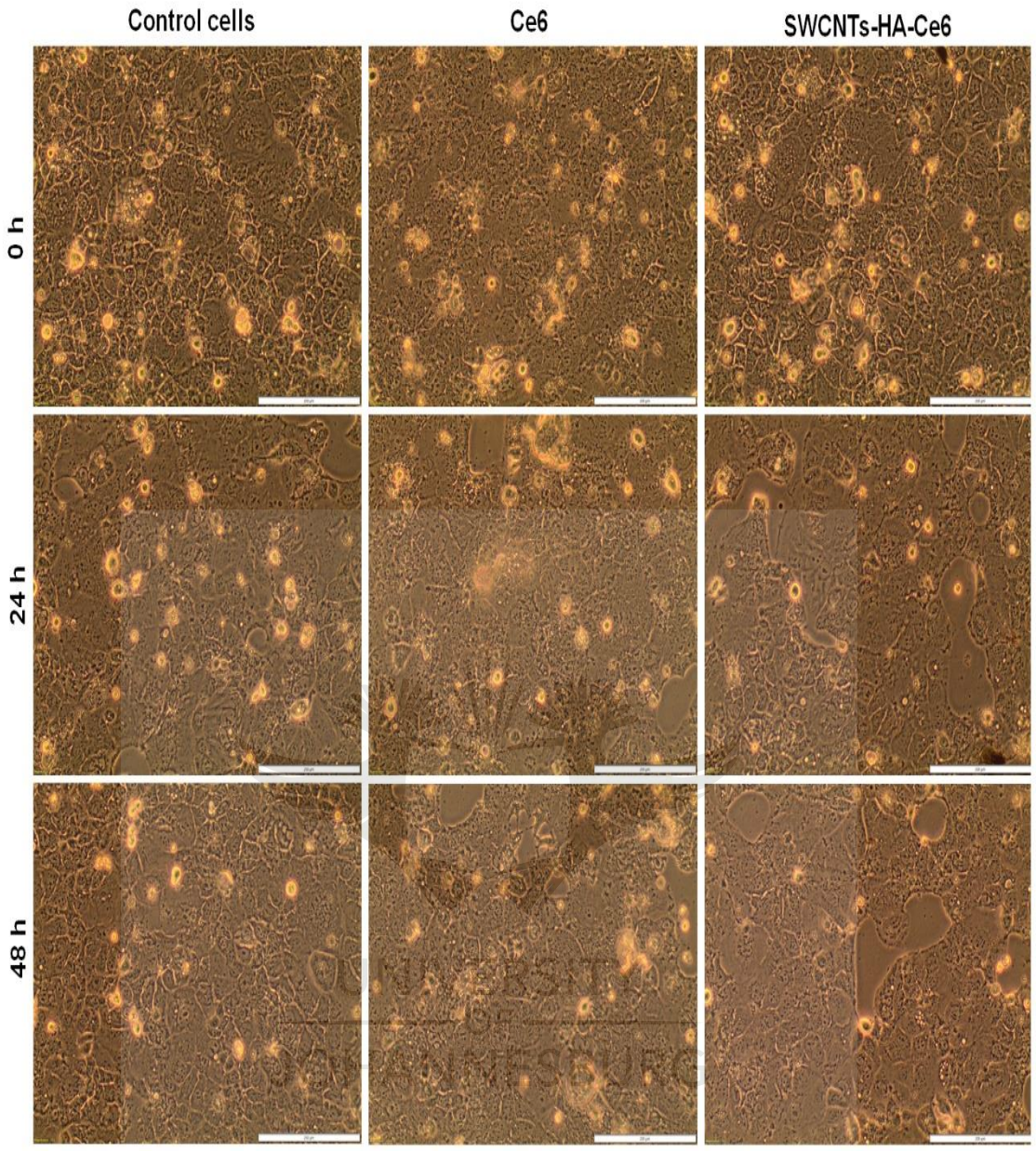

Figure 4. 20 Morphology analysis using microscopic images of treated and untreated CCSCs at 0 h, 24 h and 48 h of laser irradiated at 660 nm, 0 J/cm^2.

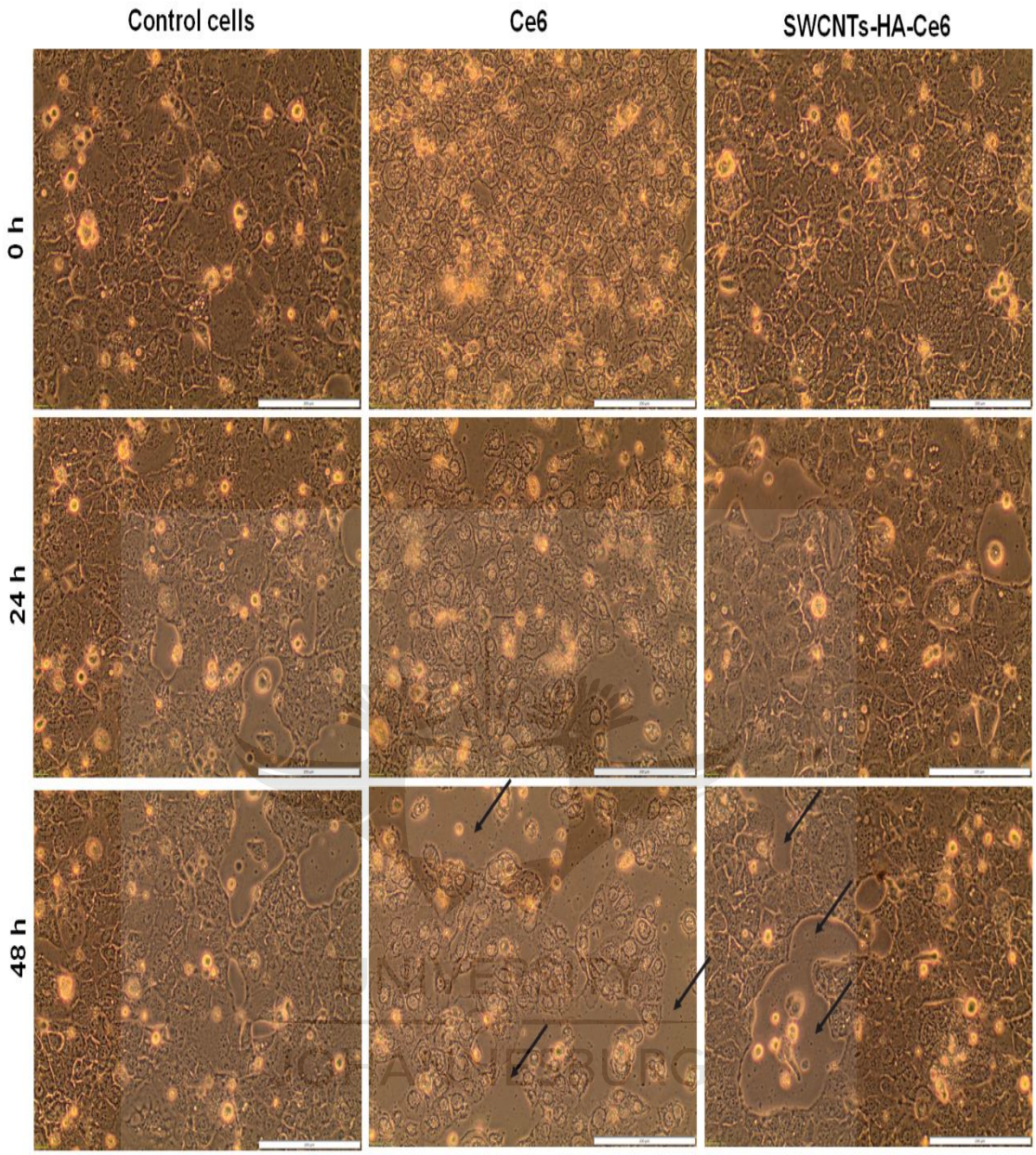

Figure 4. 21 Morphology analysis using microscopic images of treated and untreated CCSCs at 0 h, 24 h and 48 h of laser irradiated at 660 nm, 5 J/cm^2.

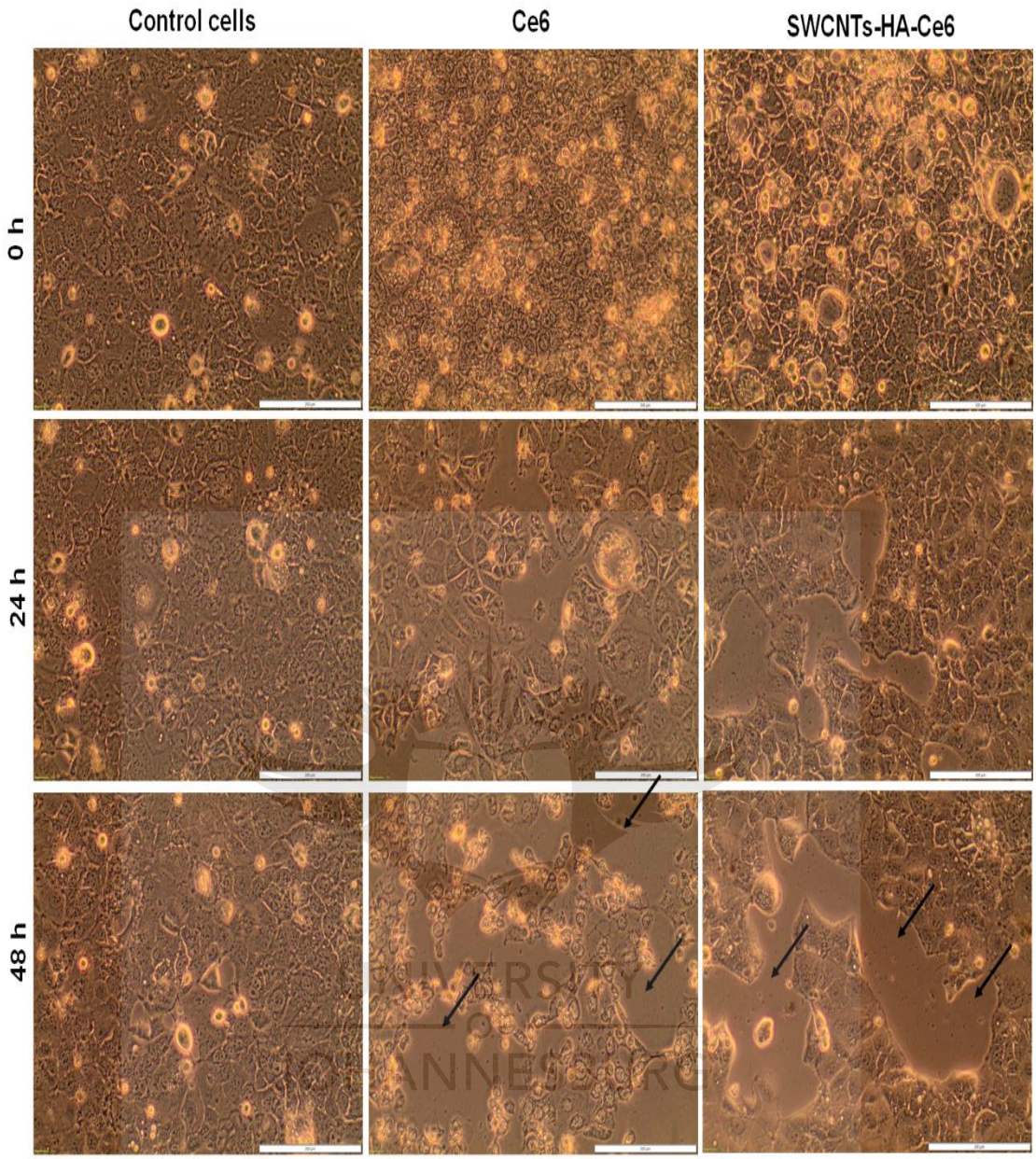

Figure 4. 22 Morphology analysis using microscopic images of treated and untreated CCSCs at 0 h, 24 h and 48 h of laser irradiated at 660 nm, 10 J/cm^2.

4.9.2 Cell death studies

4.9.2.1 LDH cytotoxicity assay

The cytotoxicity behaviour of SWCNTs-Ce6-HA was analysed using LDH cytotoxicity assay kit. The isolated CCSCs were incubated with Ce6 and SWCNTs-Ce6-HA, and then irradiated at 660 nm of laser fluence 0, 5 and 10 J/cm^2 at 24 and 48 h. After the successful PDT treatment, the damaged cancer cell was released LDH enzyme into the cell culture media, and these media were

analysed using LDH cytotoxicity assay kit. The measured absorbance value of untreated cells was kept as a control. The assay results are shown in the Figure 4.23 & 4.24.

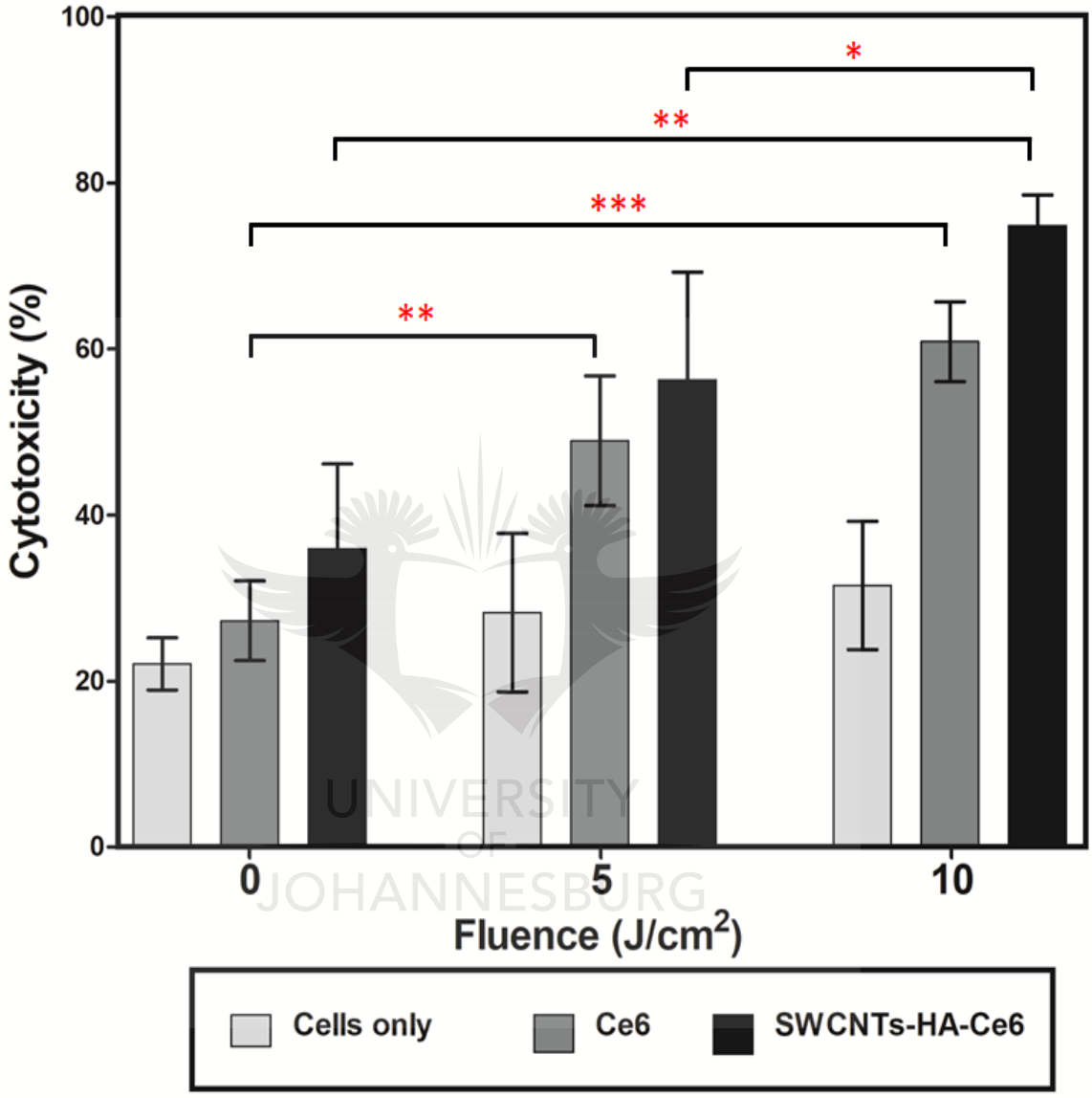

Figure 4. 23 The cytotoxicity effects of Ce6, SWCNTs-HA-Ce6 on CCSCs, laser irradiated at 660 nm of fluence 0, 5 and 10 J/cm^2 incubated for 24 h and determined cytotoxicity by LDH assay. significance is shown as * p < 0.05; ** p < 0.01; *** p 0.001.

The 24 h cytotoxicity assay results are shown in Figure 4.23, the observed results revealed that the non-irradiated 0 J/cm^2 showed lower percentage of cytotoxic behaviour for Ce6 (27.25 %) and SWCNTs-HA-Ce6 (35.94 %). The results of laser irradiation at 5 J/cm^2, revealed that the SWCNTs-HA-Ce6 treated cells

showed the cytotoxicity of 56.3% whereas the percentage cytotoxicity for Ce6 was 48.9 %. The results of laser irradiation at 10 J/cm^2, revealed that the SWCNTs-HA-Ce6 treated cells showed the cytotoxicity of 74.8% whereas the percentage cytotoxicity for Ce6 was 60.8 %. At 24 h, the percentage of cytotoxicity was significantly increased in 10 J/cm^2 irradiated and SWCNTs-HA-Ce6 treated samples compared to 5 J/cm^2 ($p < 0.05$) and 0 J/cm^2 ($p < 0.01$). The percentage of cytotoxicity was significantly increased in 10 J/cm^2 irradiated and Ce6 treated samples compared to 0 J/cm^2 ($p < 0.001$), similarly the cytotoxicity was significantly increased in 5 J/cm^2 irradiated and Ce6 treated samples compared to 0 J/cm^2 ($p < 0.01$). There was no statistical significant differences were observed in 0 J/cm^2 irradiated and SWCNTs-HA-Ce6 treated samples compared to 5 J/cm^2 ($p = 0.059$); 5 J/cm^2 irradiated and Ce6 treated samples compared to 10 J/cm^2 ($p = 0.051$).

The 48 h cytotoxicity assay results are shown in Figure 4.24, the observed results revealed that the non-irradiated 0 J/cm^2 showed lower percentage of cytotoxic behaviour for Ce6 (32.79%) and SWCNTs-HA-Ce6 (35.59%). The results of laser irradiation at 5 J/cm^2, revealed that the SWCNTs-HA-Ce6 treated cells showed the cytotoxicity of 71.85% whereas the percentage cytotoxicity for Ce6 was 60.9%. The results of laser irradiation at 10 J/cm^2, revealed that the SWCNTs-HA-Ce6 treated cells showed the cytotoxicity of 86.7% whereas the percentage cytotoxicity for Ce6 was 67.7%. At 48 h, the percentage of cytotoxicity was significantly increased in 10 J/cm^2 irradiated and SWCNTs-HA-Ce6 treated samples compared to 0 J/cm^2 ($p < 0.01$), similarly the cytotoxicity was significantly increased in 5 J/cm^2 irradiated and SWCNTs-HA-Ce6 treated samples compared to 0 J/cm^2 ($p < 0.01$). The percentage of cytotoxicity was significantly increased in 10 J/cm^2 irradiated and Ce6 treated samples compared to 0 J/cm^2 ($p < 0.05$). There was no statistical significant differences were observed in 0 J/cm^2 irradiated and SWCNTs-HA-Ce6 treated samples compared to 5 J/cm^2 ($p = 0.084$); 5 J/cm^2 irradiated and Ce6 treated samples compared to 10 J/cm^2 ($p = 0.476$); and 5 J/cm^2 irradiated and SWCNTs-HA-Ce6 treated samples compared to 10 J/cm^2 ($p = 0.117$).

The percentage of cytotoxicity results are considered as important parameter for the synthesised compounds in cancer treatments. The increased percentage of

cytotoxicity during 48h at 10 J/cm^2 results indirectly revealed the enhanced bioavailability, uptake profile and biological activity of Ce6 released from SWCNTs-HA-Ce6. The percentage of cytotoxicity results also revealed that the increased cytotoxic effects of SWCNTs-HA-Ce6 compared with Ce6 alone in 5 and 10 J/cm^2 at both 24 and 48 h.

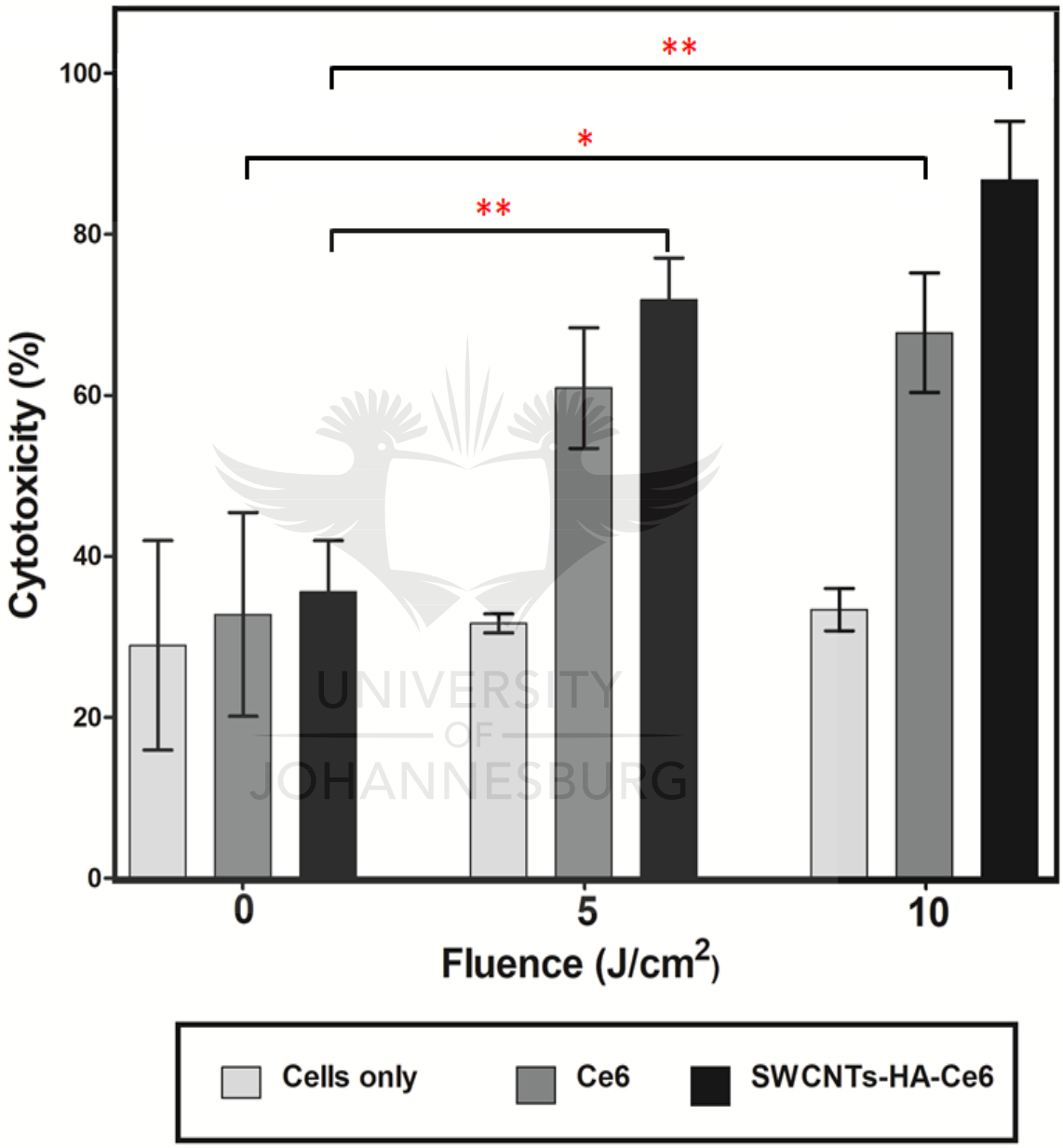

Figure 4. 24 The cytotoxicity effects of Ce6, SWCNTs-HA-Ce6 on CCSCs, laser irradiated at 660 nm of fluence 0, 5 and 10 J/cm^2 incubated for 48 h and determined cytotoxicity by LDH assay. significance is shown as * p < 0.05; ** p < 0.01; *** p 0.001.

4.9.2.2 Annexin V–fluorescein isothiocyanate (FITC) and Propidium Iodide (PI) assay using flow cytometry

The cell death mechanism of PDT was well established that directly destroy the cancer cells by apoptosis or necrosis (Yoo et al., 2012). Photodynamic effects induce the cell death by formation of ROS damage the cells by oxidizing and degrading cellular components. To estimate the cell death mechanism study of PDT in isolated CCSCs, an Annexin V PI cell death assay by flow cytometry. The CCSCs were cultured in small petri dishes and incubated with Ce6 and SWCNTs-Ce6-HA, then treated with 0, 5 and 10 J/cm^2 at 660 nm. After treatment the cells were incubated for 24 and 48 h and evaluated in this study. Flow cytometry analysis pattern as discussed early; four quadrant images are given in Figure 4.25 and 4.26. The percentage of early and late stages apoptosis cells from treated groups are comparatively higher than control cells. The percentage of cells in the early and late apoptosis quadrant will leads to cell death.

At 24 h (Figure 4.25), the SWCNTs-HA-Ce6 treated cells with no laser irradiation (0 J/cm^2) showed that the percentage of EA and LA about 12.8 and 2.9 % whereas the Ce6 treated EA and LA about 1.4 and 4.3 %. The SWCNTs-HA-Ce6 treated cells with the 5 J/cm^2 laser fluence showed that the percentage of EA and LA about 12.7 and 2.6 % whereas the Ce6 treated EA and LA about 10.5 and 2.0 %. The SWCNTs-HA-Ce6 treated cells with 10 J/cm^2 laser fluence showed that the percentage of EA and LA about 20.2 and 2.7 % whereas the Ce6 treated EA and LA about 16.9 and 4.2 %. %. The Ce6 treated samples showed lesser percentage of EA and LA cells in 0, 5 and 10 J/cm^2 irradiated samples compared to SWCNTs-HA-Ce6. The results of SWCNTs-HA-Ce6 treated and 10 J/cm^2 irradiated samples showed the prominent apoptotic effects to the CCSCs compared to the control.

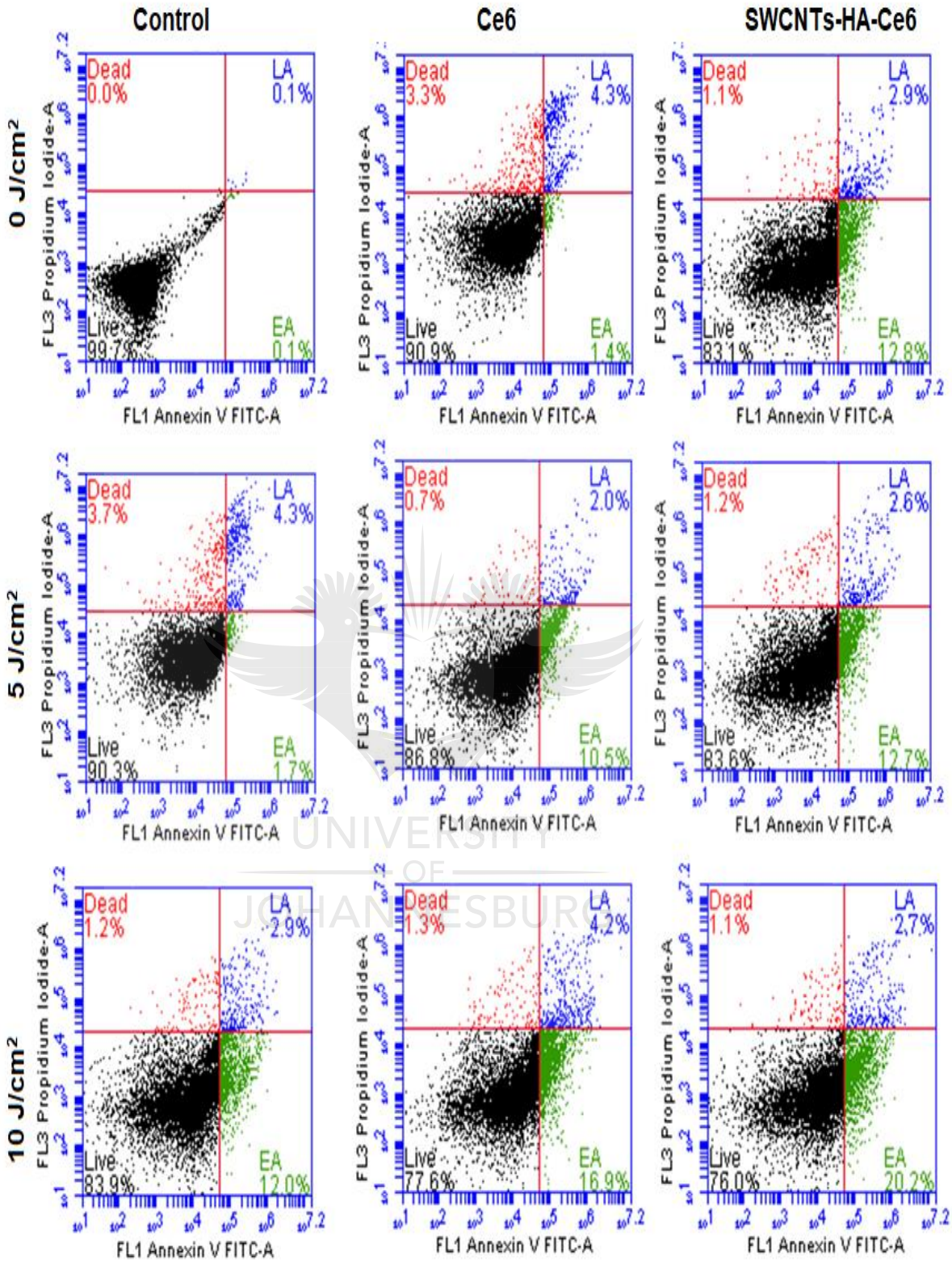

Figure 4. 25 Flow cytometry analysis using Annexin V PI for cell death, laser irradiated at 660 nm of fluence 0, 5 and 10 J/cm^2 of Ce6, SWCNTs-HA-Ce6 on CCSCs incubated for 24 h.

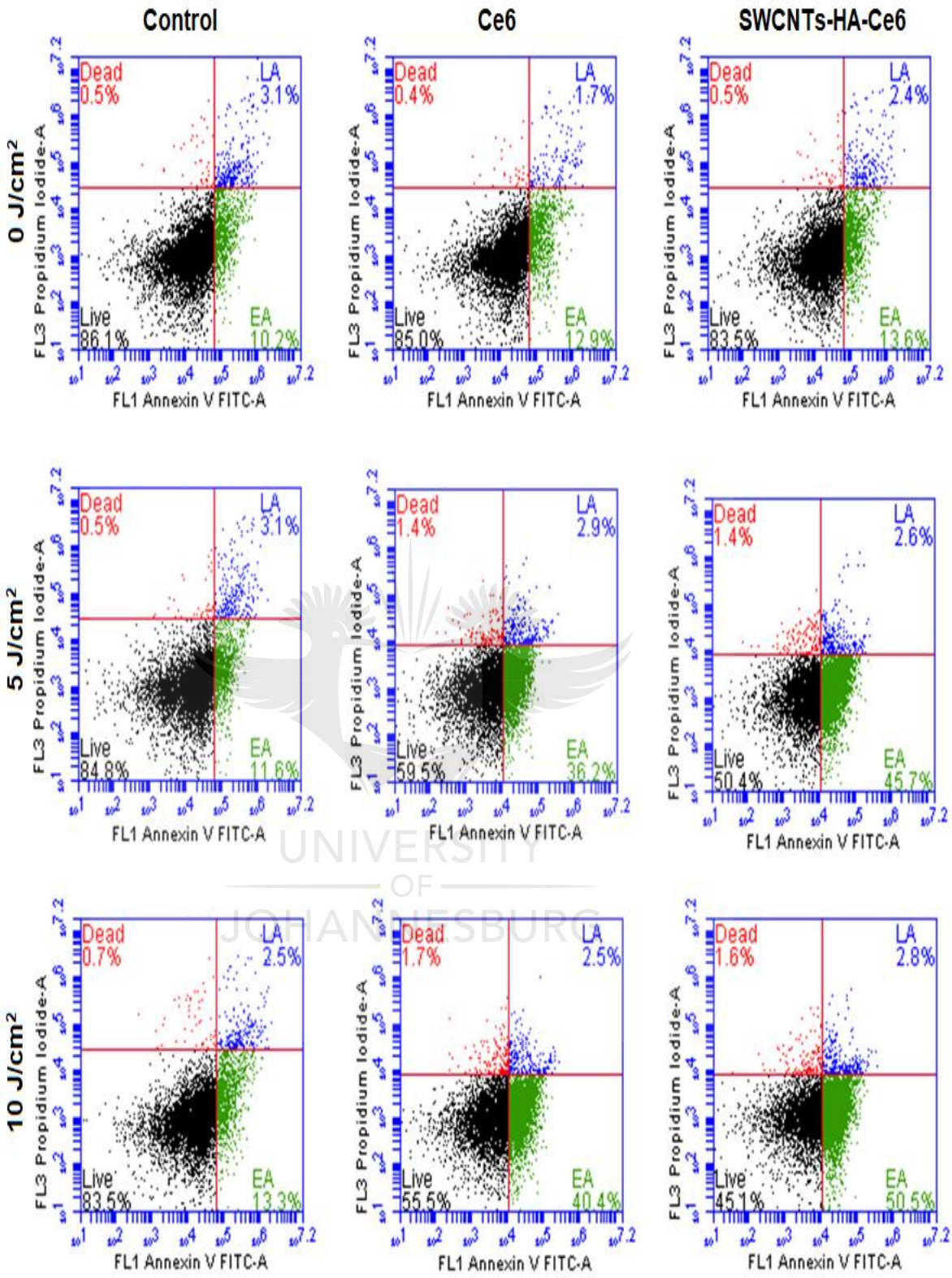

Figure 4. 26 Flow cytometry analysis using Annexin V PI for cell death, laser irradiated at 660 nm of fluence 0, 5 and 10 J/cm^2 of Ce6, SWCNTs-HA-Ce6 on CCSCs incubated for 48 h.

At 48 h (Figure 4.26), the SWCNTs-HA-Ce6 treated cells with no laser irradiation (0 J/cm^2) showed that the percentage of EA and LA about 13.6 and 2.4 % whereas the Ce6 treated EA and LA about 12.9 and 1.7 %. The SWCNTs-HA-Ce6 treated cells with the 5 J/cm^2 laser fluence showed that the percentage of EA and LA about 45.7 and 2.6 % whereas the Ce6 treated EA and LA about 36.2 and 2.9%. The SWCNTs-HA-Ce6 treated cells with 10 J/cm^2 laser fluence showed that the percentage of EA and LA about 50.5 and 2.8 % whereas the Ce6 treated EA and LA about 40.4 and 2.5 %. The Ce6 treated samples showed lesser percentage of EA and LA cells in 0, 5 and 10 J/cm^2 irradiated samples compared to SWCNTs-HA-Ce6. The results of SWCNTs-HA-Ce6 treated and 10 J/cm^2 irradiated samples showed the prominent apoptotic effects to the CCSCs compared to the control.

4.9.3 Metabolic activity of Cells using Adenosine Triphosphate (ATP) luminescence assay

Adenosine triphosphate are the energy source of cell metabolism and proliferation. Cancer cells produce more number of ATPs through aerobic glycosylation for continuous division of cells (Vander Heiden et al., 2009). The metabolic activity of the isolated CCSCs was analysed by measuring the ATP luminescence signal before and after the treatment. CCSCs were cultured and treated with Ce6 and SWCNTs-HA-Ce6 at 660 nm of fluence 5 and 10 J/cm^2, amount of ATP production was estimated at 24 and 48 h. Control cells showed higher production of ATP and it was confirmed by the luminescent RLU obtained through this study. The metabolic activity of cells slowly declined at 5 and 10 J/cm^2 laser irradiated and SWCNTs-HA-Ce6 treated samples and the calculated by ATP production rate using luminescent RLU are given in Figure 4.27 and 4.28.

The 24 h ATP luminescence assay results are shown in Figure 4.27, the observed results revealed that the non-irradiated 0 J/cm^2 and SWCNTs-HA-Ce6 treated samples showed higher luminescence compared to 5 J/cm^2 and 10 J/cm^2. It indicates the number of viable cell counts were gradually decreased in both to 5 J/cm^2 and 10 J/cm^2. The luminescence signal was significantly decreased in 10 J/cm^2 irradiated and SWCNTs-HA-Ce6 treated samples compared to 5 J/cm^2

($p < 0.001$) and 0 J/cm^2 ($p < 0.001$), similarly the luminescence signal was significantly decreased in 10 J/cm^2 irradiated and Ce6 treated samples compared to 5 J/cm^2 ($p < 0.001$) and 0 J/cm^2 ($p < 0.001$). The results of 5 J/cm^2 irradiated and Ce6 treated samples compared to 0 J/cm^2 ($p < 0.05$) and the 5 J/cm^2 irradiated and SWCNTs-HA-Ce6 treated samples compared to 0 J/cm^2 ($p < 0.001$).

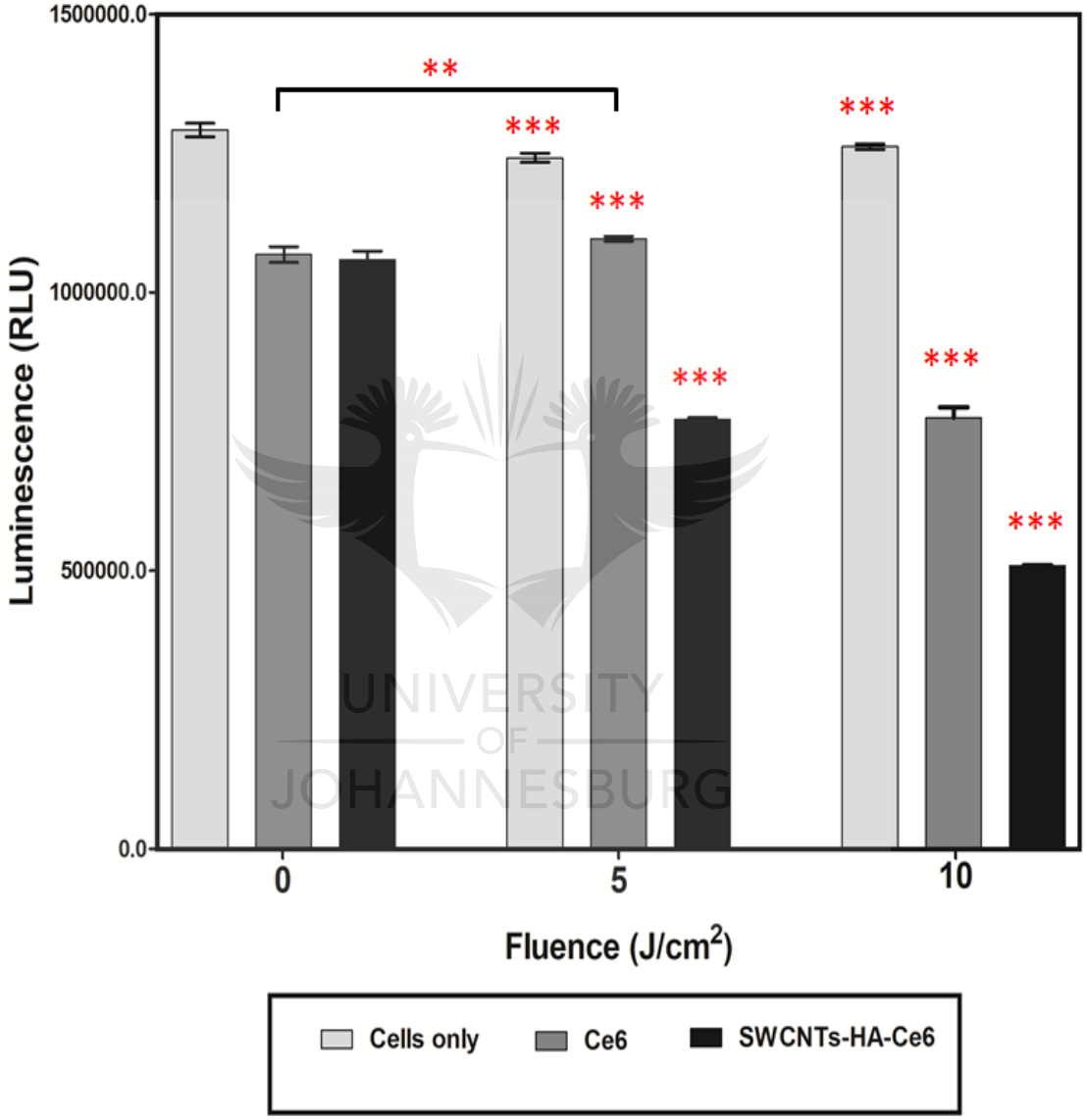

Figure 4. 27 An ATP luminescent assay of Ce6, SWCNTs-HA-Ce6 on CCSCs, laser irradiated at 660 nm of fluence 0, 5 and 10 J/cm^2 incubated for 24 h. Significance is shown as ** p < 0.01; *** p 0.001.

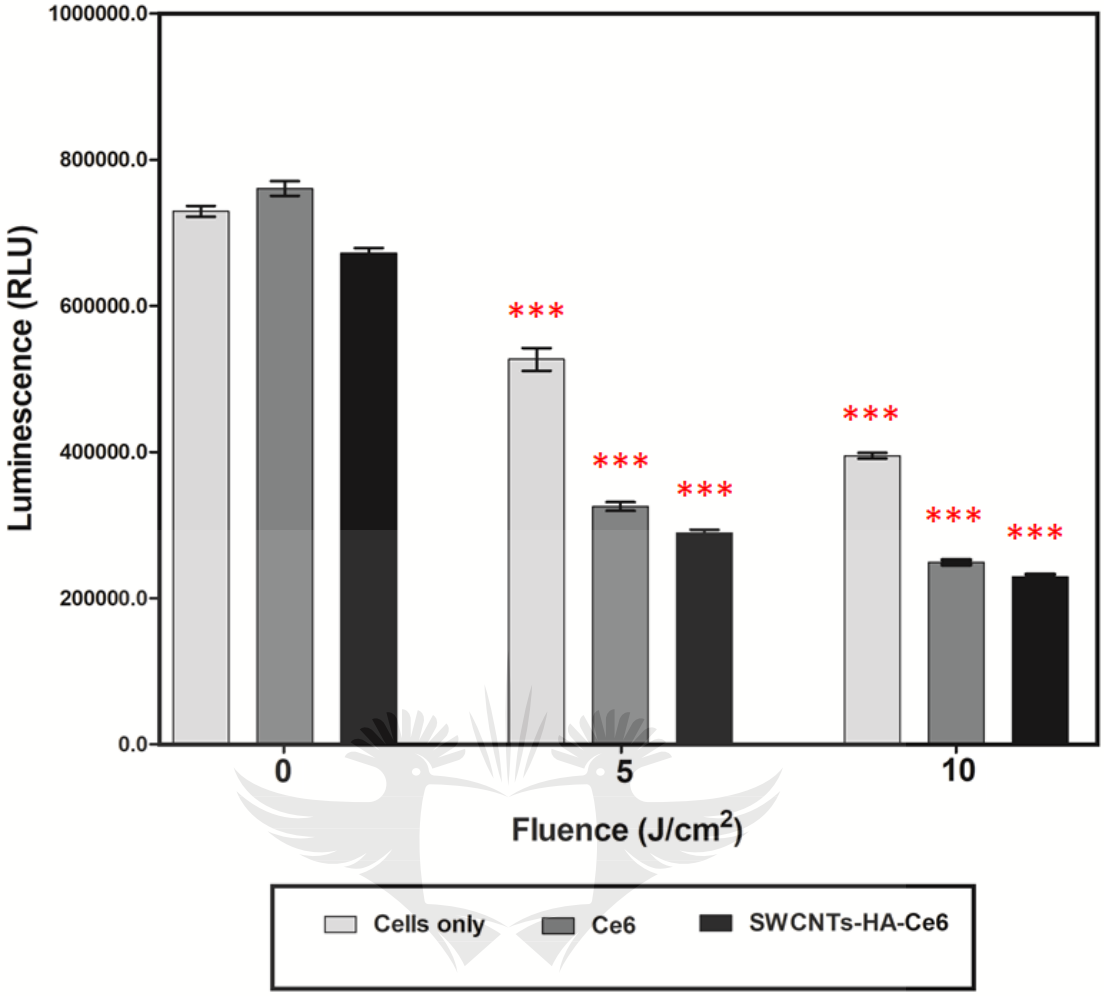

Figure 4. 28 An ATP luminescent assay of Ce6, SWCNTs-HA-Ce6 on CCSCs, laser irradiated at 660 nm of fluence 0, 5 and 10 J/cm^2 incubated for 24 h. Significance is shown as *** p 0.001.

The 48 h ATP luminescence assay results are shown in Figure 4.28, the observed results revealed that the non-irradiated 0 J/cm^2 and SWCNTs-HA-Ce6 treated samples showed higher luminescence compared to 5 J/cm^2 and 10 J/cm^2. It indicates the number of viable cell counts were gradually decreased in both to 5 J/cm^2 and 10 J/cm^2. The luminescence signal was significantly decreased in 10 J/cm^2 irradiated and SWCNTs-HA-Ce6 treated samples compared to 5 J/cm^2 ($p < 0.001$) and 0 J/cm^2 ($p < 0.001$), similarly the luminescence signal was significantly decreased in 10 J/cm^2 irradiated and Ce6 treated samples compared to 5 J/cm^2 ($p < 0.001$) and 0 J/cm^2 ($p < 0.001$). The results of 5 J/cm^2 irradiated and Ce6 treated samples compared to 0 J/cm^2 ($p < 0.001$) and the 5 J/cm^2

irradiated and SWCNTs-HA-Ce6 treated samples compared to 0 J/cm^2 ($p < 0.001$).

The metabolic activity of CSCs or SCs have decreased or quiescent, ultimately effects the growth of tumour or metastasis in the affected region (Peiris-pages et al., 2016). The results showed that RLU value of 5 and 10 J/cm^2 are lower compared with 0 J/cm^2 in both 24 and 48 h, without treatment the proliferation rate of cells was high. These results demonstrate that the SWCNTs-HA-Ce6 treated samples were showed lower metabolic rate or ATP production in the cells and it directly leads to inactive and cell death.

4.10 Nuclear Damage Studies Using Hoechst And Propidium Iodide

CCSCs were cultured in sterile glass coverslip and incubated with Ce6 and SWCNTs-HA-Ce6 and then laser irradiated at 660 nm in fluence 5 and 10 J/cm^2. The morphological changes in the nucleus were captured under fluorescent microscope, here Hoechst stain represented in blue colour and PI represented in red colour. Hoechst is a nucleic acid dye, it will permeable into the cells and nucleus to recognise chromatin condensation and fragmentation, this staining used to identify condensed nuclei of apoptotic cells. PI is a cell impairment DNA-binding dye used as counter stain for Hoechst, PI will stain the cells only where there is increase in plasma membrane permeability and enters the nucleus (Ahmed Hamdi et al., 2014).

The morphological observation of 0, 5 and 10 J/cm^2 laser irradiation and Hoechst PI staining were shown in figure 4.29. As observed in control image, the cells are seen oval nucleus and less bright blue fluorescence stained with Hoechst and no trace of red fluorescence of PI dye. The PDT treated cells exhibited features of apoptosis such as chromatin condensation, fragmentation, and cell shrinkage. The images of 5 J/cm^2 showed that bright blue fluorescence of Hoechst and less red fluorescence of PI dye, the nucleus shapes were changed. In the 10 J/cm^2 treated cell nucleus were completely damaged and irregular in shapes, and then the bright red fluorescence of PI dye and very less fluorescence of Hoechst stain in the nucleus area were observed. This result shows that nuclear damage of CCSCs were occurred during PDT treatment, there is high damage in 10 J/cm^2 laser irradiation.

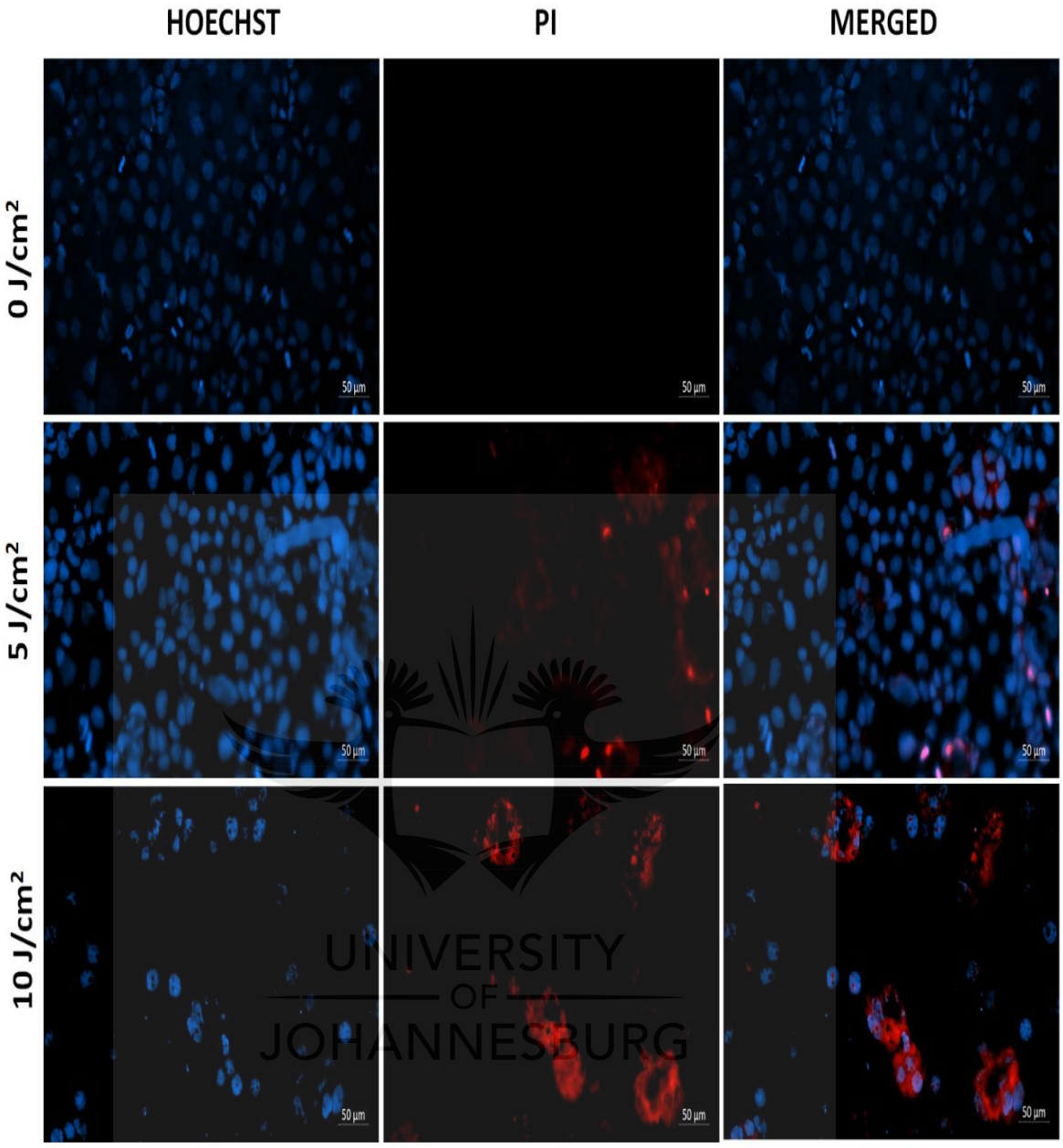

Figure 4. 29 Nuclear damage analysis of CCSCs after laser irradiation at 660 nm of fluence 0, 5 and 10 J/cm^2 of Ce6, SWCNTs-HA-Ce6 using Hoechst and PI. Scale bar 50 µm.

4.11 Oxidative Stress Visualisation Immediately Following Laser Irradiation.

Level of ROS production is important criteria in laser irradiation, PDT mechanism are type I and type II, both mechanisms based of the production of ROS leads to cellular damage or cell death. The fluorescence microscopy experiment was carried out to identify the ROS production in SWCNTs-HA-Ce6 treated and laser

irradiated CCSCs. CCSCs were cultured on glass cover slip containing petri dishes and treated with SWCNTs-HA-Ce6 at 0, 5 and 10 J/cm^2 fluence.

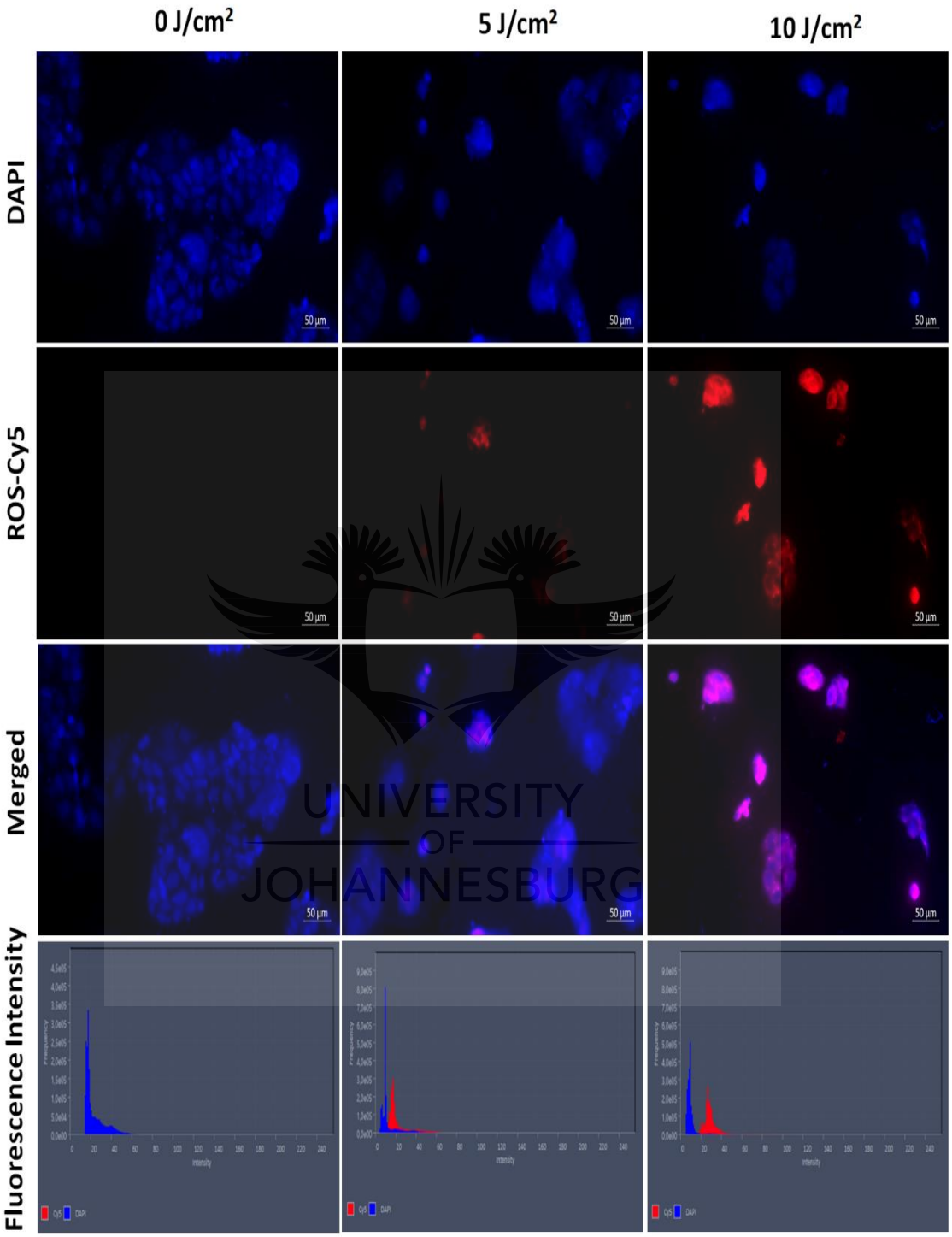

Figure 4. 30 Detection of oxidative stress on CCSCs using intracellular ROS kit. CCSCs are laser irradiation at 660 nm of fluence 0, 5 and 10 J/cm^2 of Ce6, SWCNTs-HA-Ce6 and fluorescence intensity of the merged images are represented in graph. Counter stained using DAPI. Scale bar 50 µm.

After one hour of incubation fluorometric intracellular reactive oxygen species kit was used to analysis the production of ROS in the CCSCs and visualised under fluorescent microscope and DAPI used as nuclei counter staining. The captured images are represented in figure 4.30, the results showed that 0 J/cm^2 did not produced any red fluorescence due to the absence of ROS production. Laser irradiated 5 J/cm^2 and 10 J/cm^2 fluence showed the presence of red fluorescence in different ranges and it can be measured and represented as fluorescence intensity. 5 J/cm^2 showed less ROS production compared with 10 J/cm^2, the ROS intensity were higher in increased fluence at 660 nm.

CHAPTER 5 CONCLUSION

The use of SWCNTs-based materials showed great benefits in the preparation of nanoengineered vehicles for drug delivery and biomedical application. This study aimed to use the functional applications of SWCNTs, hyaluronic acid and Chlorin e6 as a combined targeted delivery vehicle called “Nanobiocomposite (SWCNTs-HA-Ce6)” and utilizing their photodynamic effects by irradiating at 660 nm. To conclude, SWCNTs coupled biopolymer HA and coated with Ce6 were successfully synthesised which showed photodynamic effect under 660 nm to treat colon cancer cells and CCSCs.

The physicochemical characterisation of synthesised SWCNTs-HA-Ce6 showed the existence of HA and Ce6. The nanocarrier properties of synthesized SWCNTs-HA-Ce6 was confirmed through the presence of functional group bond shifting in FTIR study, surface charge of the nanotubes in DLS method, size and shape of the SWCNTs-HA-Ce6 in HRTEM study, and crystallinity and purity of the SWCNTs-HA-Ce6 in XRD. The dispersibility of the SWCNTs-HA-Ce6 were considerably improved when compared with void SWCNTs. It may due to the surface functionalisation of SWCNTs with hyaluronic acid.

The SWCNTs-based nanomaterials showed an improved loading efficiency, stability and sustained release of photosensitizers and these parameters are considered as an important criterion in photodynamic therapy. It plays major role in drug and dosage formulations in PDT related clinical trials for the treatment of cancer. An improved stability of nanobiocomposite was obtained in both physiological pH 7.4 and intracellular pH 5.5. SWCNTs-HA-Ce6 was capable of protecting the stability of loaded Ce6. The in vitro release study results revealed the slow and sustained release pattern of Ce6 from SWCNTs in both pH conditions. Ce6 release was significantly faster in pH 7.4 than compared to pH 5.5.

The synthesized nanobiocomposite was successfully studied using both colon cancer cells and CCSCs in in vitro. It shows positive outcomes in targeting CCSCs and pronounced cell death. Performance of PDT depends primarily on the release of singlet oxygen, absorbed light and their cellular penetration depth, molecular stability and PS allocation (Zhang et al., 2018). The photodynamic

effects of SWCNTs-HA-Ce6 were studied in Caco-2 cells and it showed significant cytotoxicity effect in the laser fluence of 10 J/cm^2 at 24 h compared to void Ce6 and SWCNTs. There was no significant cytotoxicity for SWCNTs at 660 nm because the maximum excitation of SWCNTs were at 808 nm under laser irradiation.

Recently, CSCs have been identified in various solid tumours and have been proposed to explain the radiotherapy and metastatic potential, recurrence, and resistance to chemotherapy caused by certain tumours. Many studies suggested that solid tumours contain small population of cells that can self-renew, proliferate infrequently initiate and metastasis the tumours (Chang et al., 2016). In cancer therapy, the current treatments methodologies are prone to destroy only tumour cells and sometimes it fails to target and eradicate CSCs; therefore, new therapies are needed to target and destroy CSCs and to completely eradicate the tumour. In our research, CCSCs were successfully isolated from colon cancer cell line (Caco-2), and then the presence of isolated CCSCs were confirmed by different characterisation techniques which includes using immunofluorescence, flow cytometry and CCSCs spheroid morphology formation in microscopy. Cellular localisation of SWCNTs-HA-Ce6 on Caco-2 cells and CCSCs were studied in fluorescence microscopy and it revealed that the Ce6 fluorescence signals were clearly seen in the mitochondrial region, so that SWCNTs-HA-Ce6 capable of damaging the powerhouse of the cell.

The synthesised SWCNTs-HA-Ce6 successfully targeted the CCSCs and release the Ce6 molecule to destroy the CCSCs. CCSCs are overexpressed with cells surface markers like CD133, EpCAM, CD24, CD44, and the functionalised HA on SWCNTs are targeting the CD44 receptors. CCSCs are irradiated at 660 nm in two different laser fluence (5 and 10 J/cm^2) for 24 and 48 h and studied various parameters to confirm the efficacy of SWCNTs-HA-Ce6. The better cytotoxic behaviour was observed on the CCSCs were irradiated with 10 J/cm^2 compared to 5 J/cm^2. The cells treated with 10 J/cm^2 indicated higher percentage of cell death, higher apoptotic activity and prominent nuclear damage inside the cells compared to 5 J/cm^2. Through the present study, a novel SWCNTs-HA-Ce6 was demonstrated as an effective nanocarrier to target and completely destroy

CCSCs. Overall, these results showed that the synthesized SWCNTs-HA-Ce6 could be a more promising material for PDT treatment of colon cancer

Future Recommendations

Future studies should be identifying the in vitro molecular pathways, which leads to the cell death in CCSCs, and then the similar in vitro approaches of SWCNTs-HA-Ce6 should be tested in in vivo mice model. These findings should be studied to find out the pharmacokinetic and pharmacodynamics effects of SWCNTs-HA-Ce6 and their targeting efficiency in the treatment of colon cancer in in vivo mice model.

REFERENCES

Abrahamse, H.; Hamblin, M.R. New photosensitizers for photodynamic therapy. Biochemical J, **2016**, 473,1347-364.

Adams, J.M.; Strasser, A. Is tumor growth sustained by rare cancer stem cells or dominant clones. J cancer res, **2008,** 68(11), 4018-4021.

Adiseshaiah, P.P.; et al. Nanomedicine strategies to overcome the pathophysiological barriers of pancreatic cancer. Nature. Rev. Clin. Oncol, **2016**, 13, 750.

Agostinis, P.; Berg, K.; Cengel, K.A.; Foster, T.H.; Girotti, A.W.; Gollnick, S.O.; Hahn, S.M.; Hamblin, M.R.; Juzeniene, A.; Kessel, D.; Korbelik, M.; Moan, J.; Mroz, P.; Nowis, D.; Piette, J.; Wilson, B.C.; Golab, J. Photodynamic therapy of cancer: an update. CA: Cancer J. Clin, **2011**, 61, 250–281.

Ahmed Hamdi, O.A.; Rahman, S.A.; Nur, S.; Awang, K.; Wahab, A.N.; Looi, C.Y.; Thomas, N.F.; Abd Malek, S.N. Cytotoxic Constituents from the Rhizomes of Curcuma zedoaria. Sci. World J, **2014**, 321943.

Alexiou, C.; Fadeel, B. Brave new world - focus on nanomedicine, Biochem. Biophys. Am. J. Res. Commun, **2015**, 468 (3), 409-410.

Al-Hajj, M.; Wicha, M.S.; Benito-Hernandez, A.; Morrison, S.J.; Clarke, M.F. Prospective identification of tumorigenic breast cancer cells. Proc Natl Acad Sci, **2003**, 100, 3983-3988.

Ali-Boucetta, H.; Kostarelos, K. Pharmacology of carbon nanotubes: Toxicokinetics, excretion and tissue accumulation. Advanced drug delivery reviews, **2013**, 65, 2111-2119.

Allen, T.M.; Martin, F.J. Advantages of liposomal delivery systems for anthracyclines. Semin. Oncol. **2004**, 31, 5–15.

Allison, R.R.; Downie, G.H.; Cuenca, R.; Xin-Hua, Hu.; Childs, C.J.; Sibata, C.H. Photosensitizers in clinical PDT. Photodiagnosis Photodyn.Ther, **2004**, 1, 27-42.

Allison, R.R.; Sibata, C.H. Oncologic photodynamic therapy photosensitizers: A clinical review. Photodiagn. Photodyn. Ther, **2010**, 7, 61–75.

Anand, P.; Kunnumakkara, A.B.; Sundaram, C.; Harikumar, K.B.; Tharakan, S.T.; Lai, O.S.; Sung, B.; Aggarwal, B.B. Cancer is a preventable disease that requires major lifestyle changes. Pharm Res. **2008**, 25, 2097-2116.

Ando, K.; Mori, K.; Corradini, N.; Redini, F.; Heymann, D. Mifamurtide for the treatment of nonmetastatic osteosarcoma. Expert Opin Pharmacother. **2011**, 12(2), 285–292.

Anindita, B.; Ganesan, K.; Nidhin, M.; et al. Chlorin e6 decorated doxorubicin encapsulated chitosan nanoparticles for photo-controlled cancer drug delivery. Int. J. Biol. Macromol, **2019**, 136, 951-961.

Asgari, M.; Gazor, R.; Abdollahifar, M.; Fadaei, Fathabady, F.; Zare, F.; Norouzian, M.; Amini, A.; Khosravipour, A.; Kiani, P.; Atashgah, R.B.; Rezaei, F.; Ghoreishi, S.K.; Chien, S.; Hamblin, M.R.; Bayat, M. Combined therapy of adipose-derived stem cells and photobiomodulation on accelerated bone healing of a critical size defect in an osteoporotic rat model. Biochem. Biophys. Res. Commun, **2020**, 530(1), 173-180.

Badea, N.; Craciun, M.M.; Dragomir, A.S.; Balas, M.; Dinischiotu, A.; Nistor, C.; Gavan, C.; Ionita, D. Systems based on carbon nanotubes with potential in cancer therapy. Mater. Chem. Phys. **2020**, 241, 1224–1235.

Bagheri, H.; Afkhami, A.; Khoshsafar, H.; Hajian, A.; Shahriyari, A. Protein capperd Cu nanoclusters-SWCNT nanocomposite as a novel candidate of high-performance platform for organophosphates enzymeless biosensor. Biosens. Bioelectron. **2017**, 89, 829–836

Bajada, S.; Mazakova, I.; Richardson, J.B.; Ashammakhi, N. Updates on stem cells and their application in regenerative medicine. J Tissue Eng Regen Med, **2008**, 2(4),169–83.

Banerjee, S.; Hemraj-Benny, T.; Wong, S.S. Covalent surface chemistry of single walled carbon nanotubes. Adv. Mater. **2005**, 17, 17–29.

Banky, B.; Raso-Barnett, L.; Barbai, T.; Timar, J.; Becsagh, P.; et al. Characteristics of CD44 alternative splice pattern in the course of human colorectal adenocarcinoma progression. Mol Cancer, **2012**, 11: 83.

Batlle, E.; Clevers, H. Cancer stem cells revisited. Nat. Med. **2017**, 23 (10), 1124–1134.

Baughman, R.H.; Zakhidov, A.A.; de Heer, W.A. Carbon nanotubes--the route toward applications. Science, **2002**, 297(5582), 787-792.

Bedikian, A.Y. et al. Pharmacokinetics and urinary excretion of vincristine sulfate liposomes injection in metastatic melanoma patients. J. Clin. Pharmacol, **2006**, 46, 727–737

Bernabeu, E. et al. Paclitaxel: what has been done and the challenges remain ahead. Int. J. Pharm, **2017**, 526, 474–495.

Besteman, K.; Lee, J.O.; Wiertz, F.G.; Heering, H.A.; Dekker, C. Enzyme-coated carbon nanotubes as single molecule biosensors. Nano Lett. **2003**, 3, 727–730.

Biehl, J.K.; Russell, B. Introduction to Stem Cell Therapy. J cardiovasc nurs, **2009**, 24, 98-103

Bidram, E.; Esmaeili, Y.; Ranji-Burachaloo, H.; Al-Zaubai, N.; Zarrabi, A.; Stewart, A.; Dunstan, D.E. A concise review on cancer treatment methods and delivery systems. J Drug Deliv Sci Technol, **2019**, 54, 101350.

Bilalis, P.; Katsigiannopoulos, D.; Avgeropoulos, A.; Sakellario, G. Noncovalent functionalization of carbon nanotubes with polymers. RSC Adv. **2014**, 4, 2911–2934.

Bishehsari, F.; Mahdavinia, M.; Vacca, M.; Malekzadeh, R.; Mariani-Costantini, R. Epidemiological transition of colorectal cancer in developing countries: environmental factors, molecular pathways, and opportunities for prevention. World J Gastroenterol, **2014**, 20, 6055–6072.

Bleau, A. M.; Huse, J. T.; Holland, E. C. The ABCG2 resistance network of glioblastoma. Cell Cycle, **2009,** 8, 2936-44.

Borga, O. et al. Maximum tolerated dose and pharmacokinetics of paclitaxel micellar in patients with recurrent malignant solid tumours: a dose-escalation study. Adv. Ther. **2019**, 36, 1150–1163

Boyle, P.; Langman, S.J. ABC of colorectal cancer. Epidemiology, **2000**, 321, 805–808.

Bray, F.; Ferlay, J.; Soerjomataram, I.; Siegel, R.L.; Torre, L.A.; Jemal, A. Global cancer statistics 2018: GLOBOCAN estimates of incidence and mortality worldwide for 36 cancers in 185 countries. CA: Cancer J. clin, **2018**, 68, 394-424.

Bray, F.; Jemal, A.; Grey, N.; Ferlay, J.; Forman, D. Global cancer transitions according to the human development index (2008–2030): A population-based study. Lancet Oncol, **2012**, 790–801.

Brunetti, C. et al. CPX-351 in acute myeloid leukemia: can a new formulation maximize the efficacy of old compounds? Expert Rev. Hematol. **2017**, 10, 853–862

Buytaert, E; Dewaele, M; Agostinis, P. Molecular effectors of multiple cell death pathways initiated by photodynamic therapy. Biochim Biophys Acta Rev Cancer, **2007**, 1776, 86–107.

Cancer country profile, WHO, **2020**: https://www.who.int/cancer/country-profiles/ZAF_2020.pdf?ua=1.

CANSA reports: https://cansa.org.za/files/2019/04/Fact-Sheet-on-How-to-Reduce-the-Risk-of-Cancer-April-**2019**.pdf.

Chang, J. C. Cancer stem cells: Role in tumor growth, recurrence, metastasis, and treatment resistance. Medicine (Baltimore), **2016**, 95, 20-5.

Chelliah, S.; Sakthivel, L.P.; Brian, C.J.; Yasodha, P.; Appavoo, U.; Maryam, S.H.; Ramasamy, T. Molecular mechanisms of curcumin and its analogs in colon cancer prevention and treatment. Life sciences, **2019**, 239, 117032.

Chen, K.; Huang, Y.H; Chen, J.L. Understanding and targeting cancer stem cells: therapeutic implications and challenges. Acta Pharmacologica Sinica, **2013**, 34, 732.

Chen, R.J.; Zhang, Y.; Wang, D.; Dai, H. Noncovalent sidewall functionalization of single-walled carbon nanotubes for protein immobilization. J. Am. Chem. Soc. **2001**, 123, 3838–3839.

Chiang, M. Y.; Shestova, O.; Xu, L.; Aster, J. C.; Pear, W. S. 2013. Divergent effects of supraphysiologic Notch signals on leukemia stem cells and hematopoietic stem cells. Blood, **2013**, 121, 905-17.

Choi, D.; Lee, H.W.; Hur, K.Y.; Kim, J.J.; Park, G.S.; et al. Cancer stem cell markers CD133 and CD24 correlate with invasiveness and differentiation in colorectal adenocarcinoma. World J Gastroenterol **2009**, 15: 2258–2264.

Choi, K. Y.; Chung, H.; Min, K.; Yoon, H.; Kim, K.; Park, J.H.; Kwon, I.C.; Jeong, S. Y. Self-Assembled hyaluronic acid nanoparticles for active tumor targeting. Biomaterials **2010**, 31, 106−114.

Chouhan, R.; Bajpai, A.K. Real time in vitro studies of doxorubicin release from PHEMA nanoparticles. J. Nanobiotechnology, **2009**, 7:5.

Chu, P.; Clanton, D.J.; Snipas, T.S.; Lee, J.; Mitchell, E.; et al. Characterization of a subpopulation of colon cancer cells with stem cell-like properties. Int J Cancer, **2009**, 124: 1312–1321.

Coco, C.; Zannoni, GF.; Caredda, E.; et al. Increased expression of CD133 and reduced dystroglycan expression are strong predictors of poor outcome in colon cancer patients. J. Exp. Clin. Cancer. Res, **2012**, 31, 71.

Darvishi, B.; Boroumandieh, S.; Majidzadeh-A, K.; Salehi, M.; Jafari, F.; Farahman, L. The role of activated leukocyte cell adhesion molecule (ALCAM) in cancer progression, invasion, metastasis and recurrence: A novel cancer stem cell marker and tumor-specific prognostic marker.Exp. Mol. Pathol, **2020**, 115, 104443.

De Adhikari, A.; Tiwari, S.K.; Ha, S.K.; Nayak, G.C. Boosted electrochemical performance of TiO2 decorated RGO/CNT hybrid nanocomposite by UV irradiation. Vacuum, **2009**, 160, 421–428.

Detty, M.R.; Gibson, S.L.; Wagner, S.J. Current clinical and preclinical photosensitizers for use in photodynamic therapy. J. Med. Chem, **2004**, 47, 3897–3915.

Ding, P.Q.; Batra, A.; Xu, Y.; McKinnon, G.P.; Cheung, W.Y. Obesity and Its Impact on Outcomes in Patients with Stage III Colon Cancer Receiving Adjuvant Chemotherapy. Clin. colorectal cancer, **2020**, 19, 209-218.

Dolmans, D.E.; Fukumura, D.; Jain, R.K. Photodynamic therapy for cancer. Nat. Rev. Cancer. **2003**, 3, 380-387.

Donaldson, K.; Aitken, R.; Tran, L.; Stone, V.; Duffin, R.; Forrest, G.; Alexander, A. Carbon nanotubes: A review of their properties in relation to pulmonary toxicology and workplace safety. Toxicol. Sci. **2006**, 92, 5–22.

Dou, Y. et al. To heat or not to heat: challenges with clinical translation of thermosensitive liposomes. J. Control. Release, **2017**, 249, 63–73

Du, L.; Wang, H.; He, L.; Zhang, J.; Ni, B.; et al. CD44 is of functional importance for colorectal cancer stem cells. Clin Cancer Res, **2008**, 14: 6751–6760.

Editors. The two directions of cancer nanomedicine. Nat. Nanotechnol, **2019**, 14, 12, 1083.

Eun Ji, H.; Dae Gun, C.; Min Suk, S. Targeted and effective photodynamic therapy for cancer using functionalized nanomaterials. Acta Pharma Sin. B. **2016**, 6, 297–307.

Fadeel, B.; Alexiou, C. Brave new world revisited: Focus on nanomedicine. Biochem. Biophys. Res. Commun, **2020,** 533, 36-49.

Fallacara, A.; Baldini, E.; Manfredini, S.; Vertuani, S. (2018). Hyaluronic acid in the third millennium. Carbohydr. Polym, **2018**, 10(7), 701.

Friedmann-Morvinski, D.; Verma, I.M. Dedifferentiation and reprogramming: origins of cancer stem cells, EMBO Rep. **2014**, 15 (3), 244–253.

Gabizon, A. et al. Pharmacokinetics of pegylated liposomal doxorubicin. Clin. Pharmacokinet, **2003**, 42, 419–436

Gabizon, A. et al. Prolonged circulation time and enhanced accumulation in malignant exudates of doxorubicin encapsulated in polyethylene-glycol coated liposomes. Cancer Res, **1994**, 54, 987–992

Gedaly, R.; Galuppo, R.; Daily, M. F.; Shah, M.; Maynard, E.; Chen, C.; Zhang, X.; Esser, K. A.; Cohen, D. A.; Evers, B. M.; Jiang, J.; Spear, B. T. Targeting the Wnt/beta-catenin signaling pathway in liver cancer stem cells and hepatocellular carcinoma cell lines with FH535. PLoS One, **2014**, 9(6), e99272.

Ghaffarzadehgan, K.; Jafarzadeh, M.; Raziee, H.R.; Sima, H.R.; Esmaili-Shandiz, E.; Hosseinnezhad, H.; et al. Expression of cell adhesion molecule CD44 in gastric adenocarcinoma and its prognostic importance. World J Gastroenterol, **2008**, 14(41), 6376-81.

Gladkova, O.L.; Parkhats, M.V.; Gorbachova, A.N.; Terekhow, S.N. FTIR spectra and normal-mode analysis of chlorin e6 and its degradation-induced impurities. Spectrochim. Acta Part A Mol. Biomol. Spectrosc. **2010**, 76, 388–394

Gouda, R.; Baishya, H.; Qing, Z. Application of mathematical models in drug release kinetics of carbide and levodopa ER tablets. J Develop Drugs, **2017**, 6:2.

Grosse-Gehling, P.; Fargeas, C.A.; Dittfeld, C.; et al. CD133 as a biomarker for putative cancer stem cells in solid tumours: limitations, problems and challenges. J Pathol, **2013**, 229, 355-378.

Grzybowski, A.; Sak, J.; Pawlikowski, J. A brief report on the history of phototherapy. Clin. Dermatol, **2016**, 34, 532–537.

Häcker, G. The morphology of apoptosis. Cell Tissue Res, **2000**, 301, 5-17.

Harrington, K. et al. Liposomes as vehicles for targeted therapy of cancer. Part 2: clinical development. Clin. Oncol. **2000**, 12, 16–24

He, H.; Pham-Huy, L.A.; Dramou, P.; Xiao, D.; Zuo, P.; Pham-Huy, C. Carbon nanotubes: Applications in pharmacy and medicine. Biomed Res. Int. **2013**, 578290.

Hiller, J.G.; Perry, N.J.; Poulogiannis, G.; Riedel, B.; Sloan, E.K. Perioperative events influence cancer recurrence risk after surgery. Nat Rev Clin Oncol, **2018**, 15, 205–18.

Hönigsmann, H. History of phototherapy in dermatology. Photochem. Photobiol. Sci, **2013**, 12, 16-21.

Hopper, C. Photodynamic therapy: a clinical reality in the treatment of cancer. Lancet Oncol, **2000**, 1, 212-219.

Hosen, N.; Park, C.Y.; Tatsumi, N.; et al. CD96 is a leukemic stem cell-specific marker in human acute myeloid leukemia. Proc Natl Acad Sci **2007**, 104, 11008-11013

Hou, L.; Zhang, H.; Wang, Y.; Wang, L.; Yang, X.; Zhang, Z. Hyaluronic acid-functionalized single-walled carbon nanotubes as tumor-targeting MRI contrast agent. Int j nanomedicine, **2015**, 10, 4507-4520.

Hou, P.; Bai, S.; Yang, Q.; Liu, C.; Cheng, H. Multi-step purification of carbon nanotubes. Carbon, **2002**, 40, 81–85.

Irollo, E.; Pirozzi, G. CD133: to be or not to be, is this the real question? Am J Transl Res **2013**, 5, 563-581

Islam, F.; Gopalan, V.; Smith, R. A.; Lam, A. K. Translational potential of cancer stem cells: A review of the detection of cancer stem cells and their roles in cancer recurrence and cancer treatment. Experimental Cell Research, **2015**, 335, 135-147.

Jaggupilli, A.; Elkord, E. Significance of CD44 and CD24 as Cancer Stem Cell Markers: An Enduring Ambiguity. Clin dev immunol, **2012**, 2012, 1-11.

Junqi, C.; Chengyun, N.; Zhengnan, Z.; Peng, Y.; Ye, Z.; Guoxin, T.; Chuanbin, M. Nanomaterials as photothermal therapeutic agents. Prog. Mater. Sci. **2019**, 99, 1-26.

Juzeniene, A. Chlorin e6-based photosensitizers for photodynamic therapy and photodiagnosis. Photodiagnosis Photodyn. Ther, **2009**, 6, 26630–26637.

Kataoka, H.; Nishie, H.; Hayashi, N.; Tanaka, M.; Nomoto, A.; Yano, S.; Joh, T. New photodynamic therapy with next-generation photosensitizers. Ann. Transl. Med. **2017**, 5.

Ke, J.; Wu, X.; He, X.; Lian, L.; Zou, Y. et al. A subpopulation of CD24(+) cells in colon cancer cell lines possess stem cell characteristics. Neoplasma, **2012**, 59:282–288.

Kessel, D.; Oleinick, N.L. Photodynamic therapy and cell death pathways. Methods Mol. Biol, **2010**, 35–46.

Khan, M. I.; Czarnecka, A. M.; Helbrecht, I.; Bartnik, E.; Lian, F.; Szczylik, C. Current approaches in identification and isolation of human renal cell carcinoma cancer stem cells. Stem cell res. ther, **2015**, 6, 178-178.

Kharkwal, G.B.; Sharma, S.K.; Huang, Y.Y.; Dai, T.; Hamblin M.R. Photodynamic therapy for infections: clinical applications, Lasers Surg. Med. **2011**, 43, 755–767.

Kim, H.; Kim, Y.; Kim, I.; Kim, K.; Choi, Y. ROS-Responsive Activatable Photosensitizing Agent for Imaging and Photodynamic Therapy of Activated Macrophages. Theranostics **2013**, 4, 1−11.

Kim, W.; Ryu, C.J. Cancer stem cell surface markers on normal stem cells. BMB Reports, **2017**, 50, 285-298

King, S.S.; Chen, D.; et al. Non-covalently functionalized single-walled carbon nanotube for topical siRNA delivery into melanoma. Biomaterials, **2014**, 35(10), 3435-42.

Kobayashi, Y.; Okamoto, A.; Nishinari, K. Viscoelasticity of hyaluronic acid with different molecular weights. Biorheology, **1994**, 31(3), 235–244.

Kou, J.; Dou, D.; Yang, L. Porphyrin photosensitizers in photodynamic therapy and its applications. Oncotarget, **2017**, 8, 81591–81603.

Krok, K.L.; Lichtenstein, G.R. Colorectal cancer in inflammatory bowel disease. Curr. Opin. Gastroenterol. **2004**, 20, 43–48.

Kumar, C.S.; Raja, M.D.; Sundar, D.S.; Antoniraj, M.G.; Ruckmani, K. Hyaluronic acid co-functionalized gold nanoparticle complex or the targeted delivery of metformin in the treatment of liver cancer (HepG2 cells). Carbohydr. Polym. **2015**, 128, 63–74

Kumar, T.H.V.; Sundramoorthy, A.K. Non-enzymatic electrochemical detection of urea on silver nanoparticles anchored nitrogen-doped single-walled carbon nanotube modified electrode. J. Electrochem. Soc. **2018**, 165, B3006–B3016.

Kuroda, Y.; Kitada, M.; Wakao, S.; et al. Unique multipotent cells in adult human mesenchymal cell populations. Proc Natl Acad Sci, **2010**, 107, 8639-8643

Kusunoki, S.; Kato, K.; Tabu, K.; Inagaki, T.; Okabe, H.; Kaneda, H.; et al. The inhibitory effect of salinomycin on the proliferation, migration and invasion of human endometrial cancer stem-like cells. Gynecol Oncol, **2013**, 129(3), 598-605

Lancet, J.E. et al. Survival following allogeneic hematopoietic cell transplantation in older high-risk acute myeloid leukemia patients initially treated with CPX–351 liposome injection versus standard cytarabine and daunorubicin: subgroup analysis of a large Phase III trial. Blood, **2016**, 128, 906

Lapidot, T.; Dar, A.; Kollet, O. How do stem cells find their way home? Blood, **2005**, 106, 1901-1910

Lathia, J.D.; Gallagher, J.; Heddleston, J.M.; et al. Integrin alpha 6 regulates glioblastoma stem cells. Cell Stem Cell, **2010**, 6, 421-432.

Lee, H.J.; Choe, G.; Jheon, S.; Sung, S.W.; Lee, C.T.; Chung, J.H. CD24, a novel cancer biomarker, predicting diseasefree survival of non-small cell lung carcinomas: a retrospective study of prognostic factor analysis from the viewpoint of forthcoming (Seventh) New TNM classification. J Thorac Oncol, 2010, 649–657.

Lei, W.; Jinjin, S.; Ruiyuan, L.; Yan, L.; Jing, Z.; Xiaoyuan, Y.; Jun, G.; Chaofeng, Z.; Zhenzhong, Z. Photodynamic effect of functionalized singlewalled carbon nanotubes: A potential sensitizer for photodynamic therapy. Nanoscale **2014**, 6, 4642–4652.

Li, C.; Heidt, D.G.; Dalerba, P.; et al. Identification of pancreatic cancer stem cells. Cancer Res, **2007**, 67, 1030-1037

Li, X.; Lee, S.; Yoon, J. Supramolecular photosensitizers rejuvenate photodynamic therapy. Chem. Soc. Rev, **2018**, 47, 1174–1188.

Liu, P.; Yue, C.; Sheng, Z.; Gao, G.; Li, M.; Yi, H.; Zheng, C.; Wang, B.; Cai, L. Photosensitizer-conjugated redox-responsive dextran theranostic nanoparticles for near-infrared cancer imaging and photodynamic therapy, Polym. Chem. 2014, 5:3, 874–881.

Liu, W.; Speranza, G. Functionalization of carbon nanomaterials for biomedical applications. J. Carbon Res. **2019**, 5, 72.

Liu, Y.; Sun, Y.; et al. Dual targeting folate-conjugated hyaluronic acid polymeric micelles for paclitaxel delivery. Int j. pharm, **2011**, 421(1):160-169.

Liu, Z.; Robinson, J.T.; Tabakman, S.M.; Yang, K.; Dai, H. Carbon materials for drug delivery & cancer therapy. Materials Today, **2011**, 14, 316-323.

Lopez-Lazaro, M. What is the main cause of cancer? Europe PMC, **2016**, 1(1):1-2.

Luksiene, Z. Photodynamic therapy: mechanism of action and ways to improve the efficiency of treatment. Med, **2003**, 39, 1137–1150.

Lundin, A.; Driscoll, B. Lung cancer stem cells: progress and prospects. Cancer Lett, **2013**, 338, 89-93.

Luo, D.; Carter, K.A.; Mirand, D.; Lovell, J.F. Chemophototherapy: an emerging treatment option for solid tumors, Adv. Sci. **2017**, 4, 1600106.

Luo, W.; Liu, R.; Zhu, J.; Li, Y.; Liu, H. Subcellular location and photodynamic therapeutic effect of chlorin e6 in the human tongue squamous cell cancer Tca8113 cell line. Oncology Letters, **2015**, 9, 551-556

Lyon, P.C. et al. Safety and feasibility of ultrasound-triggered targeted drug delivery of doxorubicin from thermosensitive liposomes in liver tumours (TARDOX): a single-centre, open-label, Phase 1 trial. Lancet Oncol, **2018**, 19, 1027–1039

Ma, L.; Zhang, G.; Miao, X.B.; Deng, X.B.; Wu, Y.; et al. Cancer stem-like cell properties are regulated by EGFR/AKT/beta-catenin signaling and preferentially inhibited by gefitinib in nasopharyngeal carcinoma. FEBS J, **2013**, 280: 2027–2041.

Mansoori, B.; Mohammadi, A.; Davudian, S.; Shirjang, S.; Baradaran, B. The different mechanisms of cancer drug resistance: a brief review. Adv. Pharm. Bull. **2017**, 7 (3), 339–348.

Marangon, I.; Ménard-Moyon, C.; Silva, A.K.A.; Bianco, A.; Luciani, N.; Gazeau, F. Synergic mechanisms of photothermal and photodynamic therapies mediated by photosensitizer/carbon nanotube complexes. Carbon **2016**, 97, 110–123.

Marhaba, R.; Zoller, M. CD44 in cancer progression: adhesion, migration and growth regulation. J Mol Histol **2004**, 35, 211–231.

Marley, A.R.; Nan, H. Epidemiology of colorectal cancer. Int J Mol Epidemiol Genet. **2016**, 7, 105-114.

Martin, TA.; Ye, L.; Sanders, A.J.; et al. Cancer Invasion and Metastasis: Molecular and Cellular Perspective. Madame curie Bioscience, **2013**, 1-56.

Mehra, N.K.; Palakurthi, S. Interactions between carbon nanotubes and bioactives: A drug delivery perspective. Drug Discov. Today, **2016**, 21, 585–597

Meyerhardt, J.A.; Heseltine, D.; Niedzwiecki, D.; Hollis, D.; Saltz, L.B.; Mayer, R.J.; et al. Impact of physical activity on cancer recurrence and survival in patients with stage III colon cancer: findings from CALGB 89803. J Clin Oncol, **2006**, 24, 3535–41.

Moan, J.; Peng, Q. An outline of the hundred-year history of PDT. Anticancer Res, **2003**, 23, 3591–3600.

Mohan K. H.; Pai S., Rao R., Sripathi H.; Prabhu, S. Techniques of immunofluorescence and their significance. Indian. J Dermatol. VE, **2008**, 74(4): 415–419.

Molofsky, A.V.; Pardal, R.; Morrison, S.J. Diverse mechanisms regulate stem cell self-renewal. Curr Opin Cell Biol, **2004**, 16(6), 700–7.

Mu, Q.; Broughton, D.L.; Yan, B. Endosomal leakage and nuclear translocation of multiwalled carbon nanotubes: Developing a model for cell uptake. Nano Lett. **2009**, 9, 4370–4375.

Mukai, H. et al. Phase I study of NK105, a nanomicellar paclitaxel formulation, administered on a weekly schedule in patients with solid tumors. Invest. New Drugs, **2016**, 34, 750–759

National Institutes of Health resource for stem cell research. July 21, **2008**. The stem cell information Stem Cell Basics page. Available at: http://stemcells.nih.gov/info/basics/ defaultpage.asp.

Napier, S.L.; Healy, Z.R.; Schnaar, R.L.; Konstantopoulos, K. Selectin ligand expression regulates the initial vascular interactions of colon carcinoma cells: the roles of CD44V and alternative sialofucosylated selectin ligands. Bio. Chem, 2007, vol. 282, no. 6, pp. 3433–3441, 2007.

Needham, J.; Gwei-Djen, L. Science and Civilisation in China. Spagyrical Discovery and Invention: Physiological Alchemy, **1983**, 5, 5.

Ng, V.Y.; Ang, S.N.; Chan, J.X.; Choo, A.B. Characterization of epithelial cell adhesion molecule as a surface marker on undifferentiated human embryonic stem cells. Stem Cells, **2010**, 28, 29-35

Nowak-Stepniowska, A.; Pergoł, P.; Padzik-Graczyk, A. Photodynamic method of cancer diagnosis and therapy–mechanisms and applications. Postepy Biochem, **2013**, 59, 53–63.

O'Brien, C.A. et al. A human colon cancer cell capable of initiating tumour growth in immunodeficient mice. Nature, **2007**, 445, 106–110.

Ogbodu, R.O.; Antunes, E.; Nyokong, T. Physicochemical properties of zinc monoamino phthalo cyanine conjugated to folic acid and single walled carbon nanotubes. Polyhedron **2013**, 60, 59–67.

Ogbodu, R.O.; Nyokong, T. The effect of ascorbic acid on the photophysical properties and photodynamic therapy activities of zinc phthalocyanine-single walled carbon nanotube conjugate on MCF-7 cancer cells. Spectrochim. Acta Part A Mol. Biomol. Spectrosc. **2015a**, 151, 174–183.

Ogbodu, R.O.; Ndhundhuma, I.; Karsten, A.; Nyokong, T. Photodynamic therapy effect of zinc monoaminophthalocyanine–folic acid conjugate adsorbed on single walled carbon nanotubes on melanoma cells. Spectrochim. Acta A **2015b**, 137, 1120–1125

Ogbodu, R.O.; Limson, J.L.; Prinsloo, E.; Nyokong, T. Photophysical properties and photodynamic therapy effect of zinc phthalocyanine-spermine-single walled carbon nanotube conjugate on MCF-7 breast cancer cell line. Synth. Metals **2015c**, 204, 122–132.

Ong, C.W.; Kim, L.G., Kong, H.H., et al. CD133 expression predicts for non-response to chemotherapy in colorectal cancer. Mod Pathol, **2010**, 23, 450-457.

Orlic, D.; Hill, J.M.; Arai, A.E. Stem cells for myocardial regeneration. Circ. Res. **2002**, 91:12, 1092-1102.

Ozvegy-Laczka, C.; Cserepes, J.; Elkind, N. B.; Sarkadi, B. Tyrosine kinase inhibitor resistance in cancer: role of ABC multidrug transporters. Drug Resist Updat, **2005**, 8, 15-26.

Pacal, I.; Karaboga, D.; Basturk, A.; Akay, B.; Nalbantoglu, U. A comprehensive review of deep learning in colon cancer. Comput. bio. med, **2020**, 126, 104003.

PanelIlche, G.; Eleftheria, G.; et.al. Evaluation of polyvinylpyrrolidone and block copolymer micelle encapsulation of serine chlorin e6 and chlorin e4 on their reactivity towards albumin and transferrin and their cell uptake. J Controlled Release, **2019**, 316, 150-167.

Park, H.; Zhao, J.; Lu, J.P. Effects of Sidewall Functionalization on Conducting Properties of Single Wall Carbon Nanotubes. Nano Lett, **2006**, 5, 916–919.

Pathak, M. A.; Fitzpatrick, T. B. The evolution of photochemotherapy with psoralens and UVA (PUVA): 2000 BC to 1992 AD. J. Photochem. Photobiol. B, **1992**, 14, 3-22

Patra, J.K.; Das, G.; Fraceto, L.F.; Campos, E.V.R.; Rodriguez-Torres, M.d.P.; Acosta-Torres, L.S.; Diaz-Torres, L.A.; Grillo, R.; Swamy, M.K.; Sharma, S.; Habtemariam, S.; Shin, H. Nano based drug delivery systems: Recent developments and future prospects. J nanobiotechnology, **2018**, 16(1), 71.

Patriarca, C.; Macchi, R.M.; Marschner, A.K.; Mellstedt, H. Epithelial cell adhesion molecule expression (CD326) in cancer: a short review. Cancer Treat Rev, **2012**, 38, 68-75.

Patrice, T.; Moan, J.; Peng, Q. An outline of the history of PDT, Comprehensive series in photochemical and photobiological sciences. RSC, **2003**, 1-18.

Peer, D. et al. Nanocarriers as an emerging platform for cancer therapy. Nat. Nanotechnol, **2007**, 2, 751–760.

Peiris-Pagès, M.; Martinez-Outschoorn, U. E.; Pestell, R. G.; Sotgia, F.; Lisanti, M. P. Cancer stem cell metabolism. Breast cancer res, **2016**, 18, 55-55.

Phi, L.T.H.; Sari, I.N.; Yang, Y.G.; Lee, S.H.; Jun, N.; Kim, K.S.; et al. Cancer stem cells (CSCs) in drug resistance and their therapeutic implications in cancer treatment. Stem Cells Int, **2018**, 5416923.

Plaetzer, K; Kiesslich, T; Verwanger, T; Krammer, B. The modes of cell death induced by PDT: an overview. Med. Laser Appl, **2003**, 18,7–19.

Pubchem: https://pubchem.ncbi.nlm.nih.gov/compound/Chlorin-e6

Raycraft, T.; Winson, Y.; Cheung; Yaling, Yin.; Speers, C.; Jenny, J. K.; Mariano, C. Causes of mortality in older patients with stage 3 colon cancer. Journal of geriatric oncology, **2019**, 10, 138-142.

Rebecca, L.S.; Kimberly, D.M.; Ahmedin, J. Cancer statistics. CA Cancer J. Clin. **2019**, 69, 7-34.

Ricci-Vitiani, L. et al. Identification and expansion of human colon-cancer-initiating cells. Nature, **2007**, 445, 111–115.

Rubin, L. L; De Sauvage, F. J. Targeting the Hedgehog pathway in cancer. Nature Reviews. Drug Discovery, **2006**, 5, 1026-1033.

Russo, J. E.; Hilton, J. Characterization of cytosolic aldehyde dehydrogenase from cyclophosphamide resistant L1210 cells. Cancer Res, **1988**, 48, 2963-8.

Sahlberg, S.H.; Spiegelberg, D.; Glimelius, B.; Stenerlöw, B.; Nestor, M. Evaluation of Cancer Stem Cell Markers CD133, CD44, CD24: Association with AKT Isoforms and Radiation Resistance in Colon Cancer Cells. PloS one **2014**, 9, e94621.

Sajid, M.I.; Jamshaid, U.; Jamshaid, T.; Zafar, N.; Fessi, H.; Elaissari, A. Carbon nanotubes from synthesis to in vivo biomedical applications. Int. J. Pharm. **2016**, 501, 278–299.

Santoro, A.; Vlachou, T.; Carminati, M.; Pelicci, P. G.; Mapelli, M. Molecular mechanisms of asymmetric divisions in mammary stem cells. EMBO reports, **2016**, 17, 1700-1720.

Seligmann, J.F.; Elliott. F.; Richman, S.; Hemmings, G.; Brown, S.; et al. Clinical and molecular characteristics and treatment outcomes of advanced right-colon, left-colon and rectal cancers: data from 1180 patients in a phase III trial of panitumumab with an extended biomarker panel. Annals of Oncology, **2020**, 31 (8), 1021-1029.

Senapati, S.; Mahanta, A.K.; Kumar, S.; Maiti, P. Controlled drug delivery vehicles for cancer treatment and their performance. Signal transduct target ther, **2018**, 3, 7-19,

Shi, S.; Chen, F.; Ehlerding, E.B.; Cai, W. Surface engineering of graphene-based nanomaterials for biomedical applications. Bioconjug. Chem. **2014**, 25, 1609–1619.

Silverman, L.; Barenholz, Y. In vitro experiments showing enhanced release of doxorubicin from Doxil1 in the presence of ammonia may explain drug release at tumor site. Nanomedicine **2015**, 11, 1841–1850.

Singh, B.; Baburao, C.; Pispati, V.; Pathipati, H.; Muthy, N.; Prassana, S.; Rathode, B.G. Carbon nanotubes: A novel drug delivery system. Int. J. Res. Pharm. Chem. **2012**, 2, 523–532

Singh, B.; Mitragotri, S. Harnessing cells to deliver nanoparticle drugs to treat cancer. Biotechnol. Adv, **2020**, 42, 107339

Slomiany, M.G.; Dai, L.; Tolliver, B.T.; Grass, G.D.; Zeng, Y.; Toole, B.P. Inhibition of functional hyaluronan-CD44 interactions in CD133 positive primary human ovarian carcinoma cells by small hyaluronan oligosaccharides. Clin Cancer Res, **2009**, 15, 24, 7593–7601.

South African National Cancer Registry. Cancer in South Africa (2010). Cited Oct 25, **2018**. Available from URL: http://www.cansa.org.za/south-african-cancer-statistics.

Spano, D.; Heck, C.; De Antonellis, P.; Christofori, G.; Zollo, M. Molecular networks that regulate cancer metastasis. Seminars Cancer Biol, **2012**, 22, 234–249

Sperandio, F.F.; Huang, Y.Y.; Hamblin, M.R. Antimicrobial photodynamic therapy to kill Gram-negative bacteria, Recent Pat. Antiinfect. Drug Discov, **2013**, 8, 108–120

Sun, M.; Zhou, W.; Zhang, Y.Y.; Wang, D.L.; Wu, X.L. CD44+ gastric cancer cells with stemness properties are chemoradioresistant and highly invasive. Oncol Lett, **2013**, 5, 1793-8.

Sundaram, P.; Abrahamse, H. Effective photodynamic therapy for colon cancer cells using chlorin e6 coated hyaluronic acid-based carbon nanotubes. Int. J. Mol. Sci, **2020a**, 21, 4745.

Sundaram, P.; Abrahamse, H. Phototherapy Combined with Carbon Nanomaterials (1D and 2D) and their Applications in Cancer Therapy. Materials **2020b**, 13, 4830.

Sundberg, M.; Jansson, L.; Ketolainen, J.; et al. CD marker expression profiles of human embryonic stem cells and their neural derivatives, determined using flow-cytometric analysis, reveal a novel CD marker for exclusion of pluripotent stem cells. Stem Cell Res, **2009**, 2, 113-124.

Swenson, C. et al. Liposome technology and the development of MyocetTM (liposomal doxorubicin citrate). Breast, **2001**, 10, 1–7

Tan, J.M.; Arulselvan, P.; Fakurazi, S.; Ithnin, H.; Hussein, M.Z. A Review on Characterizations and Biocompatibility of functionalized carbon nanotubes in drug delivery design. J. Nanomater. **2014**, 917024.

Tavianatou, A. G.; Caon, I.; Franchi, M.; Piperigkou, Z.; Galesso, D.; Karamanos, N. K. Hyaluronan: Molecular size-dependent signaling and biological functions in inflammation and cancer. The FEBS journal, **2019**, 286(15), 2883–2908.

Thapa, R.; Wilson, G.D. The Importance of CD44 as a Stem Cell Biomarker and Therapeutic Target in Cancer. Stem Cells Int, **2016**, 2087204.

The World Bank, Upper Middle Income, The World Bank Group, Washington, DC, **2016**. http://data.worldbank.org/income-level/ upper-middle-income.

Thomson, J.A.; Itskovitz-Eldor, J.; Shapiro, S.S.; et al. Embryonic stem cell lines derived from human blastocysts. Science, **1998**, 282, 1145-1147.

Tirino, V.; Desiderio, V.; Paino, F.; De Rosa, A.; Papaccio, F.; La Noce, M.; Laino, L.; De Francesco, F.; Papaccio, G. Cancer stem cells in solid tumors: an overview and new approaches for their isolation and characterization. Faseb j, **2013**, 27, 13-24.

Toole, B.P.; Wight, T.N.; Tammi, M.I. Hyaluronan-cell interactions in cancer and vascular disease. The journal of biological chemistry, **2002**, 277(7):4593-4596.

Trautinger, F.; Knobler R.; Willemze, R. et. al., EORTC consensus recommendations for the treatment of mycosis fungoides/Sézary syndrome, Eur.J. Cancer, **2006**, 42, 1014-1030.

Tuncel, D. Non-covalent interactions between carbon nanotubes and conjugated polymers. Nanoscale **2011**, 3, 3545–3554.

Valastyan, S.; Weinberg, R.A. Tumor metastasis: molecular insights and evolving paradigms. Cell **2011**, 147, 275–292.

Vander Heiden; M. G.; Cantley, L. C.; Thompson, C. B. Understanding the Warburg effect: the metabolic requirements of cell proliferation. Science (New York, N.Y.), **2009**, 324, 1029-1033

Ventimiglia, E.; Seisen, T.; Abdollah, F.; Briganti, A.; Fonteyne, V.; James, N.; Roach, M.; Thalmann, G.N.; Touijer, K.; Chen, R.C.; Cheng, L. A Systematic Review of the Role of Definitive Local Treatment in Patients with Clinically Lymph Node-positive Prostate Cancer. Eur. Urol. oncol, **2019**, 2, 294-301.

Verhaar, S.; Vissers, P.A.J.; Maas, H.; Poll-Franse, L.V.; Erning, F.N.; Mols, F. Treatment-related differences in health-related quality of life and disease specific symptoms among colon cancer survivors. Euro. J. Cancer, **2015**, 51, 1263–1273.

Virginia, M.P.; Francis C S. (2008). Anticancer therapeutics: targeting macromolecules and nanocarriers to hyaluronan or CD44, a hyaluronan receptor. Mol pharma, **2008**, 5, 474-486.

Visvader, J. E.; Lindeman, G. J. Cancer stem cells: current status and evolving complexities. Cell Stem Cell, **2012**, 10, 717-728.

Wang, C.; Chiou, S.; Chou, C.; Chen, Y.; Huang, Y.; Peng, C. Photothermolysis of glioblastoma stem-like cells targeted by carbon nanotubes conjugated with CD133 monoclonal antibody. Nanomed. Nanotechnol. Biol. Med, **2011**, 7, 69–79.

Weichert, W.; Denkert, C.; Burkhardt, M.; Gansukh, T.; Bellach, J.; et al. Cytoplasmic CD24 expression in colorectal cancer independently correlates with shortened patient survival. Clin Cancer Res, **2005**, 11: 6574–6581.

Wiskemann, A. Recent developments in light therapy. Dermatol, **1963**, 20, 377-383.

Wobus, M.; Rangwala, R.; Sheyn, I.; Hennigan, R.; Coila, B.; et al. CD44 associates with EGFR and erbB2 in metastasizing mammary carcinoma cells. Appl Immunohistochem Mol Morphol **2002**, 10, 34–39.

Wolff, K.W.; Fitzpatrick, T.B.; Parrish, J.A.; Gschnait, F.; Gilchrest, B.; Hönigsmann, H.; Pathak, M. A.; Tanenbaum, L. Photochemotherapy for psoriasis with orally administered methoxsalen, Arch Dermatol, **1976**, 112, 943-950.

World Health organisation (WHO), Cancer country profile **2020**, Available from URL: https://www.who.int/cancer/country-profiles/ZAF_2020.pdf?ua=1.

WHO, World Health organisation **2018**: https://www.who.int/news-room/fact-sheets/detail/cancer.

Wu, C.; Li, D.; Wang, L.; Guan, X.; Tian, Y.; Yang, H.; Li, S.; Liu, Y. Single wavelength light-mediated synergistic bimodal cancer photoablation and amplified photothermal performance by graphene/gold nanostar/photosensitizer theranostics. Acta Biomater. **2017**, 53, 631–642.

Xiao, H.; Zhu, B.; Wang, D.; Pang, Y.; He, L.; Ma, X.; Wang, R.; Jin, C.; Chen, Y.; Zhu, X. Photodynamic effects of chlorin e6 attached to single wall carbon nanotubes through noncovalent interactions. Carbon, **2012**, 50, 1681-1689.

Xie, L.; Wang, G.; Zhou, H.; Zhang, F.; Guo, Z.; Liu, C.; Zhang, X.; Zhu, L. Functional long circulating single walled carbon nanotubes for Fluorescent/photoacoustic imaging-guided enhanced phototherapy. Biomaterials, **2016**, 103, 219–228.

Xu, F.; Xu, J.; Ji, J.; Shen, J.Anovel biomimetic polymer as amphiphilic surfactant for soluble and biocompatible carbon nanotubes (CNTs). Colloids Surf. B, **2008**, 67, 67–72.

Yang, J.; Teng, Y.; Fu, Y.; Zhang, C. Chlorins e6 loaded silica nanoparticles coated with gastric cancer cell membrane for tumor specific photodynamic therapy of gastric cancer. International journal of nanomedicine **2019**, 14, 5061-5071

Yao, H.; Zhang, Y.; Sun, L.; Liu, Y. The effect of hyaluronic acid functionalized carbon nanotubes loaded with salinomycin on gastric cancer stem cells. Biomaterials, **2014**, 35(33), 9208-9223.

Yin, A.H.; Miraglia, S.; Zanjani, E.D.; et al. AC133, a novel marker for human hematopoietic stem and progenitor cells. Blood, **1997**, 90, 5002-5012

Yoo, C.H.; Noh, S.H.; Kim, H.; Lee, H.Y.; Min, J.S. Prognostic significance of CD44 and nm23 expression in patients with stage II and stage IIIA gastric carcinoma. J Surg Oncol **1999**, 71, 22-8

Yoo, J. O.; Ha, K. S. New insights into the mechanisms for photodynamic therapy-induced cancer cell death. Int Rev Cell Mol Biol, **2012**, 295, 139-74.

Yoon, I.; Li, J.Z.; Shim, Y.K. Advance in photosensitizers and light delivery for photodynamic therapy. Clin. Endosc, **2013**, 46, 7–23.

Yu, K.R.; Yang, S.R.; Jung, J.W.; et al. CD49f enhances multipotency and maintains stemness through the direct regulation of OCT4 and SOX2. Stem Cells **2012**, 30, 876-887.

Zhang, C.; Li, C.; He, F.; Cai, Y.; Yang, H. Identification of CD44+CD24+ gastric cancer stem cells. J Cancer Res Clin Oncol, **2011a**, 137, 1679-1686

Zhang, L.; Gao, S.; Zhang, F.; Yang, K.; Ma, Q.; Zhu, L. Activatable Hyaluronic Acid Nanoparticle as a Theranostic Agent for Optical/Photoacoustic Image-Guided Photothermal Therapy. ACS Nano **2014**, 8, 12250−12258.

Zhang, J.; Jiang, C.; Figueiro Longo, J. P.; Azevedo, R. B.; Zhang, H.; Muehlmann, L. A. An updated overview on the development of new photosensitizers for anticancer photodynamic therapy. Acta Pharm Sin B, **2018**, 8, 137-146.

Zhang, P. Y.; Yang, Y. J.; Xue, Y.; Fu, J.; Zhang, C. X.; Wang, Y.; Yang, Y.; Shi, H. Cancer stem cells: targeting tumors at the source. Eur Rev Med Pharmacol Sci, **2015**, 19, 1821-8.

Zhang, W.; Gu, Z.; Huang, D.; Liu, Z.; Guo, X.; Zhong, H. Synergistic effect of chemo photothermal therapy using PEGylated graphene Oxide. Biomaterials, **2011b**, 32, 8555–8561.

Zhang, Z.Q.; Liu, B.; Chen, Y.L.; Jiang, H.; Hwang, K.C.; Huang, Y. Mechanical properties of functionalized carbon nanotubes. Nanotechnology **2008**, 19, 395702.

Zheng, Y.B.; Luo, H.P.; Shi, Q.; Hao, N.Z.; Ding, Y.; Wang, Q.S.; et al. miR-132 inhibits colorectal cancer invasion and metastasis via directly targeting ZEB2. World J. Gastroenterology, **2014**, 20, 6515.

Zoller, M. CD44: can a cancer-initiating cell profit from an abundantly expressed molecule? Nat Rev Cancer **2011**, 11, 254-267.

Zuk, P.A.; Zhu, M.; Ashjian, P.; et al. Human adipose tissue is a source of multipotent stem cells. Mol Biol Cell, **2002**, 13, 4279-4295.

APPENDICES

APPENDIX A
Methodology flow diagram

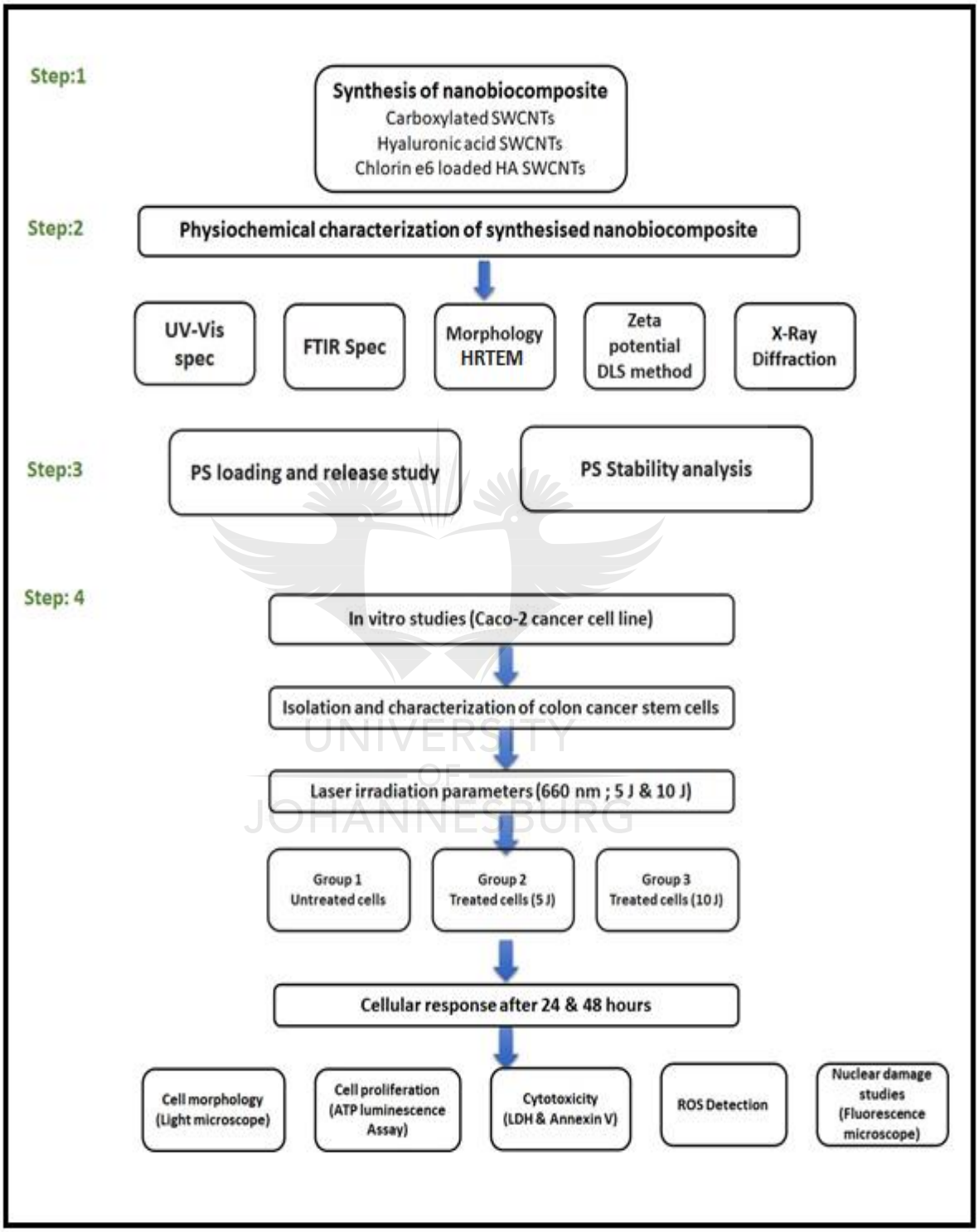

APPENDIX B
B1: List of consumables

Product	Catalogue number	Company/supplier
35mm x 10mm Style Treated Polystyrene Cell Culture Dish	430165	Corning incorporated
10 mL Disposable pipette	BD357551	Beckson Dickinson
10 mL stripette serological pipets	4488	Corning incorporated
5 mL disposable pipette	BD357543	Beckson Dickinson
5 mL stripette serological pipets	4051	Corning incorporated
Centrifuge tubes, 50 mL, PP flat top, sterile, bulk	CR430489	Corning incorporated
Eppendorf®, Microtubes	Z666521	Sigma Aldrich
Eppendorf®, Microtubes	Z666505	Sigma Aldrich
Eppendorf®, Microtubes	Z666515	Sigma Aldrich
Microplate, 96 well, F-Bottom clear, sterile	655161	Sigma Aldrich
Microplate, 96 well, F-Bottom (Chimney well), white, lumitrac, high binding, sterile	665074	Sigma Aldrich
Microscope slides, frosted one end size 25 mm x 75 mm	S8400	Sigma Aldrich
Latex Gloves powder free	EV/55620	Thermo Fisher Scientific
Falcon (5mL) Polystyrene round bottom tube	BD352054	Beckson Dickinson
Corning® cell culture flasks	CLS430639/ CLS430641/ CLS431080	Sigma
Corning® microvolume pipet tips 0.2-10 µL	CLS4840	Sigma
Corning® tissue-culture treated culture dishes	CLS430165	Sigma
Corning® non-treated culture dishes	CLS430588	Sigma
Corning® universal fit pipet tips 1-200 µL	CLS4845	Sigma
Corning® universal fit pipet tips	CLS4868	Sigma

100-1000 µL		
Countess™ Cell Counting Chamber Slide	C10228	Invitrogen™
Cryogenic vial 2 mL	CR430489	Corning
Eppendorf® LoBind microcentrifuge tubes	Z666556	Sigma
Greiner Cryo.s™ vials 5 mL	V9137	Sigma

B2: List of equipment's

Product	Catalogue number	Company/supplier
Autoclave	SA-300VL	STURDY
Barnstead™ Smart2Pure™ Water Purification System	50129688	Thermo Scientific™
Biological Safety Cabinet		Airvolution
-80 ºC Freezer United Scientific	UF440-86E	Sneijder Scientific
Ice Machine	Scotsman AF80	Lasec
Inverted Fluorescence Microscope	Axio Observer Z1	Carl Zeiss
Light Microscope	Olympus CKX41	Wirsam
High-Sensitivity Thermopile Sensor PM3	1098336	Coherent
Heraeus™ Multifuge™ X1 Centrifuge Series	75004250	Thermo Scientific™
Heraeus™ Fresco™ 17 Microcentrifuge	75002402	Thermo Scientific™
Combi-Spin	FVL-2400	BioSan
Heracell™ 150i CO2 Incubator	51026280	Thermo Scientific™

Genova 7315 Life Science Spectrophotometer	55205	Jenway®
Genova Nano	67912	Jenway®
660 nm laser		National Laser Centre, South Africa
FieldMate Laser Power Meter	1098297	Coherent
Fourier-transform infrared (FTIR) spectrometer	Spectrum 100	PerkinElmer
Countess™ II Automated Cell Counter	AMQAX1000	ThermoFischer
C6 flow cytometer	BD ACCURI C6 PLUS	BD Biosciences
Multilabel counter Victor 3	1420	Perkin Elmer
JEM 2100F	200 kV FE	JEOL Ltd
X-ray diffractometer	Ultima IV	Rigaku
Zeta sizer	ver. 7.10	Malvern Instruments Ltd
Magnetic stirrer	RCT basic	IKA
-80 ºC Freezer	UF440-86E	United Scientific Sneijder Scientific

B3: List of reagents and media

Product	**Catalogue number**	**Company/supplier**
Single walled carbon nanotubes	652490	Sigma-Aldrich
Chlorin e6	CAS 19660-77-6	Santa Cruz biotechnology

Hyaluronic acid	40583	Sigma-Aldrich
Nitric acid	438073	Sigma-Aldrich
Membrane filter pore size 0.22 µm	S2GPU05RE	Merck
Dimethyl formamide	227056	Sigma-Aldrich
N-ethylcarbodiimde hydrochloride	E6383	Sigma-Aldrich
N-hydroxysuccinimide	130672	Sigma-Aldrich
Triethylamine 99 %	T0886	Sigma-Aldrich
Dialysis bag	D9777	Sigma-Aldrich
Tween80	P1754	Sigma-Aldrich
Caco-2 cell lines	HTB-37™	ATCC®
SK-UT-1 cell lines	HTB-114™	ATCC®
Dulbecco's modified eagle's medium	D5796	Sigma-Aldrich
Dulbecco's modified eagle's medium F-12	D6421	Sigma-Aldrich
Eagle's Minimum Essential Medium	51412C	Sigma-Aldrich
foetal bovine serum	F9665	Sigma-Aldrich
L-glutamate	G7513	Sigma-Aldrich
Amphotericin B solution	A2942	Sigma-Aldrich
Bovine Serum Albumin	A2153	Sigma-Aldrich
CD133 microbead kit	130-050-801	Miltenyi Biotec
CD44 microbead kit	130-095-194	Miltenyi Biotec
CD24 microbead kit	130-095-951	Miltenyi Biotec
Anti-human CD44	MABF425, human/mouse, PE-Cy5, clone IM7	Sigma-Aldrich
Anti-human CD133	ZRB 1013, human/rabbit, clone F8, ZooAb	Merck
Anti-human CD24	555426, human/mouse, clone ML5	BD Biosciences
FTIC Mouse anti-rabbit antibodies	Sc 2359	Santa Cruz biotechnology

Cy5 goat anti mouse antibodies	NB7602	Novus Bio,
CD133 Vio® Bright FTIC	130-133-673	Miltenyi Biotec
DAPI	D1306	Invitrogen™
EDTA	60-00030-11	pluriSelect
Ethanol Absolute 99.9%	IS-O 9001	Glassworld
FITC Annexin V Apoptosis Detection Kit I	556547	BD Pharmingen™
Flow Cytometer Fluid Kit	653158	BD Biosciences
Fluoromount™ Aqueous Mounting Medium	F4680	Sigma-Aldrich
LysoTracker™ Green	L7526	Invitrogen™
MitoTracker™ Green FM	1890551	Invitrogen™
ERTracker™ Blue white DPX	E12353	Invitrogen™
4 % Paraformaldehyde	P6148	Sigma-Aldrich
Hanks Balances Salt Solution (HBSS)	55021C	Sigma-Aldrich
Hoechst 33342	H3570	Thermo Fisher Scientific
Penicillin/Streptomycin	P4333	Sigma-Aldrich
Phosphate Buffer Saline	P4417	Sigma-Aldrich
Triton X-100	T9284	Sigma-Aldrich
TrypLE™ Select	12563-029	Gibco Invitrogen
Trypan Blue	T8154	Sigma-Aldrich
Mineral Oil	DY1151	Promega
Sodium azide	S8032	Sigma-Aldrich
Trypan Blue Stain (0.4%)	T10282	Invitrogen™

APPENDIX C

Calculations

C1. Calculation of cell amount and viability

The percentage viability and number of cells per mil were retrieved using the Countess™ II Automated Cell Counter. From the results obtained Total amount of cells in suspension was calculated as follows:

$$Total\ cells\ per\ ml \times Suspension\ volume(ml) = Total\ amount\ of\ cells\ in\ suspension$$

C2. Calculation of volume of cell seeding density in a cell culture flask

Cryopreserved cells are cultured from liquid nitrogen. One ampule will be culture in a 25 cm^2 T-flask in 5 mL complete culture media. Cells are incubated and allowed to grow until confluency. Cells are passaged once confluent into a larger TC flask i.e. 75 cm^2 with complete growth media of 15 mL. Cells are detached and counted (C1). The proposed number of cells for a 75 cm^2 flask is 2×10^6. The volume of cells to be seeded from the cell suspension is as follows:

$$Total\ amount\ of\ cells\ in\ suspension = Total\ cells\ per\ mL \times Suspension\ volume(mL)$$

$$Cell\ seeding = \frac{Total\ amount\ of\ cells\ in\ suspension}{proposed\ seeding\ density}$$

C3. Calculation for cell seeding density of 3.4 cm petri dishes

The cell seeding density for culturing cells in a 3.4 cm petri dish is cell line dependant. An optimum seeding density is predetermined in order to carry out downstream biochemical applications. The optimum seeding density for Caco-2 colon cancer is at 5×10^5 cells in 3 mL media. The volume of cells to seed from a suspension is as follows:

$$Total\ amount\ of\ cells\ in\ suspension = Total\ cells\ per\ mL \times Suspension\ volume(mL)$$

$$Cell\ seeding = \frac{Total\ amount\ of\ cells\ in\ suspension}{proposed\ seeding\ density}$$

C4. Calculation for average laser irradiation times

The laser power output was measured using a Laser Power Meter and used to calculate the time of laser exposure according to the energy that is given. Laser irradiation times can be calculated as follows:

$$\frac{mW}{cm^2} = \frac{mW \times 4}{\pi \times 3.4^2}$$

$$\frac{W}{cm^2} = \frac{mW/cm^2}{1000}$$

$$Time\ (s) = \frac{J/\ cm^2}{W/cm^2}$$

C5. Calculation for PS loading efficiency

The loading efficiency of PS on SWCNTs were calculated using the below formula:

$$PLE\ (\%) = \frac{weight\ of\ loaded\ PS}{weight\ of\ PS\ infeed} \times 100$$

APPENDIX D
D1: REC Form

FACULTY OF HEALTH SCIENCES

RESEARCH ETHICS COMMITTEE
NHREC Registration no: REC-241112-035

REC-01-57- 2018

13 June 2018

TO WHOM IT MAY CONCERN:

STUDENT: **SUNDARAM, P**
STUDENT NUMBER: **201807307**

TITLE OF RESEARCH PROJECT: The Use of Biopolymer Functionalised Single Walled Carbon Nanotubes for Effective Targeted Photodynamic Therapy of Gastric Cancer Stem Cells

DEPARTMENT OR PROGRAMME: **BIOMEDICAL TECHNOLOGY**

SUPERVISOR: **Prof H Abrahamse** **CO-SUPERVISOR:** -

The Faculty Research Ethics Committee has scrutinised your research proposal and confirm that it complies with the approved ethical standards of the Faculty of Health Sciences; University of Johannesburg.

The REC would like to extend their best wishes to you with your postgraduate studies.

Yours sincerely,

Dr MA Temane
Vice Chair : Faculty of Health Sciences REC
Tel: 011 559 6972
Email: anniet@uj.ac.za

D2: HDC form

FACULTY OF HEALTH SCIENCES

HIGHER DEGREES COMMITTEE

HDC-11-40- 2018

19 June 2018

TO WHOM IT MAY CONCERN:

STUDENT: SUNDARAM, P
STUDENT NUMBER: 201807307

TITLE OF RESEARCH PROJECT: The Use of Biopolymer Functionalised Single Walled Carbon Nanotubes for Effective Targeted Photodynamic Therapy of Gastric Cancer Stem Cells

DEPARTMENT OR PROGRAMME: BIOMEDICAL TECHNOLOGY

SUPERVISOR: Prof H Abrahamse CO-SUPERVISOR: -

The Faculty Higher Degrees Committee has scrutinised your research proposal and concluded that it complies with the approved research standards of the Faculty of Health Sciences; University of Johannesburg.

The HDC would like to extend their best wishes to you with your postgraduate studies

Yours sincerely

Prof Y Coopoo
Chair: Faculty of Health Sciences HDC
Tel: 011 559 6944
Email: yogac@uj.ac.za

APPENDIX E

Publications

E1: Prabhavathi Sundaram and Heidi Abrahamse. Effective Photodynamic Therapy for Colon Cancer Cells Using Chlorin e6 Coated Hyaluronic Acid-Based Carbon Nanotubes. Int. J. Mol. Sci. 2020, 21, 4745.

International Journal of *Molecular Sciences*

MDPI

Article

Effective Photodynamic Therapy for Colon Cancer Cells Using Chlorin e6 Coated Hyaluronic Acid-Based Carbon Nanotubes

Prabhavathi Sundaram and Heidi Abrahamse *

Laser Research Centre, Faculty of Health Sciences, University of Johannesburg, Johannesburg 2028, South Africa; prabhavathis@uj.ac.za

* Correspondence: habrahamse@uj.ac.za; Tel.: +27-11-559-6550; Fax: +27-11-559-6448

Received: 27 May 2020; Accepted: 1 July 2020; Published: 3 July 2020

check for updates

Abstract: Colon cancer is the third major cancer contributor to mortality worldwide. Nanosized particles have attracted attention due to their possible contribution towards cancer treatment and diagnosis. Photodynamic therapy (PDT) is a cancer therapeutic modality that involves a light source, a photosensitizer and reactive oxygen species. Carbon nanotubes are fascinating nanocarriers for drug delivery, cancer diagnosis and numerous potential applications due to their unique physicochemical properties. In this study, single walled carbon nanotubes (SWCNTs) were coupled with hyaluronic acid (HA) and chlorin e6 (Ce6) coated on the walls of SWCNTs. The newly synthesized nanobiocomposite was characterized using ultraviolet-visible spectroscopy, Fourier transform electron microscopy (FTIR), X-ray diffraction analysis (XRD), particle size analysis and zeta potential. The loading efficiency of the SWCNTs-HA for Ce6 was calculated. The toxicity of the nanobiocomposite was tested on colon cancer cells using PDT at a fluence of 5 J/cm^2 and 10 J/cm^2. After 24 h, cellular changes were observed via microscopy, LDH cytotoxicity assay and cell death induction using annexin propidium iodide. The results showed that the newly synthesized nanobiocomposite enhanced the ability of PDT to be a photosensitizer carrier and induced cell death in colon cancer cells.

Keywords: colon cancer; chlorin e6; carbon nanotubes; hyaluronic acid; photodynamic therapy; photosensitizers

E2: Prabhavathi Sundaram and Heidi Abrahamse. Phototherapy Combined with Carbon Nanomaterials (1D and 2D) and Their Applications in Cancer Therapy. Materials 2020, 13, 4830; doi:10.3390/ma13214830.

materials

MDPI

Review

Phototherapy Combined with Carbon Nanomaterials (1D and 2D) and Their Applications in Cancer Therapy

Prabhavathi Sundaram and Heidi Abrahamse *

Laser Research Centre, Faculty of Health Sciences, University of Johannesburg, Johannesburg 2028, South Africa; prabhavathis@uj.ac.za

* Correspondence: habrahamse@uj.ac.za; Tel.: +27-11-559-6550

Received: 1 October 2020; Accepted: 26 October 2020; Published: 28 October 2020

check for updates

Abstract: Carbon-based materials have attracted research interest worldwide due to their physical and chemical properties and wide surface area, rendering them excellent carrier molecules. They are widely used in biological applications like antimicrobial activity, cancer diagnosis, bio-imaging, targeting, drug delivery, biosensors, tissue engineering, dental care, and skin care. Carbon-based nanomaterials like carbon nanotubes and graphene have drawn more attention in the field of phototherapy due to their unique properties such as thermal conductivity, large surface area, and electrical properties. Phototherapy is a promising next-generation therapeutic modality for many modern medical conditions that include cancer diagnosis, targeting, and treatment. Phototherapy involves the major administration of photosensitizers (PSs), which absorb light sources and emit reactive oxygen species under cellular environments. Several types of nontoxic PSs are functionalized on carbon-based nanomaterials and have numerous advantages in cancer therapy. In this review, we discuss the potential role and combined effect of phototherapy and carbon nanomaterials, the mechanism and functionalization of PSs on nanomaterials, and their promising advantages in cancer therapy.

Keywords: cancer; carbon nanotubes; graphene; photodynamic therapy; photosensitizers; phototherapy

APPENDIX F
Turnitin report

PS Thesis Draft-1

ORIGINALITY REPORT

20%	16%	8%	4%
SIMILARITY INDEX	INTERNET SOURCES	PUBLICATIONS	STUDENT PAPERS

PRIMARY SOURCES

1	www.mdpi.com Internet Source	5%
2	www.ncbi.nlm.nih.gov Internet Source	3%
3	hdl.handle.net Internet Source	2%
4	publications.waset.org Internet Source	1%
5	Huang, E.H.. "Colon cancer stem cells: implications for prevention and therapy", Trends in Molecular Medicine, 200811 Publication	1%
6	ujcontent.uj.ac.za Internet Source	1%
7	Stanisław Kwiatkowski, Bartosz Knap, Dawid Przystupski, Jolanta Saczko et al. "Photodynamic therapy – mechanisms, photosensitizers and combinations", Biomedicine & Pharmacotherapy, 2018	<1%